Development of Small Molecules as Chemical Tools for Investigating the Role of Metal–Protein Interactions in Neurodegenerative Diseases

by

Michael William Beck

A dissertation submitted in partial fulfillment
of the requirements for the degree of
Doctor of Philosophy
(Chemistry)
in The University of Michigan
2015

Doctoral Committee:

Associate Professor Mi Hee Lim, Co-Chair
Associate Professor Nicolai Lehnert, Co-Chair
Professor Ayyalusamy Ramamoorthy
Assistant Professor Brandon T. Ruotolo

2015

To all those who are afflicted by neurodegenerative diseases.

Acknowledgements

First and foremost, I am eternally grateful to my PhD advisor Professor Mi Hee Lim. Without her guidance, encouragement, patience, and assistance this dissertation would never have been completed. She has always been supportive of my ideas and willing to discuss my results or other scientific topics. Additionally, I want to thank her for the unique opportunity to spend a year at Ulsan National Institute of Science and Technology (UNIST) in the Republic of Korea to continue to work in her laboratory.

I would like to also thank my dissertation committee members: Professors Nicolai Lehnert, Brandon Ruotolo, and Ayyalusamy Ramamoorthy for their insights and critiques during our meetings which have made me a better scientist. I would like to particularly thank Professor Lehnert for agreeing to be a co-chair for my dissertation committee due to the transition of Professor Lim to UNIST. Additionally, I want to express my gratitude for all of my teachers and professors throughout my life especially Professor Ed Lisic, my undergraduate research advisor, who gave me my first research opportunity and encouraged me to continue with my studies at the graduate level, as well as, my internship mentors at Colgate-Palmolive, Dr. Ryan Cameron and Debbie Peru for their guidance and helpful advice.

I want to also express my sincere appreciation for the people who I have collaborated with during the course of my PhD studies who are recognized for their contributions to this thesis at the beginning of each chapter. I also want to thank all of my Lim group labmates both past and present for their assistance, mentorship, scientific discussion, and friendship, particularly the following members who have been especially influential: Dr. Xiaoming He, Dr. Joey Braymer, Dr. Alaina DeToma, Dr. Akiko Kochi, Dr. Masha Savelieff, Amit Pithadia, Hyuck Jin Lee, Kyle Korshavn, Younwoo Nam, Juhye Kang, Jeffrey Derrick, and Jeeyeon Lee. I would also like to acknowledge those who, in addition to Professor Lim, helped me with living in Korea most importantly Mi Sook Lim who made sure that I had everything in order to travel to Korea, assisted me in getting

set up there, and made sure everything else during my stay was in order, and Hyuck Jin Lee who helped me with everything else, as well as Dr. Yeon Ju Kwak, Younwoo Nam, Milim Jang, Juhye Kang, Jin Hoon Kim, Jung Ha Lee, Jeeyeon Lee, Yonghwan Ji, Eunju Nam, and Jiyeon Han.

I would also like to thank all of my friends and family for their support during the course of my PhD studies.

To my sister, for putting up with me while growing up and taking care of things while I have been unable to help out at home.

To my wonderful girlfriend, Emily, thank you for being so understanding and all of your encouragement and reassurance.

Last, but certainly not least, to my parents, Scott and Mary Beck, despite their constant reminders that “I can always quit and come live at home,” I appreciate everything they have done to ensure that I could receive a good education and to be able to follow my dreams. I also want to thank them for putting up with and feeding me while I wrote this dissertation.

Table of Contents

List of Tables

List of Figures

List of Appendices

List of Abbreviations

$(CuOTf)_2 \bullet C_6H_6$	Copper(I) trifluoromethanesulfonate benzene complex
α-Syn	α-Synuclein
3D	Three dimensional
Aβ	Amyloid-β
AD	Alzheimer's disease
Al_2O_3	Aluminium oxide
ALS	Amyotrophic lateral sclerosis
AMPA	2-Amino-3-(3-hydroxy-5-methylisoxazol-4-yl)propanoic acid
ANOVA	Analysis of variance
Asc	Sodium ascorbate
BBB	Blood-brain barrier
BSA	Bovine serum albumin
CA	Cornu amonis
CC	Corpus callosum;
C*c*O	Cytochrome c oxidase
CCS	Collision cross section
CH_3CN	Acetonitrile
*c*logP	Calculated logarithm of the octanol-water partition coefficient
CNS	Central nervous system
CO_2	Carbon dioxide
COSMO	Conductor-like screening model
CSF	Cerebral spinal fluid
CSP	Chemical shift perterbations
CTE	Chronic traumatic encephalopathy
ctx	Cortex
$Cu[(CH_3CN)_4]BF_4$	*Tetrakis*(acetonitrile)copper(I) tetrafluoroborate

$CuCl_2$	Copper(II) chloride
Cu,Zn-SOD1	Copper and zinc superoxide dismutase
CQ	Clioquinol; 5-chloro-7-iodoquinolin-8-ol
DCM	Dichloromethane
ddH_2O	Double-distilled water
DFO	Deferoxamine; *N*-{5-[acetyl(hydroxy)amino]pentyl}-*N*-[5-({4-[(5-aminopentyl)(hydroxy)amino]-4-oxobutanoyl}amino)pentyl]-*N*-hydroxysuccinamide)
DFP	Deferiprone; 3-hydroxy-1-methylpyridin-4(1*H*)-one
DFP-NP	Deferiprone functionalized with polystyrene nanoparticles
DFT	Density functional theory
dg	Dentate gyrus
DMPD	*N*,*N*-Dimethyl-*p*-phenylenediamine
DMSO	Dimethyl sulfoxide
DPA	Di-(2-picolyl)amine
DTPA	Diethylenetriaminepentaacetic acid
ECL	Enhanced chemiluminescence
ECP	Effective-core potential
EDTA	2,2',2'',2'''-(Ethane-1,2-diylbis(azanetriyl))tetraacetic acid
EGCG	Epigallocatechin-3-gallate
ELISA	Enzyme-linked immunosorbent assay
ENDIP	N_1,N_2-Bis(pyridin-2-ylmethyl)ethane-1,2-diamine
ESI-MS	Electrospray ionization mass spectrometry
ETC	Electron transport chain
Et_3N	Triethylamine
EtOAc	Ethyl acetate
Et_2O	Diethyl ether
FBS	Fetal bovine serum
FTLD	Frontotemporal lobar degeneration
Gln	Glutamine
GSH	Glutathione

H_2O_2	Hydrogen peroxide
hAPP	Human amyloid precursor protein
HD	Huntington's disease
Htt	huntingtin
HBD	Hydrogen bond donor
HBA	Hydrogen bond acceptor
Hip	Hippocampus
HEPES	4-(2-Hydroxyethyl)-1-piperazineethanesulfonic acid
HOMO	Highest occupied molecular orbital
HBSS	Hank's balanced salt solution
HSAB	Hard-soft acid base
HRMS	High-resolution mass spectrometry
IDP	Intrinsically disordered protein
IM-MS	Ion mobility-mass spectrometry
IMPY	2-(4'-Dimethylaminophenyl)-6-iodoimidazo[1,2-*a*]pyridine
IP	Ionization potential
K_d	Disassociation constant
LUMO	Lowest unoccupied molecular orbital
m/z	Mass-to-charge ratio
M17 cells	Human neuroblastoma SK-N-BE(2)-M17 cells
mf	Mossy fiber region of the brain
$MgSO_4$	Magnesium sulfate
MPAC	Metal−protein attenuating compounds
MS	Mass spectrometry
MTT	3-(4,5-Dimethylthiazol-2-yl)-2,5-diphenyltetrazolium
MW	Molecular weight
N2a cells	Murine neuroblastoma Neuro-2a cells
$Na_2H_2PO_4$	Sodium dihydrogen phosphate
NADPH	Reduced nicotinamide adenine dinucleotide phosphate
NEAA	Non-essential amino acids
nESI	Nanoelectrospray ionization

NFT	Neurofibrillary tangles
NH_4OH	Ammonium hydroxide
NMDAR	*N*-Methyl-D-aspartate receptors
NMR	Nuclear magnetic resonance spectroscopy
O_2	Dioxygen
$O_2^{\bullet-}$	Superoxide
PAMPA-BBB	Parallel artificial membrane permeability assay adapted for the blood-brain barrier
PBS	Phosphate buffered saline
PCM	Polarizable continuum model
PD	Parkinson's disease
PDVF	Polyvinylidene fluoride
PrP	Prion protein
PSA	Polar surface area
PSEN1	Presenilin
Ptau	Hyperphosphorylated tau protein
ROS	Reactive oxygen species
SDS	Sodium dodecyl sulfate
SEM	Standard errors of the mean
SMON	Subacute myelo-optic neuropathy
SOD	Superoxide dismutase
SOFAST-HMQC	Band-selective optimized flip-angle short transient heteronuclear multiple quantum coherence
SOMO	Singly occupied molecular orbitals
SPECT	Single-photon emission computed tomography
STD	Saturation transfer difference
TBS	Tris-buffered saline
TBS-T	Tris-buffered saline containing Tween 20
TEAC	Trolox equivalent antioxidant capacity
TEM	Transmission electron microscopy
TfR	Transferrin receptor

ThT	Thioflavin T; 4-(3,6-dimethylbenzothiazol-3-ium-2-yl)-*N*,*N*-dimethyl-aniline
TLC	Thin layer chromatography
TSQ	*N*-(6-Methoxy-8-quinolyl)-*p*-toluenesulfonamide
Trolox	6-Hydroxy-2,5,7,8-tetramethylchroman-2- carboxylic acid
TROSY-HSQC	Transverse relaxation-optimized heteronuclear single quantum coherence nuclear magnetic resonance spectroscopy
Tween 20	Polyoxyethylene (20) sorbitan monolaurate
UV-Vis	UV-Visible spectroscopy
WT	Wild type
$ZnCl_2$	Zinc(II) chloride
ZnTs	Zinc transporter proteins

Abstract

Metals play an essential part in biological processes in humans. When these beneficial metal ions become misregulated, the resulting metal ion dyshomeostasis can be catastrophic. This occurs in several neurodegenerative diseases where the aberrant interactions of metal ions with proteins can lead to their abnormal aggregation, production of oxidative stress, and neuronal death (reactivity). To better understand the role of metal–protein complexes in the pathogenesis of these diseases, small molecules have been developed as chemical tools that target these complexes and mediate their reactivity.

In this thesis, first, design considerations along with the approaches of developing and studying the activity of such molecules were discussed in the context of the most prevalent neurodegenerative diseases, Alzheimer's disease (AD). Next, one such compound, **L2-b**, was demonstrated to target metal complexes of amyloid-β (Aβ), an AD pathological feature, over metal-free Aβ, and reduce the reactivity of these species using biochemical and biophysical techniques. Upon application of **L2-b** to 5XFAD AD model mice, metal–Aβ was targeted and modulated in the brain; amyloid pathology was reduced; and AD-associated cognitive deficits were improved. These *in vivo* studies are the first time experimental evidence has directly linked metal–Aβ to AD pathogenesis.

Subsequent investigations developed new small molecules that could target and mediate abnormal metal-free and metal-induced reactivity. Initial studies began with a small series of stilbene-based compounds that were found to have different activity toward controlling metal-free Aβ and metal–Aβ reactivity despite their structural similarity. In-depth (bio)chemical and DFT calculations were also performed to propose modes of action for these molecules. This knowledge was then used to create a library of chemical tools that have different abilities toward mediating abnormal metal-free and

metal-induced Aβ reactivity. Additionally, two more frameworks were developed and their ability to control metal–Aβ reactivity was explored.

Overall, the small molecules designed and analyzed here demonstrate that increased mechanistic understanding of their activity allows for the development of compounds with targeted abilities to control the reactivity of metal–protein complexes. Application of such compounds *in vivo* could lead to the elucidation of the pathogenesis of these devastating diseases, which could result in effective therapeutic discovery.

Chapter 1
Ligand design to target and modulate metal-protein interactions in neurodegenerative diseases

A portion of this chapter was presented in as a publication in Beck, M. W.; Pithadia, A. S.; DeToma, A. S.; Korshavn, K. J.; Lim, M. H. In *Ligand Design in Medicinal Inorganic Chemistry*; Storr, T., Ed.; John Wiley & Sons, Ltd: Chichester, West Sussex, **2014**, pp. 257.

1.1. Introduction

1.1.1. Metals in the brain

Understanding the function of metals in different biological environments and organs especially the brain (metalloneurochemistry) has been an area of particular interest in the past 30 years.[1,2] The complex functions of the brain require suitable levels of metal ions for a variety of processes including neurotransmission, dioxygen (O_2) transport, electron transfer mechanisms, and reactive oxygen species (ROS) detoxification (Table 1.1).[1,3-13] Owing to the broad spectrum of metal ions' action within the brain, precise control of their uptake, distribution, and clearance is essential for proper function. The misregulation and miscompartmentalization of metals, particularly transition metals, have been implicated as a possible source of toxicity associated with multiple neurodegenerative diseases (*vide infra*). The recent development of both chemical tools to study the potential involvement of metals in neurodegenerative diseases and therapeutics based on this hypothesis is presented in this chapter. First,

Table 1.1. Metal ions in the brain

Metal Ion	Function in the Brain	Localization[a]
Na(I)	Action potential: depolarization of transmembrane voltage along the axon[12]	Axon
K(I)	Action potential: repolarization of transmembrane voltage along the axon[12]	Axon
Mg(II)	Synaptic plasticity: voltage dependent block of *N*-methyl-D-aspartate receptors[14]	Hippocampus
Ca(II)	Neurotransmission: neurotransmitter release and excitability[15]	Synapse
Mn(II/IV)	Enzymatic cofactor for neuronal and glial cell function, as well as neurotransmitter synthesis[16]	Globus pallidus
Fe(II/III)	Enzymatic cofactor for energy metabolism, O_2 transport, electron transfer and neurotransmitter synthesis[11]	Basal ganglia
Cu(I/II)	Enzymatic cofactor for energy metabolism, cellular respiration, ROS detoxification, and neurotransmitter synthesis[11]	Locus coeruleus
Zn(II)	Neurotransmitter and enzymatic cofactor for protein structure and conformation[11]	Hippocampus

[a]Indicates the area with highest concentration in the brain

the roles of metals in neurodegenerative diseases are briefly discussed in the context of their normal functions.

Transition metal ions, such as Cu(I/II), Zn(II), and Fe(II/III), have various functions in the brain despite occurring in trace amounts.[11,17] Copper is a redox active metal commonly found in the +1 and +2 oxidation states. Owing to its redox properties, copper is involved in the function of a number of enzymes, including those for the respiratory activity of cytochrome *c* oxidase (C*c*O) and ROS detoxification by copper and zinc superoxide dismutase (Cu,Zn-SOD1),[11] as well as the oxidation of Fe(II) to Fe(III) in ceruloplasmin.[18] Additionally, copper serves as a cofactor for enzymes and proteins that maintain neurotransmitter and neuropeptide homeostasis. Copper is distributed to various parts of the brain with average concentrations of up to 400 μM in the substantia nigra, 2.5 μM in the cerebral spinal fluid (CSF), and 30 μM in the synaptic cleft.[1,11]

Zinc is distributed in gray matter (about 500 μM), specifically the neocortex, amygdala, and hippocampus (where zinc concentrations can reach up to 300 μM).[11,19] It has been suggested that Zn(II) is released from the presynapse into the synaptic cleft during neurotransmission, and postsynaptic uptake occurs through calcium-permeable 2-amino-3-(3-hydroxy-5-methylisoxazol-4-yl)propanoic acid (AMPA)-kainate channels.[11,20] The uptake and distribution of Zn(II) throughout neuronal cells are performed by zinc transporter proteins (ZnTs).[11,21] The role of Zn(II) in neurotransmission has not been completely elucidated; however, it has been reported that Zn(II) could inhibit *N*-methyl-d-aspartate receptors (NMDARs) as well as AMPA gated channels.[11,22-25]

Iron is the most abundant metal in the body; within the brain it is primarily concentrated in the basal ganglia, oligodendrocytes, microglia, and neurons.[26,27] Iron, when bound to transferrin, can be transported across the blood brain barrier (BBB) *via* transferrin receptors (TfRs) resulting in total neuronal iron concentrations ranging between 0.5 – 1.0 mM.[28,29] Iron is typically found in the +2 and +3 oxidation states, depending on the environment and role in biological systems. Higher oxidation states can also be observed in catalytic cycles of metalloproteins (*e.g.*, cytochrome P450). The oxidation state of iron is controlled by electron transfer facilitated by ferric reductases and ferroxidases.[12,13,35] A number of functions require iron including cell respiration

Figure 1.1. Selected metals and proteins involved in the pathogenesis of neurodegenerative diseases. Alzheimer's disease (AD; Cu, Zn, and Fe; amyloid-β (Aβ) (PDB 2LFM)[30]), amyotrophic lateral sclerosis (ALS; Cu and Zn; superoxide dismutase (SOD) (PDB 1SPD)[31]), Parkinson's disease (PD; Fe and Zn; α-synuclein (α-syn) (PDB 2KKW)[32]), Huntington's disease (HD; Cu and Fe; huntingtin (htt) (PDB 4FED)[33]), and prion disease (Mn, Cu, and Zn; prion protein (PrP) (PDB 1QLX)[34]).

(C*c*O), ROS detoxification (catalase), and neurotransmitter biosynthesis (tyrosine hydroxylase).[11-13] Iron ion homeostasis is regulated through the iron storage protein, ferritin, and the iron transport protein, transferrin.[11,12,36,37]

1.1.2. Aberrant metal–protein interactions

Metals are not always beneficial in biology as metal ion misregulation can cause dysfunction. Research into neurodegenerative diseases has investigated the roles of aberrant metal–protein interactions upon various diseases (Figure 1.1); and experimental evidence has suggested that many diseases are exacerbated by metal ion dyshomeostasis. Abnormal metal binding could promote the formation and stabilization of misfolded protein conformations, accelerate protein aggregation, and/or lead to the

overproduction of ROS.[1,30-34,38-40] The non-native interaction of metal ions with proteins could interfere with the normal functioning of each component, along with the uptake, transport, and release of proteins and metal ions. For example, in Alzheimer's disease (AD), the misfolded protein, amyloid-β (Aβ) (Figure 1.1), which can bind metals, has been suggested to aggregate in the synapse where high concentrations of metal ions are found during neurotransmission (up to about 200–300 μM for Zn(II); about 30 μM for Cu(I/II)), potentially disrupting normal metal ion homeostasis.[15,18,19,30,32,38,39,41,42] Furthermore, loosely bound redox active metal ions (*e.g.*, Cu(I/II) and Fe(II/III)) can exert toxic effects *via* the production of ROS.[30,43-45]

1.1.3. Oxidative stress

Oxidative stress can be defined as an imbalance between the generation and clearance of ROS that may ultimately cause the direct oxidation and dysfunction of biomolecules (*e.g.*, DNA, proteins, and lipids).[46] The high O_2 consumption in the brain makes it especially prone to damage by ROS, and oxidative stress can easily occur if the mechanisms to detoxify ROS are dysfunctional. This can lead to more rapid aging, excitotoxicity of neurons, and neuronal death.[47,48] ROS can be produced through the Fenton reaction and Haber-Weiss cycle (Figure 1.2) when redox active metal ions, such as Fe(II/III) and Cu(I/II), are misregulated and/or miscompartmentalized.[40,49-51] Mitochondrial dysfunction could be an additional source of ROS due to its role in cellular respiration and O_2 reduction. During these processes, premature electron transfer to O_2 in the electron transport chain (ETC) could result in the generation of superoxide ($O_2^{\bullet-}$), a potent ROS.[48]

Defense mechanisms against ROS utilize metalloenzymes, such as Cu,Zn-SOD1 and catalase, as well as small molecule antioxidants, such as glutathione (GSH).[52,53] Cu,Zn-SOD1 is responsible for the disproportionation of $O_2^{\bullet-}$ to O_2 and hydrogen peroxide (H_2O_2), which is broken down to either water or O_2 and water by GSH and catalase, respectively.[52-54] In the presence of an abnormal level of redox active metal ions, however, H_2O_2 can be cycled into the Fenton and Haber-Weiss reactions instead of being broken down by catalase and GSH. Through these cycles, H_2O_2 can be converted to less stable ROS (Figure 1.2).[40,50,51]

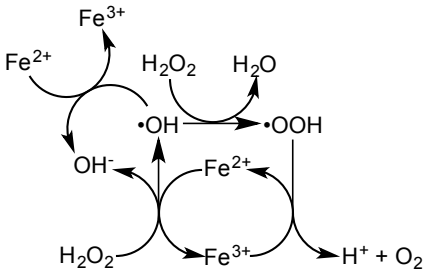

Figure 1.2. Fenton reaction and Haber-Weiss cycle for the catalytic production of ROS by Fe(II/III). Similar redox chemistry occurs for Cu(I/II).

Prolonged and elevated oxidative stress has been implicated in the pathogenesis of several neurodegenerative diseases, including AD, Parkinson's disease (PD), and amyotrophic lateral sclerosis (ALS) (*vide infra*). Metal ion dyshomeostasis and mitochondrial dysfunction could be the sources of oxidative stress in these neurodegenerative diseases. In AD, for example, the interaction of Aβ and redox active Cu(I/II) or Fe(II/III) may facilitate ROS production, resulting in oxidative damage.[30,32,45] It has also been reported that heme–Aβ complexes can have peroxidase activity in AD.[45,55] In PD, a pathological feature is the accumulation of Fe(III) in the substantia nigra of diseased neurons, which could increase the likelihood for an overabundance of ROS.[56,57] H_2O_2 has also been shown to interact with Cu,Zn-SOD1, through the oxidation of residues near the copper metal binding site, which can cause copper release and subsequently deactivate the enzyme, a concern in ALS.[58] Despite their similarities, however, each neurodegenerative disease has specific hallmarks (Figure 1.1).

1.2. Alzheimer's disease (AD)

While aberrant metal-protein interactions are involved in multiple neurodegenerative diseases (Figure 1.1), the most prevalent of these diseases is AD.[59] Thus the remainder of this chapter will focus on AD. AD is hallmarked by the accumulation of senile plaques and neurofibrillary tangles (NFTs), composed primarily of Aβ, and hyperphosphorylated tau protein (ptau), respectively, in the brain.[18,30,32,42-45,59-67] Along with these histopathological characteristics, concentrations of Cu, Zn, and Fe are found to be elevated in *ex vivo* tissue samples collected from AD brains (*ca.* 400, 1000, and 900 μM, respectively, in the plaques).[10,30,31,42-45] It remains unclear, however, whether the total concentration of metals in the brain is altered or their local pools are

miscompartmentalized upon initiation and progression of AD.[18,39,68] Still, the current consensus is that metal ion dyshomeostasis occurs in AD.[30,44,60]

Additionally, *in vitro* studies confirm that these metals can generate complexes with Aβ and tau. The coordination chemistry of Aβ with metals has been extensively studied *in vitro* as summarized in Table 1.2.[30-32,43,45,60,69-75] The interactions between metal ions and Aβ are shown to accelerate Aβ aggregation and be associated with ROS production *via* Fenton chemistry.[49] It is suggested that these interactions also stabilize toxic, oligomeric Aβ species.[30,31,76] Thus, modulation and/or disruption of these interactions could be a potential target for the future design of chemical tools, diagnostics, or therapeutics in order to understand or combat AD.[30,60,63,72,77]

Unlike Aβ, information on metal binding to tau has been relatively limited. As shown in Table 1.2, some binding studies of Cu(II), Al(III), and Fe(II/III) with both full length and fragments of tau and ptau *in vitro* have been reported.[32,78-80] Upon binding to ptau, Cu(II) has been shown to slightly promote its aggregation.[32,78] Al(III) and Fe(III), but not Fe(II), could also be involved in enhancement of ptau aggregation.[32,78-80] Despite these initial studies, the interactions of metals and tau/ptau and the role of metal–tau/ptau species in AD pathogenesis have not yet been uncovered.

1.3. Ligand design to target and modulate metal–protein interactions

The previous sections demonstrated that AD, similar to other neurodegenerative diseases, is associated with various factors. Developing adequate therapeutics is difficult due to a lack of understanding of both disease etiology and the interconnection of multiple elements with neuropathogenesis. Current treatments for AD have focused on attenuating one specific pathogenic factor and consequently only offer symptomatic relief instead of disease-modifying effects.[81-85] Given the role of metals in AD, metal chelation therapy has been suggested as a method to disrupt disease-related metal–protein interactions as well as restore metal ion homeostasis and proper protein cellular functions in the body.[81] In order to control the interactions between metal ions and misfolded proteins in AD, metal chelating agents with traditional applications in metal overload diseases, along with other common chelating compounds (Figure 1.3), were employed and shown to modulate this interaction to varying extents *in vitro.*[81,86-98]

Table 1.2. Amino acid residues and binding affinities for metal–protein complexes involved in AD[a]

Metal ion	Amyloid-β (Aβ)[40,70,73]	Tau[40,78]
Fe(II)	CN[b] = 6 Asp1, Glu3, His6, His13 or His14, Ala2 (backbone carbonyl), *N*-terminal amine (K_d = 10^{-4} M)	
Cu(I)	CN = 2 Two His residues (K_d = 10^{-14} or 10^{-7})	
Cu(II)	CN = 4 **Component I** (3N1O) [His6, His13, His14, and either Asp1-Ala2 (backbone carbonyl) or Asp1] or [N-terminal amine, two His residues, and Asp1-Ala2 (backbone carbonyl) or Asp1] **Component II** (3N1O) [His6, His13, His14, and Ala2 (backbone carbonyl)] or [N-terminal amine, Ala1-Asp2 (deprotonated backbone amide), Ala2-Glu3 (back carbonyl), one His residue] (4N) [His6, His13, His14, and either N-terminal amine or Ala1-Asp2 (deprotonated backbone amide)] (K_d[c] = 10^{-11}-10^{-7} M)	**R2 and R3 units** His299, His329, and His330 **R2 and R3 units** Cys291 and Cys322 (K_d = 10^{-6} M)
Zn(II)	CN = 4-6 His6, His13, His14, and a combination of Asp1 (N-terminal amine or carboxylate), Arg5 (backbone amide), Tyr10, Glu11, a water molecule (K_d = 10^{-9}-10^{-6} M)	

[a] Residues listed are those known to have specific interaction.
[b] CN, coordination number.
[c] K_d, dissociation constant.

For example 2,2′,2″,2‴-(ethane-1,2-diylbis(azanetriyl))tetraacetic acid (**EDTA**) was shown to resolubilize insoluble Cu(II)– and Zn(II)–Aβ aggregates and affect the morphology of Cu(II)–Aβ species generated upon co-incubation with **EDTA**.[92,93] Additionally, **EDTA** has been shown to disaggregate insoluble Al(III)-treated tau and ptau species.[99] **DFO** (Figure 1.3) has also been studied as a treatment for AD. Administration to AD patients over two years appeared to slow the clinical progression of AD-associated symptoms.[100] **Phen** (Figure 1.3), together with two of its derivatives, bathocuproine and bathophenanthroline, has been demonstrated to disaggregate metal-associated Aβ aggregates into soluble species.[101,102] These ligands also mitigated H_2O_2 production by Cu–Aβ species, suggesting a possible use for ROS scavenging or ROS production control.[103] Furthermore, **D-penicillamine** (Figure 1.3) has shown a minor ability to disaggregate Cu(II)-induced Aβ aggregates *in vitro.*[104]

The application of these traditional chelators for both the study and treatment of AD, however, has been limited due to poor brain uptake, inadequate specificity for targeting aberrant metal–protein interactions, and disruption of essential metal–protein cellular functions due to their high metal binding affinities.[81,87,88,94,105-107] Despite these

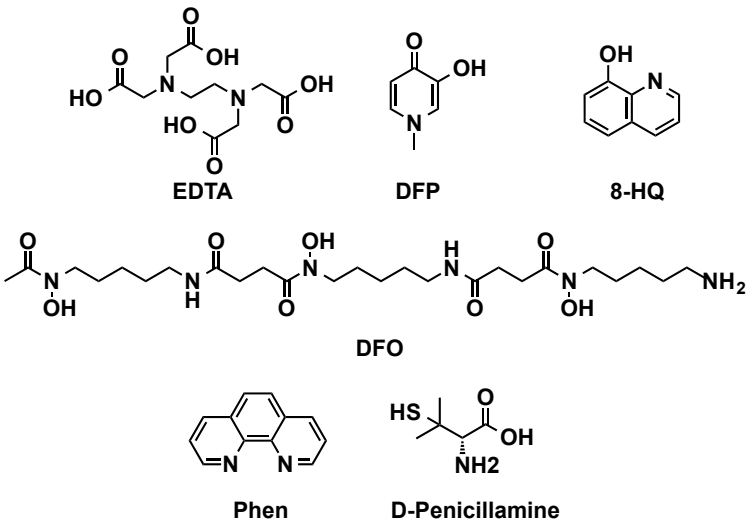

Figure 1.3. Structures of selected metal chelators. **EDTA**, 2,2',2'',2'''-(ethane-1,2-diylbis(azanetriyl))tetraacetic acid; **DFP**, 3-hydroxy-1-methylpyridin-4(1H)-one; **8-HQ**, 8-hydroxyquinoline; **DFO**, *N*'-{5-[acetyl(hydroxy)-amino]pentyl}-*N*-[5-({4-[(5-aminopentyl)(hydroxy)amino]-4-oxobutanoyl}amino)pentyl]-*N*-hydroxysuccinamide); **phen**, 1,10-phenanthroline; **D-penicillamine**, (S)-2-amino-3-mercapto-3-methylbutanoic acid.

issues, the results suggest that regulating metal–protein interactions may be a productive method in ligand design for chemical tools to uncover pathogenesis of AD and effective diagnostics or therapeutics (*vide infra*).

Recent advancements in the design of tools and treatments have sought to specifically and simultaneously target and modulate multiple disease-related factors caused by deleterious metal–protein interactions by applying a "one molecule-multiple targets" approach. In this chapter we will focus on small molecules that specifically target and modulate metal–protein interactions and regulate ROS production. Such molecules have mainly been fashioned through three design strategies: functionalization, attachment/linkage, and incorporation.[81,108,109] Using these approaches, metal binding moieties are combined with frameworks that target and regulate disease-related metal–protein interactions. To prevent the introduction of additional dyshomeostasis and misregulation of metals, the binding affinities of these designed molecules for metals must be balanced in the appropriate range. The affinity for metal ions ought to be strong enough to modulate aberrant metal–protein interactions but weak enough to avoid interference with essential metal–protein interactions for biological functions (generally, $K_d \geq 10^{-10}$ M).[30,110,111] These molecules should also demonstrate selectivity for metal ions associated with AD (*e.g.,* Cu(I/II), Fe(II), and Zn(II)) to hinder exacerbation of metal ion dyshomeostasis. Tuning these properties can often be achieved by consideration of basic inorganic chemistry concepts such as the hard-soft acid base principle, the Irving-Williams series, denticity, and the chelate effect.[94,105,106,108] Simple theories cannot always completely describe metal binding properties of small molecules in the heterogeneous *in vivo* environment, however, due to multiple parameters affecting the ability of a ligand to bind to a specific metal ion (*e.g.,* charge at local pH, oxidation state, stability, rate of complexation, and competition with biomolecules).[87,108,112-114] In addition to tuning the metal binding properties of these molecules, the design of the moiety that targets AD-related proteins is important. Unfortunately, there is no set of rules governing the interaction of small molecules with proteins, and most of the molecules known to interact are natural products, discovered through experimental observations, with little structure-interaction relationship exploration.[115] In one of the few structure-interaction relationship studies,

the presence of a methyl amino moiety, with the combined hydrogen bond donor (HBD)/hydrogen bond acceptor (HBA) properties of the amine and the hydrophobicity of the methyl group(s), in derivatives of thioflavin-T (**ThT**), a fluorescent dye that is specific for amyloid fibrils, has been suggested to be important for targeting Aβ fibrils.[116-118] Other structural moieties utilized to target AD-related proteins to identify and regulate potentially pathological metal–protein interactions are discussed later in this chapter.

Along with targeting and modulating aberrant metal–protein complexes in AD, it is critical for designed compounds to be able to penetrate the BBB. Adherence to Lipinski's rules for drug likeness and the use of calculated brain-blood partitioning values (logBB) are particularly useful in predicting passive diffusion of a ligand across the BBB. The restricted terms of Lipinski's rules dictate that molecules for brain applications should generally have a molecular weight (MW) ≤ 450 g/mol, a calculated logarithm of the octanol-water partition coefficient (*c*logP) ≤ 5, HBD ≤ 5, HBA ≤ 10, and polar surface area (PSA) ≤ 90 $Å^2$.[119,120] The logBB calculation estimates the expected permeability based on an equation (typically defined as logBB = −0.0148 × PSA + 0.152 × *c*logP + 0.139).[121] Molecules with logBB values ≤ −1.00 are expected to have poor diffusion across the BBB.[121] Alternatively, structural groups that are known to be actively transported through the BBB (*e.g.*, glucose) can be added to the parent framework to improve uptake into the brain.[95,122] Lastly, these ligands and their corresponding complexes should display low cytotoxicity. Overall, chemical structures capable of targeting and modulating abnormal metal–protein interactions, while also being nontoxic, bioavailable, and BBB permeable, could be employed to construct chemical tools to investigate the molecular basis for or as therapeutics for the treatment of neurodegenerative diseases. Design considerations for molecules and their effects on metal–protein interactions are discussed in detail in the following sections.

1.3.1. Metal chelating compounds

As discussed in the previous section, there are several issues limiting the use of metal chelators *in vivo*. This next section discusses some of the modifications made to frameworks of these compounds in order to improve their properties. A good example of several types of possible modifications comes from the work with deferiprone (**DFP**)

(Figure 1.3). Glycosylated derivatives have been developed in order to both improve **DFP**'s BBB permeability and limit the interaction of this strong chelator (K_d, approximately 10^{-21} and 10^{-13} in a 1 : 2 M(II):**DFP** stoichiometry for Cu(II) and Zn(II), respectively; 10^{-12} M in a 1 : 3 M(II):**DFP** fashion for Fe(III)) with metals outside the brain.[123] A **DFP** prochelator employed a glucose moiety that unmasks the metal binding site upon cleavage by β-glycosidase.[95] Additionally, Orvig and co-workers have capitalized on the active uptake of glucose to prepare a family of **DFP** derivatives to target and modulate metal-associated Aβ.[123] The core **DFP** framework was *O*-glycosylated, and an Aβ-interacting methylamino phenyl and benzothiazolyl moieties were appended to the *N*-position. Cu(II)- and Zn(II)-induced Aβ aggregation was attenuated using these new compounds. When benzothiazolyl derivatives were appended onto the framework at the *N*-position, selective resolubilization of Cu(II)-induced Aβ aggregates was visualized, suggesting specificity for Cu(II)–Aβ over Zn(II)–Aβ species.[123] Deferiprone, combined with polystyrene nanoparticles (**DFP-NPs**), retains the metal binding properties of the ligand while improving its viability in cells and efficacy to reach the brain.[124] The **DFP-NP** conjugates inhibited Aβ fibril formation; however, their influence on metal–Aβ interactions in AD has yet to be studied.

The most well-studied metal chelator based framework for controlling metal–protein interactions in AD is 8-hydroxyquinoline (**8-HQ**; Figure 1.3), which can act as a bidentate chelator.[125,126] Derivatives of **8-HQ** have been found to modulate aberrant metal–protein interactions in multiple neurodegenerative diseases, including AD, with sufficient success to have reached clinical trials.[125-127] The **8-HQ** derivative clioquinol (**CQ**; Figure 1.4) is an approved topical antiseptic and was once administered as an oral intestinal amebicide before being pulled from the market in 1970s due to a possible side effect, subacute myelo-optic neuropathy (SMON).[127-129] The ability of **CQ** to chelate transition metals [K_d, approximately 10^{-10} M for Cu(II) about 10^{-9} M for Zn(II)] and to passively cross the BBB suggests that this compound could be a viable treatment for neurological conditions, serving as a modulator for disease-associated metal–protein interactions.[30,127,129-133] The proposed mechanism of action for **CQ** is twofold: (i) it can chelate metal ions from disease-related proteins, which influences

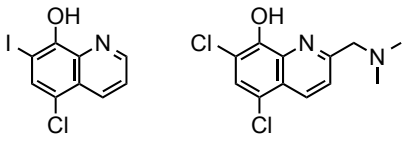

CQ **PBT2**

Figure 1.4. 8-Hydroxyquinoline (**8-HQ**) derivatives previously utilized in clinical trials for treating AD. **CQ**, 5-chloro-7-iodoquinolin-8-ol; **PBT-2**, 5,7-dicholoro-2-[(dimethylamino)methyl]quinolin-8-ol.

aggregation[128,134,135] and (ii) it can act as an ionophore, possibly mitigating changes in metal ion homeostasis by redistributing metal ions across membranes into cells and areas with lower metal ion concentrations.[89,134,136] Molecules possessing both of these properties are termed metal–protein attenuating compounds (MPACs).[134]

In AD transgenic mice, the amount of amyloid plaques was lessened upon **CQ** administration with improved symptoms and no observable adverse side effects.[127,132,137] Several human trials followed, the first of which was an uncontrolled study with 20 patients treated daily with an 80 mg dose of **CQ** for 21 days; resulting in patients displaying signs of improved cognitive function.[137,138] Subsequent phase II clinical trials had similar outcomes for AD patients with moderate dementia, but patients with more severe AD symptoms showed less significant improvement.[110,137,138]

While **CQ** has some properties that made it suitable to modulate aberrant metal–protein interactions in the brain (*e.g.*, BBB permeability, metal binding affinity in optimal range), it still lacks specificity to localize within the brain and selectively target AD-related metal–protein interactions.[139-141] In addition, scale-up reactions for clinical trials produced toxic di-iodinated byproducts of **CQ**, which prevented larger scale testing of **CQ** in humans.[141] As a result, clinical trials with **CQ** ceased and attention has shifted to another **8-HQ** derivative, **PBT-2** (Figure 1.4), which was carefully designed to avoid scale-up production problems and to maximize oral bioavailability.[140,142]

Initial *in vitro* studies of **PBT-2** demonstrated that this compound has similar metal binding affinities for Cu(II) and Zn(II) (K_d, approximately 10^{-10} M for Cu(II) and Zn(II)) as **CQ** but is a superior ionophore.[143] Studies with metal–Aβ have shown **PBT-2** is able to regulate Cu–Aβ-induced H_2O_2 production to a greater extent than **CQ**.[143] **PBT-2** was, however, unable to match **CQ**'s ability to disaggregate metal–Aβ aggregates. *In vivo*, **PBT-2** was shown to improve the cognitive abilities in AD mouse models.[144] Furthermore, **PBT-2**, but not **CQ**, could decrease abnormal tau phosphorylation in AD

mice.[143] Clinical trials of **PBT-2** on AD patients, like those of **CQ**, indicated that cognitive improvement between placebo and **PBT-2**-treated patients were only significant at earlier stages of the disease.[138,145,146] Although **PBT-2** was well tolerated in early clinical trials, more rigorous clinical trials will be beneficial to fully assess this compound's utility improving cognition in AD.[138,146]

1.3.2. Small molecules designed for metal–protein complexes

As an alternative to utilizing traditional chelators and their analogs, new small molecules containing structural moieties to target and modulate specific AD-related metal–protein interactions have been developed (*vide infra*). Some of these molecules were constructed by connecting structural moieties for metal chelation and protein interaction (*i.e.*, linkage approach), or installing a metal chelation site into a protein-targeting structure (*i.e.*, incorporation approach).[81,109,147]

ThT (Figure 1.5) has a high affinity for Aβ fibrils (nanomolar K_d).[116-118] Thus, several compounds have been based on its framework to target metal–Aβ species and modulate the interaction between metal and Aβ. The first reported example is **XH1** (Figure 1.5) which is composed of two **ThT**-like molecules linked with diethylenetriaminepentaacetic acid (**DTPA**), a strong metal chelator for Fe(II), Fe(III), Cu(II), and Zn(II) (K_d, about 10^{-16}, 10^{-28}, 10^{-21}, and 10^{-18} M, respectively).[148] **XH1** influenced Zn(II)-induced Aβ aggregation *in vitro* and reduced plaque load in an AD mouse model.[148] Moreover, when compared with **DTPA**'s effects on Zn(II)-triggered Aβ aggregation *in vitro*, **XH1** was able to decrease aggregation by about 50% more, which demonstrates the value of having moieties targeting both metal ions and proteins simultaneously to disrupt aberrant metal–protein interactions.

FC1 (Figure 1.5) is another multifunctional molecule derived from the **ThT** framework. The molecule is based on a neutral **ThT** backbone in which the dimethylamino group is replaced with the moderate metal binding moiety di-(2-picolyl)amine (**DPA**) (K_d, about 10^{-9} M for Cu(II) and 10^{-7} M for Zn(II)).[149] **FC1** was found to partially transform Cu(II)– and Zn(II)–Aβ aggregates into small, amorphous aggregates. When HeLa cells exposed to metal–Aβ were treated with **FC1**, however,

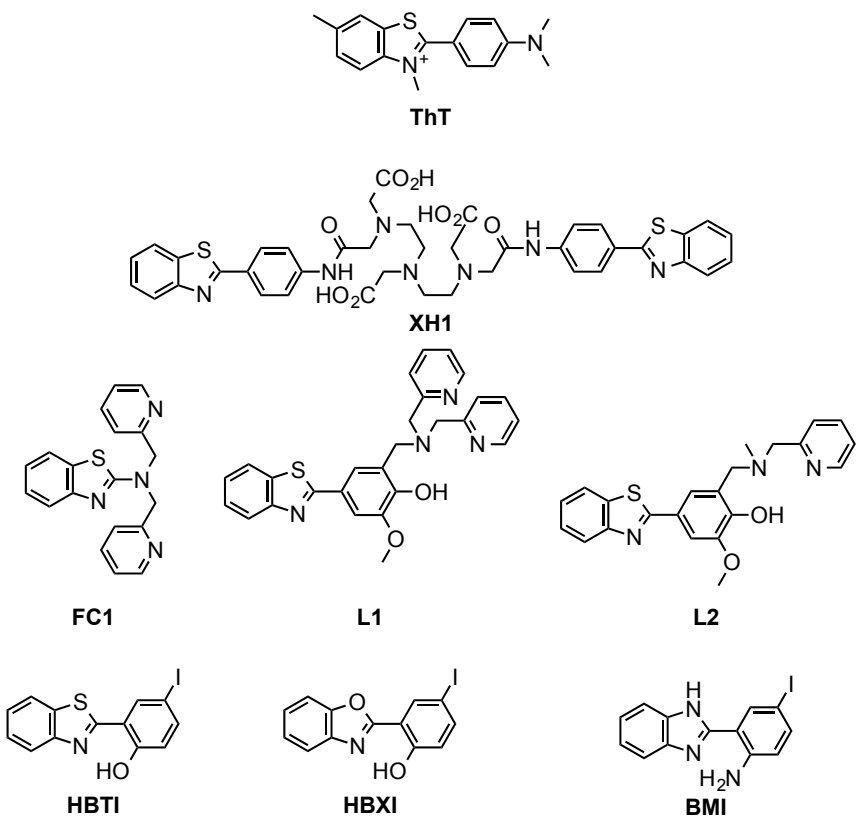

Figure 1.5. Structures of thioflavin-T (**ThT**) derivatives. **ThT**, 4-(3,6-dimethylbenzothiazol-3-ium-2-yl)-*N*,*N*-dimethylaniline; **XH1**, ([(4-(benzothiazol-2-yl)phenylcarbamoyl)methyl]-{2-[(2-{[(4-(benzothiazol-2-yl)phenylcarbamoyl)methyl](carboxymethyl)amino}ethyl)(carboxymethyl)amino] ethyl}amino)acetic acid; **FC1**, *N*,*N*-bis(pyridin-2-ylmethyl)-3*a*,7*a*-dihydrobenzothiazol-2-amine; **L1**, 4-(3*a*,7*a*-dihydrobenzothiazol-2-yl)-2-methoxy-6-((methyl(pyridin-2-ylmethyl)amino)methyl)phenol; **L2**, 2-((bis(pyridin-2-ylmethyl)amino)methyl)-4-(3*a*,7*a*-dihydrobenzothiazol-2-yl)-6-methoxyphenol; **HBTI**, 2-(benzothiazol-2-yl)-4-iodophenol; **HBXI**, 2-(benzoxazol-2-yl)-4-iodophenol; and **BMI**, 2-(1*H*-benzimidazol-2-yl)-4-iodoaniline.

increased toxicity was observed, implying that **FC1** may stabilize the generation of toxic Aβ oligomers.[149]

Mirica and co-workers took a similar approach to the design of **L1** and **L2** (Figure 1.5) where a dipyridylmethyl (**L1**) or a pyridylmethyl (**L2**) group was installed onto a **ThT** derivative with the dimethylaminophenyl group replaced with one derived from *o*-vanillin, previously shown to interact with Aβ.[150] As expected, tetradentate **L1** could bind Cu(II) and Zn(II) more strongly than tridentate **L2** (K_d, about 10^{-10} M *versus* 10^{-8} M for Cu(II); about 10^{-8} M *versus* 10^{-7} M for Zn(II)). Moreover, for Aβ interaction, **L2** (K_i about 30 nM) was able to bind more strongly to Aβ fibrils than **L1** (K_i about 200 nM). Despite these differences both **L1** and **L2** were capable of inhibiting the formation of metal–Aβ aggregates as well as disaggregate preformed aggregates. Similar to **FC1**, however,

treatment of N2a cells with Aβ, Cu(II) or Zn(II), and **L1** or **L2** resulted in increased toxicity over **L1**- or **L2**-untreated cells.[150]

HBX, **HBT**, and **BM** (iodinated forms; Figure 1.5) were discovered by *in silico* screening commercially available **ThT** derivatives for BBB permeability, antioxidant properties, and synthetic ease of iodination for possible use as imaging agents.[151] The properties of Aβ interaction (**ThT**) and metal chelation (a portion of **ThT** and a phenol or aniline ring) were introduced into one framework. The iodinated forms of these compounds, **HBXI**, **HBTI**, and **BMI** (Figure 1.5), were found to be mostly neutral at physiological pH, suggesting that they may passively cross the BBB. Furthermore, all of the derivatives were able to coordinate Cu(II) and Zn(II) with K_d values similar to **CQ** as well as inhibit metal-induced Aβ aggregation.[151]

Stilbene derivatives, previously used as imaging agents for Aβ aggregates, have demonstrated an ability to target Aβ fibrils with nanomolar binding affinities (Figure 1.6a).[152-154] **L1-b** (Figure 1.6a) was designed by incorporating two nitrogen donor atoms into the structure of the stilbene derivative (for Aβ interaction) to impart metal chelation.[102] This compound was able to modulate metal-induced Aβ aggregation and diminish metal–Aβ-induced cytotoxicity.[155] Owing to limited solubility of **L1-b** in aqueous media, the reduced amine form, **L2-b** (Figure 1.6a), was designed to combat this problem.[156] **L2-b** was capable of binding metal ions with affinities for Cu(II) and Zn(II) (K_d, about 10^{-10} and 10^{-6} M, respectively) in the appropriate range needed to target metal-associated Aβ. Two dimensional ^{1}H-^{15}N Transverse relaxation-optimized-heteronuclear single quantum coherence nuclear magnetic resonance spectroscopy (TROSY-HSQC) NMR demonstrated **L2-b** could interact directly with Aβ near the metal binding region. As a result, **L2-b** could control metal-mediated Aβ aggregation pathways *in vitro* and reduce the toxicity induced by metal–Aβ species in human neuroblastoma M17 cells. Additionally, it was shown to disaggregate *ex vivo* Aβ plaques in brain homogenates obtained from human AD patients.[156]

Another compound, **IMPY** (2-(4′-dimethylaminophenyl)-6-iodoimidazo[1,2-*a*]pyridine) (Figure 1.6b), was developed as an imaging agent for Aβ plaques.[153] **IMPY** binds to Aβ fibrils, and this property was exploited by using this framework as a

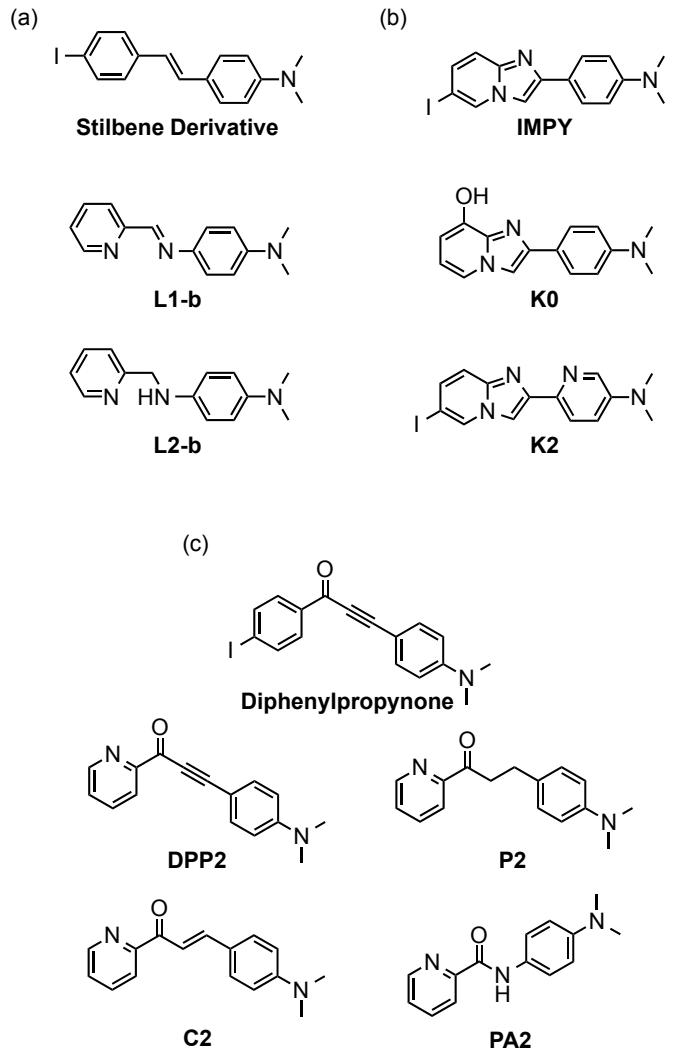

Figure 1.6. Structures of small molecules designed based on the frameworks of (a) the stilbene derivative, (4-(dimethylamino)-4'-iodostilbene); (b) **IMPY**, ((2-(4'-dimethylaminophenyl)-6-iodoimidazo[1,2-*a*]pyridine)); and (c) diphenylpropynone, (3-(4-(dimethylamino)phenyl)-1-(4-iodophenyl)-2-propyn-1-one. **L1-b**, N^1,N^1-dimethyl-N^4-(pyridin-2-ylmethylene)benzene-1,4-diamine; **L2-b**, N^1,N^1-dimethyl-N^4-(pyridin-2-ylmethyl)benzene-1,4-diamine; **K0**, 2-[4-(dimethylamino)phenyl]imidazo[1,2-*a*]pyridin-8-ol; **K2**, 6-(6-iodoimidazo[1,2-*a*]pyridin-2-yl)-*N*,*N*-dimethylpyridin-3-amine; **DPP2**, 3-(4-(dimethylamino)phenyl)-1-(pyridin-2-yl)prop-2-yn-1-one; **C2**, (*E*)-3-(4-(dimethylamino)phenyl)-1-(pyridin-2-yl)prop-2-en-1-one; **P2**, 3-(4-(dimethylamino)phenyl)-1-(pyridin-2-yl)propan-1-one; **PA2**, *N*-(4-(dimethylamino)phenyl) picolinamide.

template to design new molecules for targeting and controlling metal–Aβ interactions. A hydroxy group was incorporated into the **IMPY** framework to produce **K0** (Figure 1.6b) which could bind Cu(II) and modulate Cu(II)-triggered Aβ aggregation *in vitro*.[102] For the second generation of compounds, the metal chelation site was modified from an N,O donor atom site to an N,N donor atom site by incorporating a single N donor atom into the **IMPY** structure, generating **K2**.[157] These compounds were able to moderately regulate Cu(II)- and Zn(II)-mediated Aβ aggregate formation and disassembly.[157]

The compound **DPP2** (Figure 1.6c) was generated by the installation of an N donor atom into a proposed Aβ imaging agent based on a diphenylpropynone framework.[158] The N,O donor atom metal binding site of **DPP2** could bind Cu(II) with high nanomolar K_d, control both metal-free and metal-induced Aβ aggregation, and disaggregate preformed aggregates. Moreover, **DPP2** has the potential to cross the BBB passively, as confirmed by an *in vitro* assay.[158] The application of **DPP2**, however, was limited by its low micromolar cytotoxicity, possibly due to the carbonyl-triple bond moiety acting as a Michael acceptor which could react with biomolecules forming covalent adducts.[158,159] Thus, **DPP2** was recently structurally modified to ameliorate its cytotoxicity while maintaining BBB permeability.[159] The triple bond of **DPP2** was reduced to a double or single bond, to generate new compounds, **C2** and **P2** (Figure 1.6c), respectively. In addition, **PA2** (Figure 1.6c) was designed by replacing the 2-methylpyridine in **L2-b** (Figure 1.6a) with the 2-pyridyl ketone from **DPP2** (Figure 1.6c). All of these derivatives maintained **DPP2**'s BBB permeability; noticeably, their reactivity with metal-free Aβ and metal–Aβ species was altered.[159] The diminished reactivity of **P2** and **C2**, compared with **DPP2**, is believed to stem from increased flexibility of the overall structure. In contrast to **DPP2** and **C2** which could modulate metal-free as well as metal–Aβ aggregation, **PA2** was only able to modulate the aggregation of metal–Aβ species. Structural modification of **DPP2** was shown to reduce cytotoxicity.[159] **C2** with a double bond was slightly less cytotoxic than **DPP2**; complete removal of an unsaturated bond in **P2** and **PA2** demonstrated the greatest reduction in cytotoxicity.[159] In all of the above Aβ imaging agent-based molecules, maintaining the dimethylamino group in the frameworks proved important for activity. This highlights the value of selecting and retaining key structural groups and backbones from molecules known to interact with Aβ for the design of new compounds to target and modulate metal–Aβ species.[102,156,157,159,160]

1.3.3. Other relevant compounds

Pyridine-based compounds have been developed to interrogate metal–Aβ interactions in AD (*vide infra*). Specifically, **ENDIP** (N^1,N^2-bis(pyridin-2-ylmethyl)ethane-1,2-diamine) (Figure 1.7), a tetradentate ligand, has demonstrated its ability to modulate

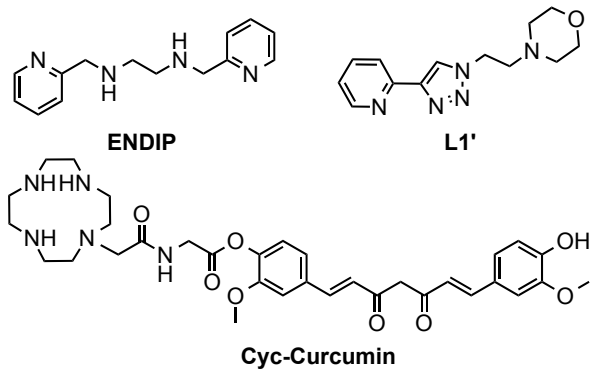

Figure 1.7. Structures of pyridine- and cyclen-based ligands. **ENDIP**, N^1,N^2-bis(pyridin-2-ylmethyl)ethane-1,2-diamine; **L1'**, 4-(2-(4-(pyridin-2-yl)-1H-1,2,3-triazol-1-yl)ethyl)morpholine; and **cyc-curcumin**, 4-((1E,6E)-7-(4-hydroxy-3-methoxyphenyl)-3,5-dioxohepta-1,6-dienyl)-2-methoxyphenyl (2-(1,4,7,10-tetraazacyclododecan-1-yl)acetyl)glycinate.

Cu(II)- and Zn(II)-induced Aβ aggregation by chelating the metal from Aβ.[161] The binding affinities of this ligand (K_d, about 10^{-12} M for Cu(II); about 10^{-7} M for Zn(II)) are also appropriate for interaction with metal–Aβ species rather than other metalloproteins present in the brain.[71,161] Compound **L1'** (Figure 1.7) also contains a pyridyl group, along with a triazole moiety, to manipulate metal–Aβ interactions.[162] **L1'** was shown to influence Cu(II)- and Zn(II)-mediated Aβ aggregation *in vitro.*[162] These data suggest that pyridine moieties could be utilized for the development of small molecules for the regulation of metal–protein interactions, if optimized for specific protein targets (*vide infra*).

Derivatives of cyclam and cyclen (K_d, approximately 10^{-28} and 10^{-23} M for Cu(II), respectively)[163,164] are also of interest in the design of agents to target metal–Aβ species and modulate their interaction and reactivity in AD. Initial studies suggested that Co(III)-cyclen (**Co(III)-cyc**) complexes were able to proteolytically cleave Aβ by hydrolysis of amide bonds.[165] This finding has led to the construction of **cyc-KLVFF** and **cyc-curcumin** (Figure 1.7), two synthetic analogs of Aβ targeting molecules produced through the linkage approach.[163] KLVFF is the self-recognition motif in Aβ.[163] This compound could coordinate Cu(II) and disrupt Cu–Aβ aggregates *in vitro* as well as cleave Aβ oligomers.[163] **Cyc-curcumin** has shown a similar ability to modulate Cu-induced aggregation and proteolytically cleave Aβ; however, it has been neither as potent nor as stable under aqueous conditions as **cyc-KLVFF**. One drawback to the use of cyclen and cyclam are their high binding affinities for Cu(II) and Zn(II), which may

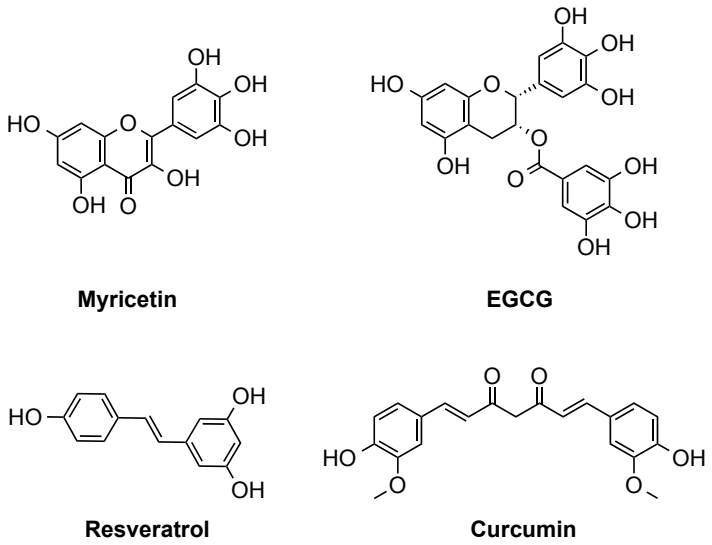

Figure 1.8. Structures of selected, naturally occurring compounds. **Myricetin**, 3,5,7-trihydroxy-2-(3,4,5-trihydroxyphenyl)-4-chromenone; **EGCG**, [(2*R*,3*R*)-5,7-dihydroxy-2-(3,4,5-trihydroxyphenyl)chroman-3-yl] 3,4,5-trihydroxybenzoate; **resveratrol**, 3,4',5-trihydroxy-trans-stilbene; **curcumin**, (1*E*,6*E*)-1,7-bis-(4-hydroxy-3-methoxyphenyl)-1,6-heptadiene-3,5-dione.

allow them to perturb metalloproteins nonspecifically and further disrupt metal ion homeostasis (*vide supra*). These results, however, lend support to the potential of covalently linked small molecules and peptides to target and mediate metal–protein interactions in neurodegenerative diseases.[163]

1.3.4. Naturally occurring molecules

Naturally occurring compounds (in particular, polyphenolic compounds) have also been investigated for their ability to probe and influence metal–protein interactions in neurodegenerative diseases.[43,81] A polyphenolic flavonoid, myricetin (Figure 1.8), was studied by Lim and co-workers.[166] **Myricetin** was observed to influence metal-induced Aβ aggregation to a greater extent than metal-free Aβ aggregation *in vitro*, as well as diminish toxicity related to metal–Aβ species, proposing a possible use in AD research and treatment.[166] The polyphenolic compound from green tea, epigallocatechin-3-gallate (**EGCG**; Figure 1.8), has been studied to understand and treat numerous diseases, including AD (*vide infra*). **EGCG** could lower Aβ-related neurotoxicity and generate non-toxic Aβ oligomers under both metal-free and metal-present conditions.[167-169] The molecular mechanisms of these effects toward Aβ and metal–Aβ were recently investigated using biochemical and biophysical methods.[170] **EGCG** could form

complexes with metal-free Aβ as well as metal-associated Aβ, showing compaction of Aβ conformations.[170,171]

Another polyphenol, **resveratrol** (Figure 1.8), a plant-derived antioxidant, is of particular interest in the study of metal–Aβ species. Conflicting reports on the effects of resveratrol on Aβ aggregation have been made, and these discrepancies arise from the different methodologies employed in sample preparation.[172-174] Based on these studies, no significant alteration in Cu(II)-associated Aβ aggregation by **resveratrol** has been shown.[172] Studies have indicated, however, that **resveratrol** could be a potent antioxidant against ROS generated by Cu(I/II)–Aβ and Fe(II/III)–Aβ, suggesting that further investigations on this framework are warranted.[172]

Additionally, **curcumin** (Figure 1.8), a naturally occurring curcuminoid found in turmeric, has been studied for its ability to interact with metal–protein complexes found in neurodegenerative diseases.[175-177] **Curcumin** has antioxidative, anti-inflammatory, and anti-microbial properties similar to other natural products used as possible therapeutic agents for multiple neurodegenerative diseases.[176] **Curcumin** is also shown to interact with metal–Aβ species.[176,177] It has an approximately micromolar and nanomolar K_d values for Cu(II) and Aβ, respectively.[177,178] These properties allow it to alter the aggregation pathway of Aβ in the presence of metal ions and, at low concentrations, scavenge ROS generated by metal ions.[179] Owing to its poor solubility and bioavailability as well as its instability in aqueous media, structural modifications are needed to improve the viability of this framework prior to further use as a chemical tool or in therapeutic applications.[175]

1.4. Methods to study the ability of small molecules to mediate the aberrant interaction of metal ions and proteins

There are many different methods to analyze and characterize the ability of small molecules discussed above to mediate the interaction of metal ions and proteins involved in AD. In the following sections, the techniques employed in this thesis to determine and describe the activity of these molecules to modulate the metal-free and metal-induced aggregation of proteins, mediation of oxidative stress, and alleviation of

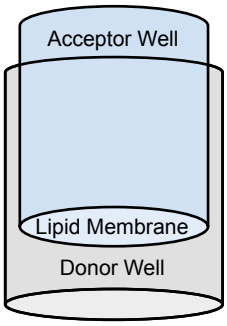

Figure 1.9. Illustration of the 'sandwiched' wells of the PAMPA-BBB assay. Compound in the donor well diffuses across a lipid membrane in the acceptor well. After a set amount of time the concentration of the compound in both wells is determined and used to calculate its permeability value ($\log P_e$).

toxicity are outlined. Additionally, techniques to understand the molecular level interactions between the compounds described herein and metal-free and metalated proteins are discussed along with methods used to characterize physical properties, such as BBB permeability and metal binding.

1.4.1. Techniques for determining blood brain barrier permeability

As BBB permeability is an important feature it should be one of the first design features considered. In addition to using calculated logBB values and Lipiniski's rules to determine possible blood brain barrier permeability, as previously discussed, other *in vitro* and *in vivo* methods were employed herein. The parallel artificial membrane permeability assay adapted for the blood brain barrier (PAMPA-BBB) is a common assay for determining ability to passively diffuse across the blood brain barrier.[180-182] This assay simulates the blood brain barrier using a porcine brain lipid-soaked membrane (Figure 1.9). The diffusion of a compound across this membrane from a buffer that contains the molecule (donor well) to a new buffer (acceptor well) is measured and $\log P_e$ values are calculated using the following 'two-way flux' equation: $C_A(t) = M/(V_D + V_A) + (C_A(0) - M/(V_D + V_A))e^{-PeA(1/VD + 1/VA)t}$ where $C_A(t)$ is the concentration of the compound in the acceptor well at time t, M is the total amount of compound in the system, V_D is the volume of donor well, V_A is the volume of the acceptor well, $C_A(0)$ is the concentration of the compound in the acceptor well at the beginning of the experiment, P_e is the effective artificial-membrane permeability, and A is the area of the membrane.[180-182]

Another factor for BBB permeability that needs to be considered is the charge of the compound, since neutral molecules typically passively diffuse across the BBB more readily.[119,183] pK_a values and thus the charge at physiological pH (7.4) can be obtained through multiple methods,[184] however, variable pH titrations, monitored by UV-Vis, were employed here. This method was chosen as it is very sensitive and does not require for high concentrations of compound (> 10^{-6} M).[184] To obtain pK_a values, the assumption that each species has different UV-Vis spectra is made and special software is typically employed to fit the spectral data.[184,185]

While calculations and *in vitro* methods are useful to screen for passive diffusion across the BBB, measuring uptake of a compound *in vivo* is required to confirm BBB permeability due to the complexity of the BBB and the *in vivo* environment.[186] In principle, these studies are straight forward: the amount of compound in the brain is determined after a one time dose.[186] The animal model utilized, however, must be carefully considered as different phenotypes may result in varied BBB permeabilities.[187,188] Thus, CD1 mice are typically employed for these studies as their heterozygosity is similar to wild mice and humans.[188]

1.4.2. Strategies for studying the interaction of compounds with metal ions, proteins, and metal–protein complexes

The ability of the molecules to interact with metal ions can be explored by observing changes in the UV-Vis spectra of the molecules upon addition of metal ions. More detailed studies, however, are required to determine the K_d values and the stoichiometry of the metal complexes at physiological pH. UV-Vis variable pH titration studies can be carried out on compounds that are stable in the presence of metal ions and their K_d estimated by utilizing the concentrations of unchelated metal in the solution at a given pH (pM = $-\log[M_{unchelated}]$).[102,158,189,190]

To observe the molecular level interactions between molecules, proteins, and metal–protein complexes, mass spectrometry (MS) and nuclear magnetic resonance spectroscopy (NMR) can be employed (*vide infra*). MS can be used to observe monomeric up to soluble oligomeric forms of aggregated proteins and their complexes with compounds.[191-195] This typically requires using nano electrospray ionization (nESI)

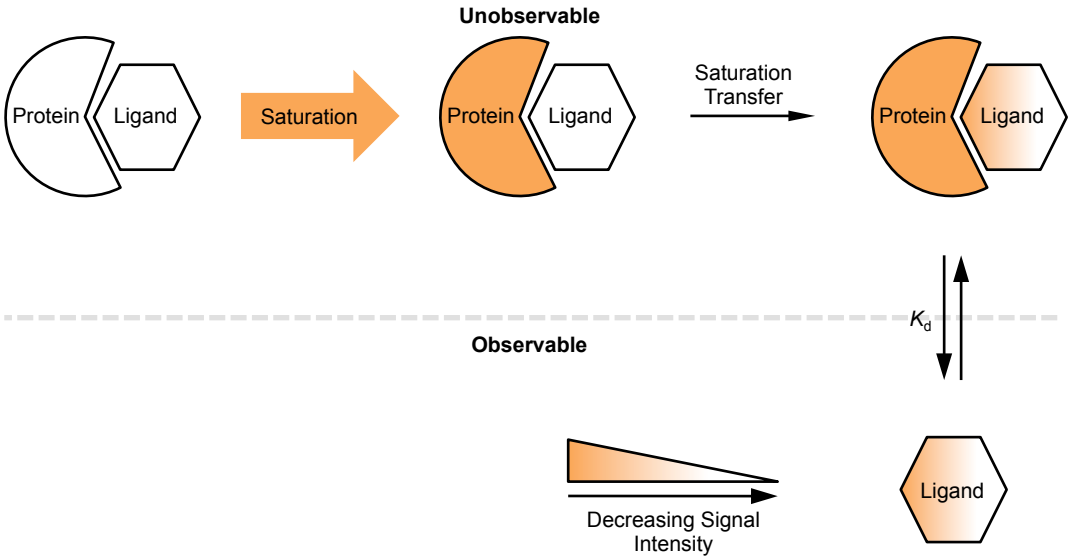

Figure 1.10. Schematic representation of the basic principles of STD NMR. The protein is selectively magnetically saturated (represented by orange color) and the saturation is then transferred to the bound ligand. The disassociation of the saturated ligand before relaxation gives rise to the STD signal, which is proportional in intensity to the previous proximity of ligand atoms to the protein.

which allows for the use of small sample volumes (1-3 μL of nanomolar to micromolar solutions) and is less sensitive to salts present in buffer.[196,197] Most importantly, nESI is also a very soft method of ionization allowing for the observation of relatively weak, biologically relevant non-covalent interactions.[196,197]

In addition to being able to identify the species and stoichiometry of the molecule binding, ion mobility MS (IM-MS) methods can be utilized to provide structural information on the resulting protein–ligand and metal–protein–ligand complexes.[191,195,198,199] IM-MS measures the transit time of ions in a chamber pressurized an inert gas under the influence of a weak electric field which is dependent on their ion-neutral collisional cross section (CCS).[191,195,198,199] Thus IM-MS can be used to study if the compound of interest causes structural changes to the protein.[170,195]

NMR can also be employed to study the molecular level interactions between molecules and multiple metal-free protein and metal–protein forms depending on the methods used. 2D $^{1}H–^{15}N$ band-selective optimized flip-angle short transient heteronuclear multiple quantum coherence (SOFAST-HMQC) NMR can be used to observe changes in the spectra of a ^{15}N-backbone-labeled protein upon titration of a compound.[200,201] These changes result from the interactions of the molecule with

specific residues and if the $^{1}H–^{15}N$ cross-peaks are assigned for the protein, their binding site can be determined.[202,203] Additionally, the reappearance, partial reappearance, or change in signal corresponding to residues involved in metal binding can also give information on the compound's interaction with the metal ion component of the metal–protein complex.[156,204]

Another NMR method, saturation transfer difference (STD), can also be employed to study the interaction of small molecules with proteins in the absence and presence of metal ions.[201,205] STD NMR produces an atomic-level map of the compound's atoms that are in contact with the protein species of interest allowing for the determination of moieties that are important for interaction.[205-207] This is achieved by exploiting the dynamics of ligand binding (Figure 1.10).[205-207] Since the noncovalent binding of a compound with a protein and metal–protein species is labile, the protein is magnetically saturated and when the ligand binds the saturation is transferred to the compound. If the saturated molecule disassociates before relaxing, signal is produced proportional to the previous proximity of the ligand atoms to the protein or metal–protein complex.[205-207] Furthermore, unlike SOFAST-HMQC NMR, which requires the target of interest to be soluble during the experiment, this method can be used to study the interaction of compounds with aggregated forms.[201]

1.4.3. Systems for exploring the metal-induced protein aggregation

The classical methods of measuring the aggregation of amyloidogenic proteins are to use **ThT** (Figure 1.4) or turbidity assays to measure the progression of aggregation.[116,117,128,208] These assays, however, can be significantly interfered with in the presence of small molecules and their metal complexes when their absorbance overlap with the assay (λ_{ex} = *ca.* 440 nm, λ_{em} = 490 nm for **ThT**; *ca*. 350−450 nm for turbidity).[128] Additionally, many metal ions are known to quench the fluorescence of a fluorophore like **ThT**, further limiting the application of this assay when studying metal-induced protein aggregation.[209-211] Thus, other methods outlined below were employed for this work.

Gel electrophoresis can separate protein aggregates based on size, charge, and molecular weight.[212,213] When paired with Western blotting (gel electrophoresis/Western

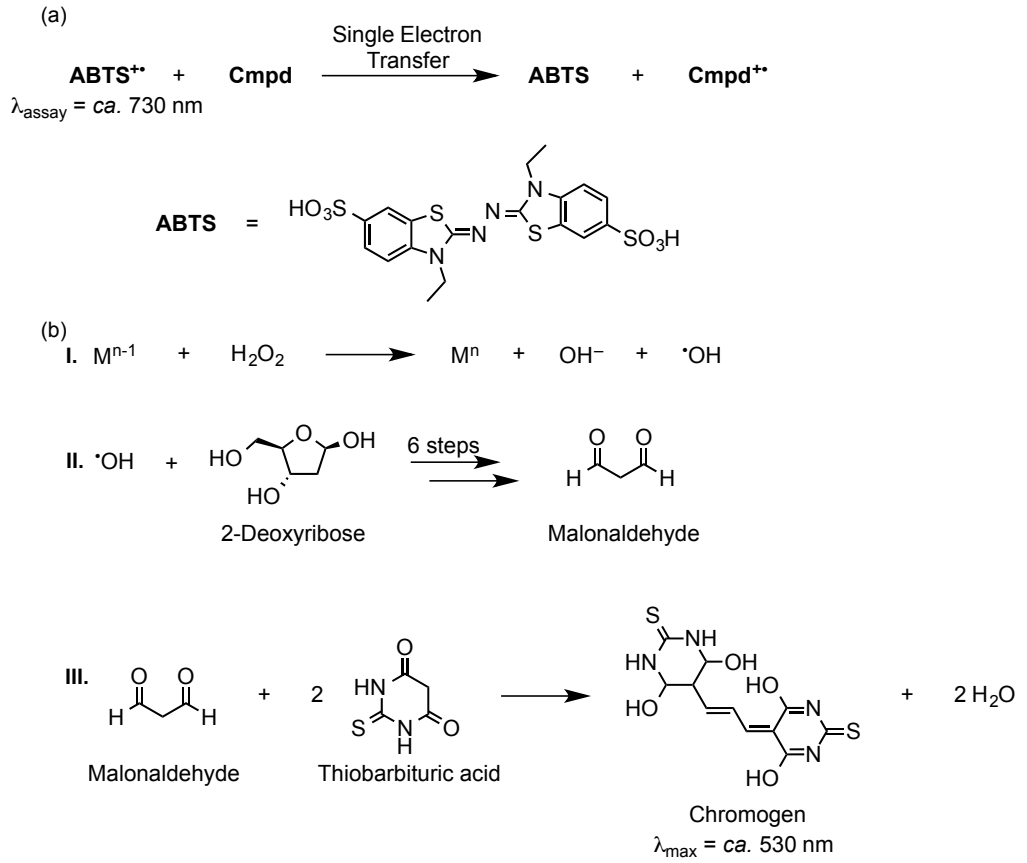

Figure 1.11. Schemes of the mechanisms of antioxidant assays. (a) The ABTS assay depends on the quenching of the **ABTS** cationic radical (**ABTS**$^{+\bullet}$) by a single electron transfer from the compound (**Cmpd**) being studied. **ABTS** = 2,2'-azino-bis(3-ethylbenzothiazoline-6-sulfonic acid. (b) In the deoxyribose assay, I. reduced redox active metal ions (M^{n-1}) oxidize in the presence of hydrogen peroxide (H_2O_2) to produce hydroxyl molecules and hydroxyl radicals. II. Hydroxyl radicals then react with and degrade 2-deoxyribose to form malonaldehyde in six steps. III. After a set time interval, excess thiobarbituric acid is added and reacted with the malonaldehyde formed in the previous step producing a chromogen with a strong absorbance at *ca.* 530 nm and water.

blotting) this method can provide information on the distribution of species present in solution. Gel electrophoresis/Western blotting is limited, however. This method cannot provide any information of the type of species present (*e.g.*, amorphous, oligomeric, and fibrillar) and it is only able detect forms that can penetrate into the gels.[213]

Thus, other methods are required to better study the ability of small molecules to modulate the aggregation of metal–protein complexes. Dot blots with conformation specific antibodies such as A11[214] and OC[215] can provide identification of specific forms of aggregates.[213,216] A11 can identify oligomeric forms which are believed to be particularly toxic while OC can identify aggregates having a fibrillar structure.[213-215]

An additional method of studying the aggregates present in solution is to identify the morphology visually using microscopy techniques, such as transmission electron microscopy (TEM).[208,217] Using this technique, structures can be classified as fibrils, protofibrils, or amorphous aggregates.[217,218] Comparing morphologies produced after treatment with the compound can provide a more complete understanding of the effect of small molecules on the larger aggregates of metal–protein species.

1.4.4. Approaches for studying the ability of compounds to mediate oxidative stress

There are many assays for determining the ability to mediate oxidative stress.[219-222] Careful selection of the correct assay is required in order to obtain meaningful results from these experiments. A particularly important point to consider is the compound's mechanism of modulating oxidative stress as most of the assays are mechanism specific. In the following chapters, the Trolox Equivalent Antioxidant Capacity (TEAC) and deoxyribose assays are employed to characterize the ability of the molecules studied to reduce oxidative stress.

The TEAC assay measures the ability of a compound to neutralize the organic radical of ABTS compared to Trolox, a water soluble vitamin E analog. This method was chosen as it can be used for molecules that undergo electron transfer mechanisms to scavenge radicals and can be monitored at a wavelength which does not interfere with the compounds studied (λ_{assay} = *ca.* 730 nm; Figure 1.11a).[219,223,224] Additionally, this experiment is robust and can be ran in a variety of solvents including solutions which can simulate the complexity of biological environments such as cell lysates.[201,221]

The ability to reduce oxidative stress from Fenton-like chemistry (Figure 1.2) can be studied using the deoxyribose assay.[201,221] In this assay, the ability of a compound to prevent the production of or scavenge hydroxy radicals (•OH) generated by a redox active metal (typically, Cu(I/II) or Fe(II/III)) through Fenton-like chemistry in the presence of hydrogen peroxide can be determined.[225-227] This is measured by reacting thiobarbituric acid with the malonaldehyde (MDA) produced from the oxidation of 2-deoxyribose by •OH producing a chromogen (λ_{max} = *ca.* 530 nm; Figure 1.11b).[226]

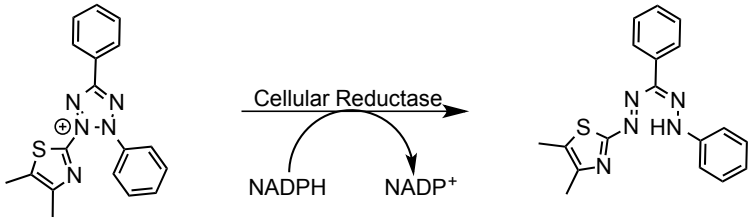

Figure 1.12. Scheme of **MTT** reduction in living cells exploited by the MTT assay. **MTT** is reduced by an NADPH-dependent cellular reductase to produce the highly colored **MTT Formazan**. **MTT** = 3-(4,5-dimethylthiazol-2-yl)-2,5-diphenyltetrazolium; **MTT Formazan** = 1-(4,5-Dimethylthiazol-2-yl)-3,5-diphenylformazan.

1.4.5. Experiments for determining the ability to relieve metal-protein complex cytotoxicity

Cytotoxicity is typically determined by measuring cell viability in the presence of the metal–protein complex of interest. Cell types employed should reflect the disease of interest and cell viability can be determined through a variety of methods.[228,229] Studies employed here utilize mouse and human neuroblastoma cell lines as well as primary neuron cultures taken from fetal wild type mice. These experiments utilize the popular MTT assay which monitors the production of a strongly colored formazan (λ_{max} = *ca.* 600 nm) generated by the reduction of **MTT** is classically believed to happen in the mitochondria, however, there is evidence which suggests the reduction can occur in the cytoplasm as well (Figure 1.12).[228,230] This reduction is NADPH dependent, thus it only can occur in living cells.[228,230] The absorbance values of treated cells are compared to control cells that were not exposed to metal−protein complexes or compound to determine the percent cell viability.[228]

1.5. Conclusions

Neurodegenerative diseases have been the focus of intense research recently, especially given their broad impact on public health. The complex and relatively unknown etiology of many of these illnesses and the relative lack of diagnostic and treatment methodologies make progress of paramount importance. It has been well established that metal ion dyshomeostasis and subsequent interaction between metal ions and proteins are two of a number of common factors in a variety of neurological

diseases, including AD. Research efforts have striven to develop selective ligands and probes to target and mediate or interrupt the metal–protein interactions which are suggested to promote toxic protein aggregation in AD. The current understanding of the specific interactions between metal ions and proteins that can contribute to the onset and/or progression of neurodegenerative diseases has resulted in the design of molecules that target these potentially pathological metal–protein interactions. Several of these frameworks have shown initial promise as chemical tools to provide insights into the relationship between metal–protein interactions and pathogenesis in neurodegenerative diseases. Clarification of the link between metal ions, misfolded proteins, and neurodegeneration could lead to the design of compounds with more promising therapeutic qualities in the future.

1.6. Scope of thesis

As described above, multiple small molecules have been developed that can target and mediate aberrant metal–protein interactions to varying degrees. In this thesis, studies are carried out to better understand how small molecules interact with and mediate the formation of aggregates, oxidative stress, and cell death (reactivity) caused by the formation of metal–protein complexes. This better understanding of the activity of these molecules is then used to design new compounds that have different abilities to mediate metal-free and metal-induced abnormal protein *reactivity*.

In Chapter 2, the ability to control metal–Aβ reactivity by **L2-b** is explored in detail using more in depth *in vitro* experiments as well as utilizing an *in vivo* animal model of AD. Building off of the promising results from Chapter 2, Chapter 3 explores the activity of several compounds based on the same stilbene framework as **L2-b** that have small structural differences and provides an understanding of their mode of action. Chapter 4 utilizes the molecular level knowledge of the activity of the stilbene derivatives from Chapter 3 to design a series of molecules with differing activities. Additionally, in Appendices 1 and 2, new molecules are designed based off of a diazo form of the same stilbene derivative as **L2-b** and a 1,2,3-triazole Aβ imaging agent, respectively, and their abilities to mediate Aβ and metal–Aβ reactivity are evaluated.

Overall, the small molecules designed and studied as a part of this thesis demonstrate that a more complete understanding of the mode of actions behind their activity can allow for the development of chemical tools with targeted abilities to mediate metal-free protein and metal-induced protein aggregation, oxidative stress, and toxicity. The ability to generate a chemical toolbox of molecules that can target and modulate misfolded proteins and their metalated counterparts *in vivo* could lead to better comprehension of their roles in the pathogenesis of neurodegenerative diseases. This increased knowledge could eventually lead to the development of effective interventions to treat these devastating diseases.

1.7. References

(1) Bush, A. I. *Curr. Opin. Chem. Biol*. **2000**, *4*, 184.
(2) Burdette, S. C.; Lippard, S. J. *Proc. Natl. Acad. Sci. U.S.A.* **2003**, *100* 3605.
(3) Kandel, E. R.; Schwartz, J. H.; Jessell, T. M.; Siegelbaum, S. A.; Hudspeth, A. J. *Principles of Neural Science*, 5th ed.; McGraw-Hill Professional: New York, NY, 2012.
(4) Gerhardsson, L.; Lundh, T.; Minthon, L.; Londos, E. *Dement. Geriatr. Cogn. Disord.* **2008**, *25*, 508.
(5) Frederickson, C. J.; Koh, J. Y.; Bush, A. I. *Nat. Rev. Neurosci.* **2005**, *6*, 449.
(6) Frederickson, C. J.; Bush, A. I. *BioMetals* **2001**, *14*, 353.
(7) Li, Y. V.; Hough, C. J.; Sarvey, J. M. *Sci. STKE* **2003**, *182*, pe19.
(8) Frederickson, C. *Sci. STKE* **2003**, *182*, pe18.
(9) Kay, A. R. *Trends Neurosci.* **2006**, *29*, 200.
(10) Lovell, M. A.; Robertson, J. D.; Teesdale, W. J.; Markesbery, W. R. *J. Neurol. Sci.* **1998,** *158*, 47.
(11) Que, E. L.; Domaille, D. W.; Chang, C. J. *Chem. Rev.* **2008**, *108*, 1517.
(12) Lippard, S. J.; Berg, J. M. *Principles of Bioinorganic Chemistry*; University Science Books: Mill Valley, CA, 1994.
(13) Gray, H. B.; Stiefel, E. I.; Valentine, J. S.; Bertini, I. *Biological Inorganic Chemistry: Structure and Reactivity*; University Science Books: Sausalito, CA, 2006.
(14) Slutsky, I.; Abumaria, N.; Wu, L.-J.; Huang, C.; Zhang, L.; Li, B.; Zhao, X.; Govindarajan, A.; Zhao, M.-G.; Zhuo, M.; Tonegawa, S.; Lui, G. *Neuron* **2010**, *65*, 165.
(15) Leal, S. S.; Botelho, H. M.; Gomes, C. M. *Coord. Chem. Rev.* **2012**, *256*, 2253.
(16) Bowman, A. B.; Kwakye, G. F.; Herrero Hernández, E.; Aschner, M. *J. Trace Elem. Med. Biol.* **2011**, *25*, 191.
(17) Zheng, W.; Monnot, A. D. *Pharmacol. Ther.* **2012**, *133*, 177.
(18) Ayton, S.; Lei, P.; Bush, A. I. *Free Radical Biol. Med.* **2013**, *65*, 76.
(19) Frederickson, C. J. *Int. Rev. Neurobiol.* **1989**, *31*, 145.
(20) Levenson, C. W.; Tassabehji, N. M. In *Handbook of Neurochemistry and Molecular Neurobiology*, 3rd ed., Lajtha, A.; Reith, M. E. A. Eds. Springer: New York, NY, 2007, pp. 257.
(21) Kambe, T.; Yamaguchi-Iwai, Y.; Sasaki, R.; Nagao, M. *Cell. Mol. Life Sci.* **2004**, *61*, 49.
(22) Assaf, S. Y.; Chung, S. H *Nature* **1984**, *308*, 734.
(23) Howell, G. A.; Welch, M. G.; Frederickson, C. J. *Nature* **1984**, *308*, 736.
(24) Li, Y.; Hough, C. J.; Suh, S. W.; Sarvey, J. M.; Frederickson, C. J. *J. Neurophysiol.* **2001**, *86*, 2597.
(25) Sensi, S. L.; Canzoniero, L. M. T.; Yu, S. P.; Ying, H. S.; Koh, J.-Y.; Kierchner, G. A.; Choi, D. W. *J. Neurosci.* **1997**, *17*, 9554.
(26) Connor, J. R.; Menzies, S. L. *J. Neurol. Sci.* **1995**, *134*, 33.
(27) Hill, J. M.; Switzer, R. C. III *Neuroscience* **1984**, *11*, 595.
(28) Jefferies, W. A.; Brandon, M. R.; Hunt, S. V.; Williams, A. F.; Gatter, K. C.; Mason, D. Y. *Nature* **1984**, *312*, 162.
(29) Fiedler, A.; Reinert, T.; Morawski, M.; Brückner, G.; Arendt, T; Butz, T. *Nucl.*

Instrum. Methods Phys. Res., Sect. B **2007**, *260*, 153.
(30) Kepp, K. P. *Chem. Rev.* **2012**, *112*, 5193.
(31) Viles, J. H. *Coord. Chem. Rev.* **2012**, *256*, 2271.
(32) Savelieff, M. G.; Lee, S.; Liu, Y.; Lim, M. H. *ACS Chem. Biol.* **2013**, *8*, 856.
(33) Outten, F. W.; Twining, B. S. In *Wiley Encyclopedia of Chemical Biology*; John Wiley & Sons, Inc.: Hoboken, NJ, 2008, pp. 1
(34) Bleackley, M. R.; Macgillivray, R. T. *BioMetals* **2012**, *24*, 785.
(35) Kosman, D. J. *J. Biol. Chem.* **2010**, *285*, 26729.
(36) Schade, A. L.; Caroline, L. *Science* **1946**, *104*, 340.
(37) Connor, J. R., Boeshore, K. L., Benkovic, S. A.; Menzies, S. L. *J. Neurosci. Res.* **1994**, *37*, 461.
(38) Barnham, K. J.; Bush, A.I. *Curr. Opin. Chem. Biol.* **2008**, *12*, 222.
(39) Greenough, M. A.; Camakaris, J.; Bush, A. I. *Neurochem. Int.* **2013**, *62*, 540.
(40) Rivera-Mancía, S.; Pérez-Neri, I.; Ríos, C.; Tristán-López, L.; Rivera-Espinosa; L.; Montes, S. *Chem. Biol. Interact.* **2010**, *186*, 184.
(41) Tamano, H.; Takeda, A. *Metallomics* **2011**, *3*, 656.
(42) Faller, P.; Hureau, C.; Berthoumieu, O. *Inorg. Chem.* **2013**, *52*, 12193.
(43) DeToma, A. S.; Salamekh, S.; Ramamoorthy, A.; Lim, M. H. *Chem. Soc. Rev*. **2012**, *41*, 608.
(44) Rauk, A. *Chem. Soc. Rev.* **2009**, *38,* 2698.
(45) Pithadia, A. S.; Lim, M. H. *Curr. Opin. Chem. Biol.* **2012**, *16*, 67.
(46) Molina-Holgado, F.; Hider, R. C.; Gaeta, A.; Williams, R.; Francis, P. *BioMetals* **2007**, *20*, 639.
(47) Reddy, P. H. *J. Biomed. Biotechnol*. **2006**, *2006*, 31372.
(48) Adam-Vizi, V. *Antioxid. Redox Sign.* **2005**, *7*, 1140.
(49) Huang, X.; Atwood, C.S.; Hartshorn, M.A.; Multhaup, G.; Goldstein, L. E.; Scarpa, R. C.; Cuajungco, M. P.; Gray, D. N.; Lim, J.; Moir, R. D.; Tanzi, R. E.; Bush, A. I.; *Biochemistry* **1999**, *38*, 7609.
(50) Koppenol, W. H. *Redox Rep.* **2001**, *6*, 229.
(51) Wardman, P.; Candeias, L. P. *Radiat. Res.* **1996**, *145*, 523.
(52) Briner, W. *Oxid. Med. Cell. Longev.* **2012**, *2012*, 981561.
(53) Nicholls, P. *Arch. Biochem. Biophys.* **2012**, 525, 95.
(54) Lushchak, V. I. *J. Amino Acids* **2012**, 2012, 736837.
(55) Atamna, H.; Boyle, K. *Proc. Natl. Acad. Sci. U.S.A.* **2006**, *103*, 3381.
(56) Mounsey, R. B.; Teismann, P. *Int. J. Cell Biol*. **2012**, *2012*, 983245.
(57) Bisaglia, M.; Tessari, I.; Mammi, S.; Bubacco, L. *Neuromol. Med.* **2009**, *11*, 239.
(58) Valentine, J. S.; Doucette, P. A.; Potter, S. Z. *Annu. Rev. Biochem.* **2005**, *74*, 563.
(59) Alzheimer's Association, *Alzheimers Dement.* **2012**, *8*, 131.
(60) Jakob-Roetne, R.; Jacobsen, H. *Angew. Chem. Int. Ed.* **2009**, *48*, 3030.
(61) Rauk, A. *Dalton Trans.*, **2008**, *2008*, 1273.
(62) Mayeux, R. *N. Engl. J. Med.*, **2010**, *362*, 2194.
(63) Biran, Y.; Masters, C. L.; Barnham, K. J.; Bush, A. I.; Adlard, P. A. *J. Cell. Mol. Med.* **2009**, *13*, 61.
(64) Alonso, A. C.; Grundke-Iqbal, I.; Iqbal, K. *Nat. Med.* **1996**, *2*, 783.
(65) Wang, J.-Z.; Xia, Y.-Y.; Grundke-Iqbal, I.; Iqbal, K. *J. Alzheimers Dis.* **2013**, *33*,

S123.
(66) Morris, M.; Maeda, S.; Vossel, K.; Mucke, L. *Neuron* **2011**, *70*, 410.
(67) Köpke, E.; Tung, Y.-C.; Shaikh, S.; del C. Alonso, A.; Iqbal, K.; Grundke-Iqbal, I. *J. Biol. Chem.* **1993**, *268*, 24374.
(68) Schrag, M.; Mueller, C.; Oyoyo, U. *Prog. Neurobiol.* **2011**, *94*, 296.
(69) Alies, B.; Hureau, C.; Faller, P. *Metallomics*, **2013**, *5*, 183.
(70) Telpoukhovskaia, M.A.; Orvig, C. *Chem. Soc. Rev.* **2013**, *42*, 1836.
(71) Faller, P.; Hureau, C. *Dalton Trans.* **2009**, 1080.
(72) Hureau, C. *Coord. Chem. Rev.* **2012**, *256*, 2164.
(73) Feaga, H. A.; Maduka, R. C.; Foster, M. N.; Szalai, V. A. *Inorg. Chem.* **2011**, *50*, 1614.
(74) Alies, B.; Badei, B.; Faller, P.; Hureau, C. *Chem. Eur. J.* **2012** *18*, 1161.
(75) Bousejra-El Garah, F.; Bijani, C.; Coppel, Y.; Faller, P.; Hureau, C. *Inorg. Chem.*, **2011**, *50*, 9024.
(76) Solomonov, I.; Korkotian, E.; Born, B.; Feldman, Y.; Bitler, A; Rahimi, F.; Li, H.; Bitan, G.; Sagi, I. *J. Biol. Chem.* **2012**, *287*, 20555.
(77) Crouch, P. J.; Barnham, K. J. *Acc. Chem. Res.* **2012**, *45*, 1604.
(78) Soragni, A.; Zambelli, B.; Mukrasch, M. D. *Biochemistry* **2008**, *47*, 10841.
(79) Shin, R.-W.; Lee, V. M.-Y.; Trojanowski, J. Q. *J. Neurosci.* **1994**, *14*, 7221.
(80) Yamamoto, A.; Shin, R.-W.; Hasegawa, K.; Naiki, H.; Sato, H.; Yoshimasu, F.; Kitamoto, T. *J. Neurochem.* **2002**, *82*, 1137.
(81) Faller, P.; Hureau, C.; Berthoumieu, O. *Inorg. Chem.* **2013**, *52***,** 12193.
(82) Zhang, H.-Y. *FEBS Lett.* **2005**, *579*, 5260.
(83) Massoud, F.; Léger, G.C. *Can. J. Psychiatry* **2011**, *56*, 579.
(84) Lleó, A. *Curr. Genomics* **2007**, *8*, 550.
(85) Ross, C. A.; Tabrizi, S. J. *Lancet Neurol.*, **2011**, *10*, 83.
(86) Bourassa, M. W.; Miller, L. M. *Metallomics* **2012**, *4*, 721.
(87) Andersen, O. *Chem. Rev.* **1999**, *99*, 2683.
(88) Blanusa, M.; Varnai, V. M.; Piasek, M.; Kostial, K. *Curr. Med. Chem.* **2005**, 12, 2771.
(89) Bolognin, S.; Drago, D.; Messori, L.; Zatta, P. *Med. Res. Rev.* **2009**, *29*, 547.
(90) Olzscha, H.; Schermann, S. M.; Woerner, A. C. *Cell* **2011**, 144, 67.
(91) Born, T.; Kontoghiorghe, C. N.; Spyrou, A.; Kolngaou, A.; Kontoghiorghes, G. J. *Toxicol. Mech. Methods* **2013**, 23, 11.
(92) Huang, X.; Atwood, C. S.; Moir, R. D.; Hartshorn, M. A.; Vonsattel, J.-P.; Tanzi, R. E.; Bush, A. I. *J. Biol. Chem.* **1997**, *272*, 26464.
(93) Atwood, C. S.; Moir, R. D.; Huang, X. *J. Biol. Chem.* **1998**, *273*, 12817.
(94) Liu, Z. D.; Hider, R. C. *Coord. Chem. Rev.* **2002**, *232*, 151.
(95) Schugar, H.; Green, D. E.; Bowen, M. L.; Scott, L. E.; Storr, T.; Böhmerle, K.; Thomas, F.; Allen, D. D.; Lockman, P. R.; Merkel, M.; Thompson, K. H.; Orvig, C. *Angew. Chem. Int. Ed.* **2007**, *46*, 1716.
(96) Bebbington, D.; Monck, N. J. T.; Gaur, S.; Palmer, A. M.; Benwell, K.; Harvey, V.; Malcolm, C. S.; Porter, R. H. P. *J. Med. Chem.* **2000**, *43***,** 2779.
(97) Bebbington, D.; Dawson, C. E.; Gaur, S.; Spencer, J. *Bioorg. Med. Chem. Lett.* **2002**, *12*, 3297.
(98) Ferenci, P. *Aliment. Pharmacol. Ther.* **2004**, *19*, 157.

(99) Li, W.; Ma, K. K. Y.; Sun, W.; Paudel, H. K. *Neurochem. Res.* **1998**, *23*, 1467.
(100) Crapper McLachlan, D. R.; Dalton, A. J.; Kruck, T. P. A.; Bell, M. Y.; Smith, W. L.; Kalow, W.; Andrews, D. F. *Lancet* **1991**, *337*, 1304.
(101) Cherny, R. A.; Barnham, K. J.; Lynch, T.; Volitakis, I.; Li, Q.-X.; McLean, C. A.; Multhaup, G.; Beyreuther, K.; Tanzi, R. E.; Masters, C. L.; Bush, A. I. *J. Struct. Biol.* **2000** *130*, 209.
(102) Hindo, S. S.; Mancino, A. M.; Braymer, J. J.; Liu, Y.; Vivekanandan, S.; Ramamoorthy, A.; Lim, M. H. *J. Am. Chem. Soc.* **2009** *131*, 16663.
(103) Bush, A. I.; Huang, X.; Fairlie, D. P. *Neurobiol. Aging* **1999**, *20*, 335.
(104) Cui, Z.; Lockman, P. R.; Atwood, C. S.; Hsu, C.-H.; Gupte, A.; Allen, D. D.; Mumper, R. J. *Eur. J. Pharm. Biopharm.* **2005**, *59*, 263.
(105) Gaeta, A.; Hider, R. C. *Br. J. Pharmacol.* **2005**, *146*, 1041.
(106) Liu, Z. D.; Hider, R. C. *Med. Res. Rev.* **2002**, *22*, 26.
(107) Budimir, A. *Acta Pharm.* **2011**, *61*, 1.
(108) Scott, L. E.; Orvig, C. *Chem. Rev.* **2009**,*109*, 4885.
(109) Braymer, J. J.; DeToma, A.S.; Choi, J.-S.; Ko, K. S.; Lim, M. H. *Int. J. Alzheimers Dis.* **2011**, *2011*, Article ID 623051.
(110) Ritchie, C. W.; Bush, A. I.; Mackinnon, A.; Macfarlane, S.; Mastwyk, M.; MacGregor, L.; Kier, L.; Cherny, R.; Li, Q.-X.; Tammer, A.; Carrington, D.; Mavors, C.; Beyreuther, K.; Tanzi, R. E.; Masters, C. L. *Arch. Neurol.* **2003**, *60*, 1685.
(111) Rimola, A.; Alí-Torres, J.; Rodríguez-Rodríguez, C.; Poater, J.; Matito, E.; Solà, M.; Sodupe, M. *J. Phys. Chem. A*, **2011**, *115*, 12659.
(112) Martell, A. E. *J. Chem. Educ.*, **1952**, *29*, 270.
(113) Jones, C. J.; Thornback, J. R. In *Medicinal Applications of Coordination Chemistry*; Royal Society of Chemistry: Cambridge, England, 2007, pp. 324.
(114) Andersen, O.; Aaseth, J. *Environ. Health Perspect.* **2002**, *110*, 887.
(115) Stains, C. I.; Mondal, K.; Ghosh, I. *ChemMedChem* **2007**, *2*,1674.
(116) LeVine, H. III *Methods Enzymol.* **1999**, *309*, 274.
(117) LeVine, H. III *Protein Sci.* **1993**, *2*, 404.
(118) Yona, R. L.; Mazeres, S.; Faller, P.; Gras, E. *ChemMedChem* **2008**, *3*, 63.
(119) Clark, D.E. *Annu. Rep. Med. Chem.*, **2005**, *40*, 403.
(120) Rodríguez-Rodríguez, C.; Rimola, A.; Alí-Torres, J.; Sodupe, M.; González-Duatre, P. *J. Comput. Aided Mol. Des.* **2011**, *25*, 21.
(121) Clark, D.E.; Pickett, S.D. *Drug Discov. Today* **2000**, *5*, 49.
(122) Gabathuler, R. *Neurobiol. Dis.* **2010**, *37*, 48.
(123) Scott, L.E.; Telpoukhovskaia, M.; Rodríguez-Rodríguez, C.; Merkel, M.; Bowen, M. L.; Page, B. D. G.; Green, D. E.; Storr, T.; Thomas, F.; Allen, D. D.; Lockman, P. R.; Patrick, B. O.; Adam, M. J.; Orvig, C. *Chem. Sci.* **2011**, *2*, 642.
(124) Liu, G.; Men, P.; Kudo, W.; Perry, G.; Smith, M. A. *Neurosci. Lett.* **2009**, *455*, 187.
(125) Collin, G.; Höke, H. In *Ullman's Encyclopedia of Industrial Chemistry*; Wiley-VCH Verlag GmbH: Weinheim, Germany, 2000; pp. 1.
(126) Pierre, J.-L.; Baret, P.; Serratrice, G. *Curr. Med. Chem.* **2003**, *10*, 1077.
(127) Bareggi, S. R.; Cornelli, U. *CNS Neurosci. Ther.* **2012**, *18*, 41.
(128) Mancino, A. M.; Hindo, S. S.; Kochi, A.; Lim, M. H. *Inorg. Chem.* **2009**, *48*, 9596.

(129) Mao, X.; Schimmer, A. D. *Toxicol. Lett.* **2008**, *182*, 1.
(130) Di Vaira, M.; Bazzicalupi, C.; Orioli, P.; Messori, L.; Bruni, B. Zatta, P. *Inorg. Chem.* **2004**, *43*, 3795.
(131) Jenagaratnam, L.; McShane, R. *Cochrane Database Syst. Rev.* **2006**, CD005380.
(132) Cherny, R. A.; Atwood, C. S.; Xilinas, M. E.; Gray, D. N.; Jones, W. D.; McLean, C. A.; Barnham, K. J.; Volitakis, I.; Fraser, F. W.; Kim, Y.-S.; Huang, X.; Goldstein, L. E.; Moir, R. D.; Lim, J. T.; Beyreuther, K.; Zheng, H.; Tanzi, R. E.; Masters, C. L.; Bush, A. I. *Neuron* **2001**, *30*, 665.
(133) Ferrada, E.; Arancibia, V.; Loeb, B.; Norambuena, E.; Olea-Azar, C.; Huidobro-Toro, J. P. *Neurotoxicology* **2007**, *28*, 445.
(134) Bush, A. I.; Tanzi, R. E. *Neurotherapeutics* **2008,** 5, 421.
(135) Raman, B.; Ban, T.; Yamaguchi, K.; Sakai, M.; Kawai, T.; Naiki, H.; Goto, Y. *J. Biol. Chem.* **2005**, *280*, 16157.
(136) Tardiff, D. F.; Tucci, M. L.; Caldwell, K. A.; Caldwell, G. A.; Lindquest, S. *J. Biol. Chem.* **2012**, *287*, 4107.
(137) Doraiswamy, P. M.; Finefrock, A. E. *Lancet Neurol.* **2004**, *3*, 431.
(138) Sampson, E. L.; Jenagaratnam, L.; McShane, R. *Cochrane Database Syst. Rev.* **2012**, CD005380.
(139) Dickens, M. G.; Franz, K. J.; *ChemBioChem*, **2010**, *11*, 59.
(140) Relkin, N. R. *Lancet Neurol.* **2008**, *7*, 762.
(141) *CINAPS Compound Dossier: 'Clioquinol'*; National Institute of Neurological Disorders and Stroke: 2009.
(142) Filiz, G.; Caragounis, A.; Bica, L.; Du, T.; Masters, C. L.; Crouch, P. J; White, A. R. *Int. J. Biochem. Cell Biol.* **2008**, *40*, 1030.
(143) Adlard, P. A.; Cherny, R. A.; Finkelstein, D. I.; Gautier, E.; Robb, E.; Cortes, M.; Volitakis, I.; Liu, X.; Smith, J. P.; Perez, K.; Laughton, K.; Li, Q.-X.; Charman, S. A.; Nicolazzo, J. A.; Wilkins, S.; Deleva, K.; Lynch, T.; Kok, G.; Ritchie, C. W.; Tanzi, R. E.; Cappai, R.; Masters, C. L.; Barnham, K. J.; Bush, A. I. *Neuron* **2008**, 59, 43.
(144) Cherny, R. A.; Ayton, S.; Finkelstein, D. I.; Bush, A. I.; McColl, G. *J. Huntington's Dis.* **2012**, *2012*, 211.
(145) Faux, N. G.; Ritchie, C. W.; Gunn, A.; Rembach, A.; Tsatsanis, A.; Bedo, J.; Harrison, J.; Lannfelt, L.; Blennow, K.; Zetterberg, H.; Ingelsson, M.; Masters, C. L.; Rudolph, E. T.; Cummings, J. L.; Herd, C. M.; Bush, A. I. *J. Alzheimers Dis.* **2010**, *20*, 509.
(146) Lannfelt, L.; Blennow, K.; Zetterberg, H.; Batsman, S.; Ames, D.; Harrison, J.; Masters, C. L.; Targum, S.; Bush, A. I.; Murdoch, R.; Wilson, J.; Ritchie, C. W *Lancet Neurol.* **2008**, *7*, 779.
(147) Hureau, C.; Sasaki, I.; Gras, E.; Faller, P. *ChemBioChem* **2010**, *11*, 950.
(148) Dedeoglu, A.; Cormier, K.; Payton, S.; Tseitlin, K. A.; Kremsky, J. N.; Lai, L.; Li, X.; Moir, R. D.; Tanzi, R. E.; Bush, A. I.; Kowall, N. W.; Rogers, J. T.; Huang, X. *Exp. Gerontol.* **2010**, *39*, 1641.
(149) Wang, Q.; Zhang, X.; Chen, S.; Zhang, X.; Zhang, S.; Youdium, M. Le, W. *Neurodegener. Dis.* **2011**, 8, 310.
(150) Sharma, A. K.; Pavlova, S. T.; Kim, J.; Finkelstein, D.; Hawco, N. J.; Rath, N. P.;

Kim, J.; Mirica, L. M. *J. Am. Chem. Soc.* **2012**, *134*, 6625.
(151) Rodríguez-Rodríguez, C.; Sánchez de Groot, N.; Rimola, A.; Álvarez-Larena, Á.; Lloveras, V.; Videl-Gancedo, J.; Ventura, S.; Vendrell, J.; Sodupe, M.; González-Duarte, P. *J. Am. Chem. Soc.* **2009**, *131*, 1436.
(152) Kung, H. F.; Lee, C.-W.; Zhuang, Z.-P.; Kung, M.-P.; Hou, C.; Plössl, K. *J. Am. Chem. Soc.* **2001** *123*, 12740.
(153) Ono, M.; Wilson, A.; Nobrega, J.; Westaway, D.; Verhoeff, P.; Zhuang, Z.-P.; Kung, M. P.; Kung, H. F. *Nucl. Med. Biol.* **2003**, *30*, 565.
(154) Zhang, W.; Oya, S.; Kung, M.-P.; Hou, C.; Maier, D. L.; Kung, H. F. *Nucl. Med. Biol.* **2005**, *32*, 799.
(155) Braymer, J. J.; Choi, J-S.; DeToma, A. S.; Wang, C.; Nam, K.; Kampf, J. W.; Ramamoorthy, A.; Lim, M. H. *Inorg. Chem.* **2011**, *50*, 10724.
(156) Choi, J.-S.; Braymer, J. J.; Nanga, R. P. R.; Ramamoorthy, A.; Lim, M. H. *Proc. Natl. Acad. Sci. U.S.A.* **2010**, *107*, 21990.
(157) Choi, J.-S.; Braymer, J. J.; Park, S. K.; Mustafa, S.; Chae, J.; Lim, M. H. *Metallomics* **2011**, *3*, 284.
(158) Pithadia, A. S.; Kochi, A.; Soper, M. T.; Beck, M. W.; Liu, Y.; Lee, S.; DeToma, A. S.; Ruotolo, B. T.; Lim, M. H. *Inorg. Chem.* **2012**, 51, 12959.
(159) Liu, Y.; Kochi, A.; Pithadia, A. S.; Lee, S.; Nam, Y.; Beck, M. W.; He, X.; Lee, D.; Lim, M. H. *Inorg. Chem.* **2013**, *52*, 8121.
(160) Li, X.; Jankovic, J.; Le, W. *J. Neural Transm.* **2011**, *118*, 473.
(161) Lakatos, A. Zsigó, É., Hollender, D.; Nagy, N. V.; Fülöp, L.; Simon, D.; Bozsó, Z.; Kiss, T. *Dalton Trans.* **2010**, 1302.
(162) Jones, M. R.; Service, E. L.; Thompson, J. R.; Wang, M. C. P.; Kimsey, I. J.; DeToma, A. S.; Ramamoorthy, A.; Lim, M. H.; Storr, T. *Metallomics* **2012**, *4*, 910.
(163) Wu, W.-H.; Lei, P.; Liu, Q.; Hu, J.; Gunn, A. P.; Chen, M.-S.; Rui, Y.-F.; Su, X.-Y.; Xie, Z.-P.; Zhao, Y.-F; Bush, A. I.; Li, Y.-M *J. Biol. Chem.* **2008**, *283*, 31657.
(164) Lima, L. M. P.; Esteban-Gómez, D.; Delgado, R.; Platas-Iglesias, C.; Tripier, R. *Inorg. Chem.* **2012**, *51*, 6916.
(165) Suh, J.; Yoo, S. H.; Kim, M. G. *et al*. *Angew. Chem. Int. Ed.* **2007**, *46*, 7064.
(166) DeToma, A. S.; Choi, J.-S.; Braymer, J. J.; Lim, M. H. *ChemBioChem* **2011**, *12*, 1198.
(167) Lopez del Amo, J. M.; Fink, U.; Dasari, M.; Grelle, G.; Wanker, E. E.; Bieschke, J.; Reif, B. *J. Mol. Biol.* **2012** *421*, 517.
(168) Bieschke, J.; Russ, J.; Friedrich, R. P.; Ehrnhoefer, D. E.; Wobst, H.; Neugebauer, K.; Wanker, E. E. *Proc. Natl. Acad. Sci. U.S.A.* **2010**, *107*, 7710.
(169) Ehrnhoefer, D. E.; Bieschke, J.; Boeddrich, A.; Herbst, M.; Masino, L.; Lurz, R.; Engemann, S.; Pastore, A.; Wanker, E. E. *Nat. Struct. Mol. Biol.* **2008**, *15*, 558.
(170) Hyung, S.-J.; DeToma, A. S.; Brender, J. R.; Lee, S.; Vivekanandan, S.; Kochi, A.; Choi, J.-S.; Ramamoorthy, A.; Ruotolo, B. T.; Lim, M. H. *Proc. Natl. Acad. Sci. U.S.A.* **2013**, *110*, 3743.
(171) Zhang, B.; Cheng, X. R.; daSilva, I. S.; Hung, V. W. S.; Veloso, A. J.; Angnes, L.; Kerman, K. *Metallomics* **2013**, *5*, 259.
(172) Granzotto, A.; Zatta, P. *PLoS One* **2011**, *6*, e21565.
(173) Ono, K.; Yoshiike, Y.; Takashima, A.; Hasegawal, K.; Naiki, H.; Yamada, M. *J. Neurochem.* **2003**, *87*, 172.

(174) Rivière, C.; Richard, T.; Quentin, L.; Krisa, S.; Mérillon, J.-M.; Monti, J.-M. *Bioorg. Med. Chem.* **2007**, *15*, 1160.
(175) Anand, P.; Kunnumakkara, A. B.; Newman, R. A.; Aggarwal, B. B. *Mol. Pharm.* **2007**, *4*, 807.
(176) Hatcher, H.; Planalp, R.; Cho, J.; Torti, F. M.; Torti, S. V. *Cell. Mol. Life Sci.* **2008**, *65*, 1631.
(177) Ryu, E. K.; Choe, Y. S.; Lee, K.-H. Choi, Y.; Kim B.-T. *J. Med. Chem.* **2006**, *49*, 6111.
(178) Baum, L.; Ng, A. *J. Alzheimers Dis.* **2004**, *6*, 367.
(179) Huang, H.-C.; Lin, C.-J.; Liu, W.-J.; Jiang, R.-R.; Jiang, Z.-F. *Food Chem. Toxicol.* **2011**, *49*, 1578.
(180) Palm, K.; Luthman, K.; Ros, J.; Gråsjo, J.; Artursson, P. *J. Pharmacol. Exp. Ther.* **1999**, *291*, 435.
(181) Avdeef, A.; Strafford, M.; Block, E.; Balogh, M. P.; Chambliss, W.; Khan, I. *Eur. J. Pharm. Sci.* **2001**, *14*, 271.
(182) Avdeef, A. In *Absorption and Drug Development: Solubility, Permeability, and Charge State*, 2nd ed.; Wiley: Hoboken, New Jersey, 2012; pp. 575
(183) Mikitsh, J. L.; Chacko, A.-M *Perspect. Medicin*. *Chem.* **2014**, *6*, 11.
(184) Babić, S.; Horvat, A. J. M.; Pavlović, D. M.; Kaštelan-Macan, M. *TrAC-Trend Anal. Chem.* **2007**, *26*, 1043.
(185) Gans, P.; Sabatini, A.; Vacca, A. *Ann. Chim.* **1999**, *89*, 45.
(186) Nicolazzo, J. A.; Charman, S. A.; Charman, W. N. *J. Pharm. Pharmacol.* **2006**, *58*, 281.
(187) Banks, W. A. *BBA-Mol. Basis Dis.* **2010**, *1802*, 881.
(188) Rice, M. C.; O'Brien, S. J. *Nature* **1980**, *283*, 157.
(189) Rodríguez-Rodríguez, C., Telpoukhovskaia, M. and Orvig, C. *Coord. Chem. Rev.* **2012**, *256*, 2308.
(190) Braymer, J. J.; Merrill, N. M.; Lim, M. H. *Inorg. Chim. Acta* **2012**, *380*, 261.
(191) Benesch, J. L. P.; Ruotolo, B. T. *Curr. Opin. Struct. Biol.* **2011**, *21*, 641.
(192) Bernstein, S. L.; Dupuis, N. F.; Lazo, N. D.; Wyttenbach, T.; Condron, M. M.; Bitan, G.; Teplow, D. B.; Shea, J.-E.; Ruotolo, B. T.; Robinson, C. V.; Bowers, M. T. *Nat. Chem.* **2009**, *1*, 326.
(193) Hernández, H.; Robinson, C. V. *Nat. Protoc.* **2007**, *2*, 715.
(194) Suzuki, Y.; Brender, J. R.; Soper, M. T.; Krishnamoorthy, J.; Zhou, Y.; Ruotolo, B. T.; Kotov, N. A.; Ramamoorthy, A.; Marsh, E. N. G. *Biochemistry* **2013**, *52*, 1903.
(195) Niu, S.; Rabuck, J. N.; Ruotolo, B. T. *Curr. Opin. Chem. Biol.* **2013**, *17*, 809.
(196) Benesch, J. L. P.; Ruotolo, B. T.; Simmons, D. A.; Robinson, C. V. *Chem. Rev.* **2007**, *107*, 3544.
(197) Karas, M.; Bahr, U.; Dülcks, T. *Fresen. J. Anal. Chem.* **2000**, *366*, 669.
(198) Uetrecht, C.; Rose, R. J.; van Duijn, E.; Lorenzen, K.; Heck, A. J. R. *Chem. Soc. Rev.* **2010**, *39*, 1633.
(199) Verbeck, G. F.; Ruotolo, B. T.; Sawyer, H. A.; Gillig, K. J.; Russell, D. H. *J. Biomol. Tech.* **2002**, *13*, 56.
(200) Schanda, P.; Brutscher, B. *J. Am. Chem. Soc.* **2005**, *127*, 8014.

(201) Lee, S.; Zheng, X.; Krishnamoorthy, J.; Savelieff, M. G.; Park, H. M.; Brender, J. R.; Kim, J. H.; Derrick, J. S.; Kochi, A.; Lee, H. J.; Kim, C.; Ramamoorthy, A.; Bowers, M. T.; Lim, M. H. *J. Am. Chem. Soc.* **2014**, *136*, 299.
(202) Clarkson, J.; Campbell, I. D. *Biochem. Soc. Trans.* **2003**, *31*, 1006.
(203) Ziarek, J. J.; Peterson, F. C.; Lytle, B. L.; Volkman, B. F. *Methods Enzymol.* **2011**, *493*, 241.
(204) Jensen, M. R.; Hass, M. A. S.; Hansen, D. F.; Led, J. J. *Cell. Mol. Life Sci.* **2007**, *64*, 1085.
(205) Mayer, M.; Meyer, B. *J. Am. Chem. Soc.* **2001**, *123*, 6108.
(206) Bhunia, A.; Bhattacharjya, S.; Chatterjee, S. *Drug Discov. Today* **2012**, *17*, 505.
(207) Zartler, E. R.; Mo, H. *Curr. Top. Med. Chem.* **2007**, *7*, 1568.
(208) Nilsson, M. R. *Methods* **2004**, *34*, 151.
(209) Varnes, A. W.; Dodson, R. B.; Wehry, E. L. *J. Am. Chem. Soc.* **1972**, *94*, 946.
(210) Kemlo, J. A.; Shepherd, T. M. *Chem. Phys. Lett.* **1977**, *47*, 158.
(211) Fabbrizzi, L.; Licchelli, M.; Pallavicini, P.; Perotti, A.; Taglietti, A.; Sacchi, D. *Chem. Eur. J.* **1996**, *2*, 75.
(212) Kavoosi, G.; Ardestani, S. K. In *Gel Electrophoresis-Principles and Basics*; Magdeldin, S., Ed.; InTech, Rijeka, Croatia, 2012; pp. 69.
(213) Pryor, N. E.; Moss, M. A.; Hestekin, C. N. *Int. J. Mol. Sci.* **2012**, *13*, 3038.
(214) Kayed, R.; Head, E.; Thompson, J. L.; McIntire, T. M.; Milton, S. C.; Cotman, C. W.; Glabe, C. G. *Science* **2003**, *300*, 486.
(215) Kayed, R.; Head, E.; Sarsoza, F.; Saing, T.; Cotman, C. W.; Necula, M.; Margol, L.; Wu, J.; Breydo, L.; Thompson, J. L.; Rasool, S.; Gurlo, T.; Butler, P.; Glabe, C. G. *Mol. Neurodegener.* **2007**, *2*, 18.
(216) Krishnan, R.; Goodman, J. L.; Mukhopadhyay, S.; Pacheco, C. D.; Lemke, E. A.; Deniz, A. A.; Lindquist, S. *Proc. Natl. Acad. Sci. U.S.A.* **2012**, *109*, 11172.
(217) Tosoni, A.; Barbiano di Belgiojoso, G.; Nebuloni, M. In Amyloidosis-Mechanisms and Prospects for Therapy, Sarantseva, S., Ed.; InTech, Rijeka, Croatia, 2011; pp. 121.
(218) Fändrich, M. *Cell. Mol. Life Sci.* **2007**, *64*, 2066.
(219) Prior, R. L.; Wu, X.; Schaich, K. *J. Agric. Food. Chem.* **2005**, *53*, 4290.
(220) Antolovich, M.; Prenzler, P. D.; Patsalides, E.; McDonald, S.; Robards, K. *Analyst* **2002**, *127*, 183.
(221) Aruoma, O. I. *Mutat. Res.-Fund. Mol. M.* **2003**, *523-524*, 9.
(222) Nile, S. H.; Khobragade, C. N.; Park, S. W. *Mini-Rev. Med. Chem.* **2012**, *12*, 1007.
(223) Tang, Y.-Z.; Liu, Z.-Q. *J. Am. Oil Chem. Soc.* **2007**, *84*, 1095.
(224) Re, R.; Pellegrini, N.; Proteggente, A.; Pannala, A.; Yang, M.; Rice-Evans, C. *Free Radic. Biol. Med.* **1999**, *26*, 1231.
(225) Gutteridge, J. M. C.; Halliwell, B. *Biochem. J.* **1988**, *253*, 932.
(226) Halliwell, B.; Gutteridge, J. M. C.; Aruoma, O. I. *Anal. Biochem.* **1987**, *165*, 215.
(227) Gutteridge, J. M. C. *FEBS Letters* **1981**, *128*, 343.
(228) Riss, T. L.; Moravec, R. A.; Niles, A. L.; Benink, H. A.; Worzella, T. J.; Minor, L. In *Assay Guidance Manual*; Sittampalam, G. S., Gal-Edd, N.; Arkin, M.; Auld, D.; Austin, C.; Bejcek, B.; Glicksman, M.; Inglese, J.; Lemmon, V.; Li, Z.; McGee, J.; McManus, O.; Minor, L.; Napper, A.; Riss, T.; Trask, O. J.; Weidner, J. Eds.; Eli

Lilly & Company and the National Center for Advancing Translational Sciences: Bethesda, MD, 2004, http://www.ncbi.nlm.nih.gov/books/NBK144065/
(229) Riss, T. *Cell Notes* **2005**, *13*, 16.
(230) Berridge, M. V.; Tan, A. S. *Arch. Biochem. Biophys*. **1993**, *303*, 474.

Chapter 2
A rationally designed small molecule for identifying an in vivo link between metal-amyloid-β complexes and the pathogenesis of Alzheimer's disease

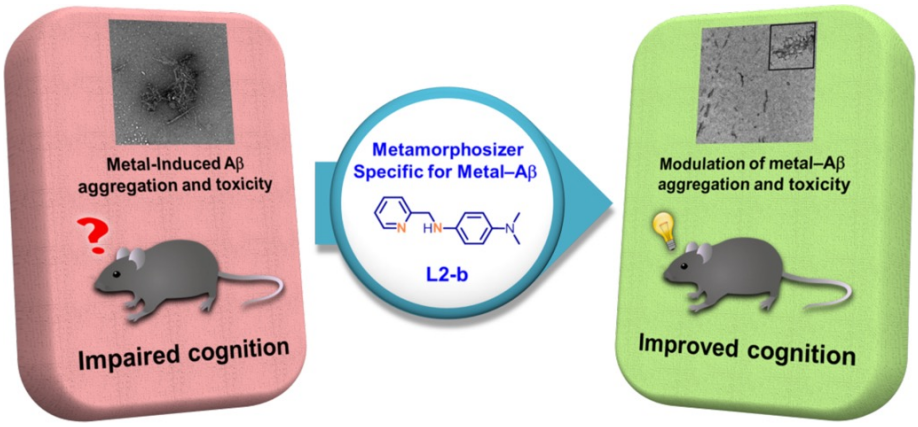

The results presented in this chapter were previously published (Beck, M. W.[‡]; Oh, S. B.[‡]; Kerr, R. A.; Lee, H. J.; Kim, S. H.; Kim, S.; Jang, M.; Ruotolo, B. T.; Lee, J.-Y.; Lim, M. H. Chem. Sci., 2015, 6, 1879. [‡]Equal contribution). I thank Professor Joo-Yong Lee, Shin Bi Oh, So Hee Kim, and Sujeong Kim for the mouse model studies, as well as Professor Brandon Ruotolo and Dr. Richard A. Kerr for the nESI-IM-MS studies. Hyuck Jin Lee obtained TEM images. Milim Jang conducted cell culture and antioxidant experiments. I conducted the Western blot and dot blot investigations of in vitro Aβ aggregation and mainly handled manuscript writing with Professor Lim.

2.1. Introduction

Alzheimer's disease (AD), a progressive neurodegenerative disease, is the most common form of dementia afflicting 24 million people worldwide.[1] Despite AD being the sixth leading cause of death in the United States, there are currently no disease modifying treatments; approved therapies only offer symptomatic relief without having an effect on the underlying pathogenesis.[1,2] Development of effective therapeutics has been hindered by the fact that AD pathogenesis is still poorly understood. Pathologically, AD is characterized by the accumulation of aggregated, misfolded proteins, such as amyloid-β (Aβ) peptides (two major forms exist, $A\beta_{40}$ and $A\beta_{42}$).[3,4] The amyloid cascade hypothesis suggests that Aβ is the causative agent in AD;[5] however, the etiology of AD can be multifactorial; of particular interest is the role of Aβ with other factors (*i.e.*, metals) toward AD development.[4,6-11]

High concentrations of Fe, Cu, and Zn (*ca.* low mM) are found within Aβ deposits in ex vivo tissues from the AD-afflicted brain.[12,13] These metal ions are observed to coordinate to Aβ peptides *in vitro* forming metal–Aβ complexes which could direct toxicity *via* two possible pathways:[4,6-11,14-19] (i) metals could influence the Aβ aggregation pathways leading to the generation and stabilization of toxic Aβ oligomers;[4,7-9,14] (ii) redox active metal ions [*i.e.,* Cu(I/II) and Fe(II/III)] associated with Aβ are shown to produce reactive oxygen species (ROS) under physiological conditions through Fenton-like reactions.[4,6-11,16-19] Overproduction of ROS by metal–Aβ can result in oxidative stress and eventually neuronal death in the AD-affected brain. Although the reactivity of metal–Aβ [*i.e.*, (i) metal–Aβ aggregation (toxic Aβ oligomer formation) and (ii) redox active metal–Aβ-triggered ROS generation, *vide supra*] has been indicated *in vitro*,[4,6-11,14-19] the direct involvement of metal–Aβ complexes in AD pathogenesis *in vivo* is uncertain.

Metal chelating agents have shown that the interference of metal–Aβ interactions as well as the modulation of metal distribution in the brain could lead to an improvement in AD pathology.[4,19-24] 8-Hydroxyquinoline derivatives have been employed to regulate metal-related neurotoxicity in AD; some small molecules, including clioquinol (**CQ**) and **PBT2**, have indicated promising results for possible AD treatment in clinical trials.[4,22,23]

The effects of **CQ** and **PBT2** are mainly from their ability to act as an ionophore to redistribute metal ions in the brain instead of directly disrupting metal–Aβ complexes;[4,19,23-25] thus, these compounds would not be able to directly probe the relation between metal–Aβ complexes and AD pathogenesis. Therefore, chemical tools, termed as metamorphosizers, have been recently developed in order to (i) specifically target metal–Aβ complexes and (ii) alter the interaction between the metal and Aβ, consequently (iii) redirecting the toxic aggregation pathway of metal–Aβ into off-pathway, less toxic unstructured Aβ forms and (iv) reducing metal–Aβ-induced ROS production, which eventually alle*via*tes metal–Aβ-linked toxicity.[4,24]

Herein, we demonstrate that a chemical tool (**L2-b**, Figure 2.1a) stands out as being well suited *in vivo* for identifying the association of metal–$A\beta_{40}$/$A\beta_{42}$ with AD pathogenesis, through *in vitro* biochemical/biophysical/cytotoxicity/metabolism investigations, as well as *in vivo* brain uptake studies. Our *in vivo* tool specifically interacts with metal–Aβ over metal-free Aβ and generates a ternary **L2-b**–metal–Aβ complex causing structural compaction, as validated by mass spectrometry (MS) and ion mobility-mass spectrometry (IM-MS). Most significantly, we present the first report that the control of metal–Aβ interaction and reactivity by an *in vivo* chemical tool mitigates amyloid pathology and improves cognitive deficits in the 5XFAD AD mouse model. This robust AD mouse model develops severe amyloid pathology and cognitive decline at an early age through high expression of three familial mutant types of human amyloid precursor protein (hAPP; Swedish, Florida, and London) and two mutant forms of presenilin (PSEN1; M146L and L286V).[26] Overall, our studies establish strong experimental evidence for an *in vivo* link between metal–Aβ and AD development, implying that targeting metal–Aβ complexes could be an effective strategy for the future development of new therapeutics.

2.2. Results and discussion

2.2.1. Design principle and characterization of a chemical tool for investigating metal–Aβ complexes *in vivo*

L2-b (Figure 2.1a) was designed to target metal–Aβ complexes and modulate heir interaction/reactivity with subsequent reduction of toxicity,[27] in order to determine whether they are connected with AD pathology. For *in vivo* applications, first, chemical tools for this purpose must have specificity toward metal–Aβ complexes in order to limit

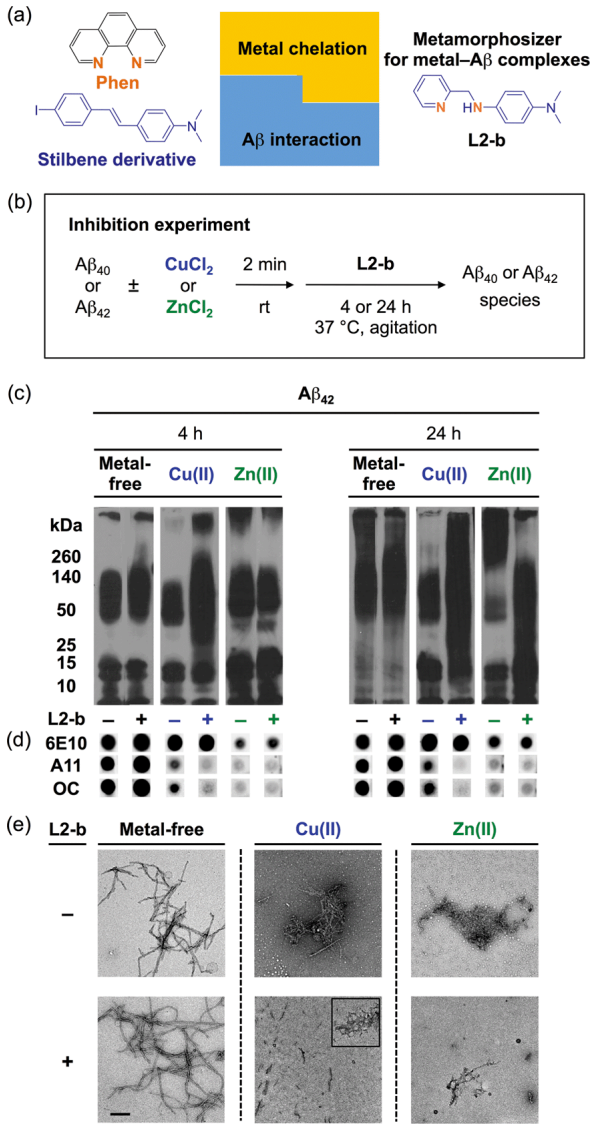

Figure 2.1. Design principle of **L2-b** and its effect on metal-free and metal-induced Aβ aggregation. (a) Design principle of **L2-b**, a metamorphosizer for metal–Aβ complexes: a metal binding site (orange) is incorporated into an Aβ interacting framework (blue). (b) Scheme showing the inhibition experiment: metal-free or metal-treated [$CuCl_2$ (blue) or $ZnCl_2$ (green)] $Aβ_{40}$/$Aβ_{42}$ was incubated with (+) or without (−) **L2-b** for 4 h (left) and 24 h (right). Conditions: [Aβ] = 25 μM; [Cu(II) or Zn(II)] = 25 μM; [**L2-b**] = 50 μM; pH 6.6 (for Cu(II) samples) or pH 7.4 (for metal-free and Zn(II) samples); 37 °C; constant agitation. (c) Analysis of the size distribution of the resultant $Aβ_{42}$ species by gel electrophoresis and Western blotting with an anti-Aβ antibody (6E10). (d) Dot blot analysis of the resulting $Aβ_{42}$ species employing 6E10, an anti-Aβ oligomer antibody (A11), and an anti-Aβ fibril antibody (OC). (e) TEM images of the 24 h incubated samples (scale bar = 200 nm).

the disruption of other metalloproteins.[4,24] This property can be imparted into small molecules by using inorganic chemistry concepts to allow specificity for disease-relevant metal ions (Fe(II/III), Cu(I/II), and Zn(II)), along with limiting the metal binding affinity (K_d) to ≥ 10^{-10} M, and by including structural components for Aβ interaction.[4,24] To satisfy this aspect, **L2-b** (a bidentate ligand; Figure 2.1a) was constructed upon incorporation of two nitrogen donor atoms (for metal chelation) into the structure of an Aβ aggregate imaging agent (stilbene derivative; for Aβ interaction),[28] which could interact with metal–Aβ complexes (Figure 2.1a).[27] **L2-b** is shown to have apparent K_d values of *ca.* 10^{-10} and 10^{-6} M for Cu(II) and Zn(II), respectively, and is relatively selective for Cu(II) over other biologically relevant bivalent ions.[27] Secondly, the blood–brain barrier (BBB) permeability of **L2-b** is critical for applications in the brain, which was first predicted by considering Lipinski's rules of drug-likeness and observing calculated logBB values.[27] Employing CD1 mice, *in vivo* brain uptake studies of **L2-b** newly confirmed its BBB penetration. **L2-b** (*ca.* 250 ng g^{-1}) is observed to be available in the brain when administered by oral gavage (10 mg kg^{-1}) to the mice (Table 2.1). Thirdly, the metabolic stability of **L2-b** for *in vivo* applications was also verified utilizing human liver microsomes. Susceptibility of **L2-b** to metabolism is between 30 min and 120 min indicating that this compound has moderate metabolic stability, suggesting its suitability for use *in vivo*. Lastly, **L2-b** acts as an antioxidant as well as an inhibitor of Cu(I/II)– or Cu(I/II)–Aβ-induced ROS production as presented in previous studies.[27,29] From our newly performed study using the Trolox equivalent antioxidant capacity in a cellular environment [*i.e.*, murine neuroblastoma Neuro-2a (N2a) cell lysates],[30] **L2-b** exhibits a greater free radical scavenging capacity (2.3 ± 0.2) than Trolox (1.0 ± 0.1), a known antioxidant vitamin E analogue. Therefore, **L2-b** is clearly demonstrated to be *via*ble for *in vivo* use as a chemical tool for exploring the association of metal–Aβ complexes with AD pathogenesis.

Table 2.1. Distribution of L2-b in male CD1 mice after its administration by oral gavage.

Brain (ng/g)	CSF (ng/mL)	Plasma (ng/mL)	Brain-to-plasma ratio
253 ± 175	289 ± 126	1347 ± 671	0.19 ± 0.16

2.2.2. Specific modulation of metal-induced over metal-free Aβ aggregation pathways *in vitro*

To elucidate whether **L2-b** could redirect metal–Aβ aggregation into off-pathway amorphous Aβ aggregates, suggested to be less toxic or nontoxic,[31] while leaving metal-free Aβ cases unaffected, inhibition (Figure 2.1b) and disaggregation (Figure 2.2a) experiments[30] were performed employing $A\beta_{40}$ and $A\beta_{42}$, the two main Aβ forms found in the AD-affected brain. The influence of **L2-b** on both metal-free and metal-mediated Aβ aggregation was monitored at short and long incubation time points.[32] Gel electrophoresis and Western blotting (gel/Western blot utilizing an anti-Aβ antibody, 6E10)[30] were conducted to determine the molecular weight (MW) distribution of the

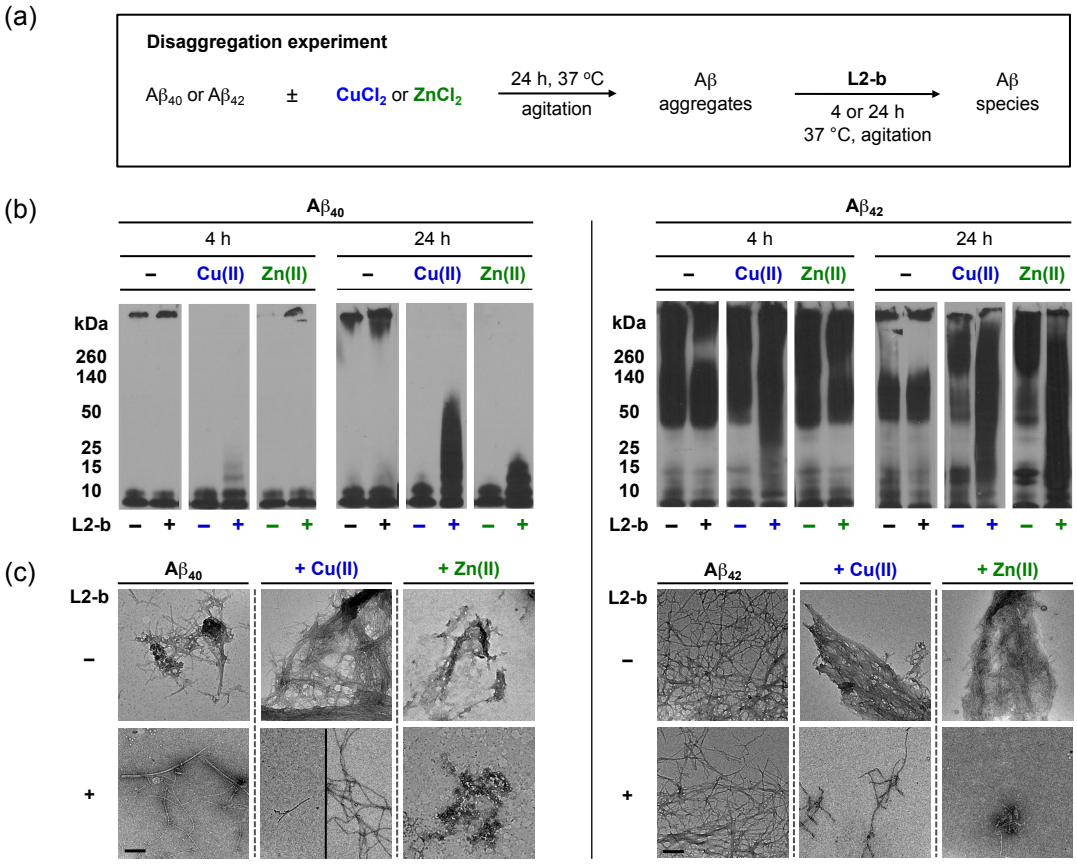

Figure 2.2. Effect of **L2-b** on preformed aggregates of $A\beta_{40}$ and $A\beta_{42}$. (a) Scheme of the disaggregation experiment: $A\beta_{40}$ (left) or $A\beta_{42}$ (right) aggregates, generated by 24 h incubation of peptides with and without $CuCl_2$ (blue) or $ZnCl_2$ (green), were treated with **L2-b** (+) followed by an additional incubation of 4 h or 24 h. Conditions: [Aβ] = 25 μM; [Cu(II) or Zn(II)] = 25 μM; [**L2-b**] = 50 μM; pH 6.6 (for $CuCl_2$ samples) or pH 7.4 (for metal-free and Zn(II) samples); 37 °C; constant agitation. (b) Analysis of the size distribution of the resultant Aβ species by gel electrophoresis and Western blotting with an anti-Aβ antibody (6E10). (c) TEM images of the 24 h incubated samples (scale bar = 200 nm).

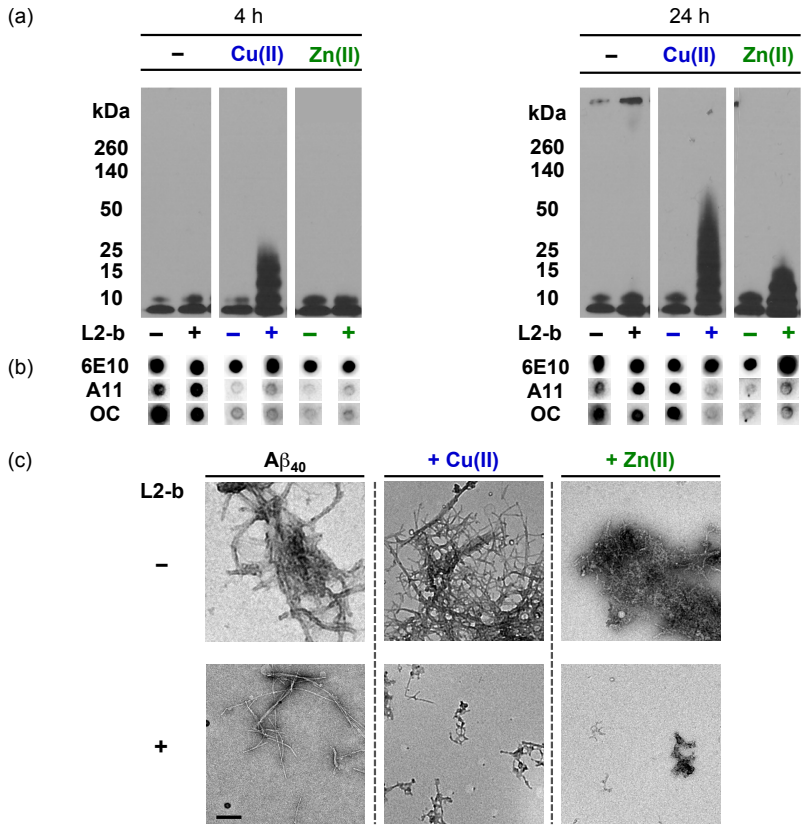

Figure 2.3. Effect of **L2-b** on the formation of metal-free and metal-induced $A\beta_{40}$ aggregation (inhibition experiment). The experimental conditions are described in Figure 2.1b. (a) Analyses of the size distribution of the resultant $A\beta_{40}$ species by gel electrophoresis and Western blotting with an anti-Aβ antibody (6E10). (b) Dot blot analysis of the resulting $A\beta_{40}$ species employing 6E10, an anti-Aβ oligomer antibody (A11), and an anti-Aβ fibril antibody (OC). (c) TEM images of the 24 h incubated samples (scale bar = 200 nm).

resulting Aβ aggregates. Dot blot analysis with an anti-Aβ oligomer antibody A11[33] and an anti-Aβ fibril antibody OC,[34] along with 6E10, was carried out to identify the type of Aβ species produced. Moreover, transmission electron microscopy (TEM) images were taken to visualize the morphologies of the resultant Aβ aggregates.[30]

Both the inhibition and disaggregation experiments indicate that **L2-b** does not modulate the aggregation pathways of both $A\beta_{40}$ and $A\beta_{42}$ under metal-free conditions after either short or long incubation periods. Nearly identical MW distributions of the Aβ species in the absence and presence of **L2-b** were observed in the gel/Western blots (Figures 2.1c, 2.2b, and 2.3a). The dot blots of the inhibition samples indicated A11 (oligomer)- and OC (fibril)-positive aggregates for metal-free $A\beta_{40}$/$A\beta_{42}$ even when

treated with **L2-b** (Figure 2.1d and 2.3b). TEM images revealed that Aβ fibrils were mainly present in both the inhibition and disaggregation experiments of metal-free $A\beta_{40}$/$A\beta_{42}$ with and without **L2-b** after 24 h of incubation (Figures 2.1e, 2.2c, and 2.3c). Thus, metal-free Aβ aggregation is not noticeably influenced upon treatment with **L2-b**.

In contrast to the metal-free conditions, significantly noticeable changes in the metal [Cu(II) or Zn(II)]-induced $A\beta_{40}$ and $A\beta_{42}$ aggregation pathways by **L2-b** were observed compared to **L2-b**-untreated analogues. In both the inhibition and disaggregation experiments, after 24 h of incubation of the Cu(II)–Aβ species with **L2-b**, the resulting peptide species with a wide range of MWs were visualized by gel/Western blot (Figure 2.1c, 2.2b, and 2.3a). In the inhibition studies of both $A\beta_{40}$ and $A\beta_{42}$, as well as in the disaggregation experiment of $A\beta_{42}$, Cu(II)–Aβ samples treated with **L2-b** even for 4 h also exhibited the distinct MW distribution of Aβ (Figures 2.1c, 2.2b, and 2.3a). Distinguishably, **L2-b** was capable of limiting the formation of A11- and OC-positive Cu(II)-induced $A\beta_{40}$/$A\beta_{42}$ aggregates at both short and longer incubation times (Figures 2.1d and 2.3b). Morphologies of **L2-b**-incubated Cu(II)–Aβ, analyzed by TEM, displayed both narrower and shorter fibrils, as well as unstructured Aβ aggregates in the inhibition experiments (Figure 2.1e and 2.3c); while less dense, thinner fibrils were mainly observed in the disaggregation experiments (Fig. 2.2c). In the case of Zn(II)–Aβ, **L2-b** could also transform the aggregation pathways (Figure 2.1c, 2.2b, and 2.3a). The TEM studies revealed **L2-b**-triggered, smaller amorphous Zn(II)–Aβ aggregates in both the inhibition and disaggregation experiments (Figure 2.1e, 2.2c, and 2.3c). Overall, **L2-b** is observed to redirect metal–Aβ aggregation mainly into unstructured Aβ aggregates that are generated *via* the off-pathway aggregation and are known to be less toxic or nontoxic.[31] Thus, **L2-b** could be used as a chemical tool specific for such anti-amyloidogenic activity toward metal–Aβ complexes over metal-free Aβ in this manner.

2.2.3. Formation of structurally-compact complexes with metal–Aβ not metal-free Aβ *in vitro*

In order to explore the specific interaction of **L2-b** with metal–Aβ over metal-free Aβ, nanoelectrospray ionization-MS (nESI-MS) studies were employed (Figure 2.4a).

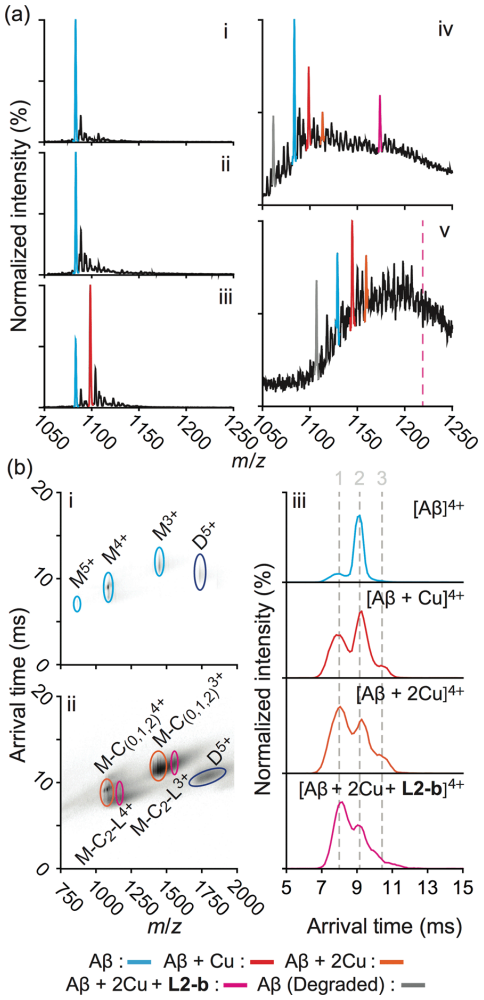

Figure 2.4. Mass spectrometric (MS) and ion mobility-mass spectrometric (IM-MS) analyses of Aβ in the presence of **L2-b** and/or Cu(II). (a) Comparison of incubated Aβ 4+ charge states in the samples containing (i) $A\beta_{40}$ (18 μM) alone and $A\beta_{40}$ co-incubated with (ii) excess **L2-b** (120 μM), (iii) Cu(II) (40 μM), and (iv) both **L2-b** (40 μM) and Cu(II) (40 μM) [(v) $A\beta_{42}$ (pH 9, 18 μM) with **L2-b** (40 μM) and Cu(II) (40 μM) is also presented]. Consistent with data shown here, the gray signal represents a currently unidentified chemical modification of the N-terminus up to, and including, residue 5 (Figure 2.5) but not F4 (Figure 2.6). The projected location of the complex consisting of $A\beta_{42}$, Cu(II), and **L2-b** in a ratio of 1:2:1 is indicated in pink. (b) IM-MS analysis of $A\beta_{40}$ (18 μM) incubated in the (i) absence and (ii) presence of **L2-b** (40 μM) and Cu(II) (40 μM). Extracted arrival time distributions support the existence of three resolvable structural populations [Collision Cross Section (CCS) data, Table 2.2].

When metal-free $A\beta_{40}$ was allowed to react with **L2-b**, no binding events were observed, even with a six fold excess of the ligand (Figure 2.4a(ii)). In comparison, incubating a comparatively smaller concentration of **L2-b** with $A\beta_{40}$ and Cu(II) promoted readily observed levels of complexes containing $A\beta_{40}$, Cu(II), and **L2-b** approximately in the ratio 1:2:1, supporting the metal specific nature of the interaction (Figure 2.4(iv)). The

Table 2.2. Calculated collision cross section (CCS) values* of the 4+ species of $A\beta_{40}$.

Species	Conformation 1 ($Å^2$)	Conformation 2 ($Å^2$)	Conformation 3 ($Å^2$)
$A\beta_{40}$	656.25 ± 29.01	720.35 ± 24.36	782.02 ± 23.86
$A\beta_{40}$ + Cu(II)	663.53 ± 26.70	728.28 ± 29.17	790.08 ± 26.96
$A\beta_{40}$ + 2Cu(II)	664.00 ± 33.33	729.18 ± 24.11	785.98 ± 33.51
$A\beta_{40}$ + 2Cu(II) + **L2-b**	669.26 ± 25.92	722.04 ± 23.77	794.39 ± 47.19

formation of a ternary complex between **L2-b** and Cu(II)–$A\beta_{40}$ is supported by the previously reported NMR studies of **L2-b** with Zn(II)–$A\beta_{40}$ in solution.[27]

Additionally, another MS signal was observed. This signal corresponds to an intact molecular mass of 89.24 Da less than the full-length $A\beta_{40}$ peptide in good agreement with ternary $A\beta_{40}$–Cu(II)–**L2-b** complex formation (gray, Figure 2.4a(iv)). Tandem MS data (Figure 2.5) and subsequent analysis of the fragment ions indicate that this new signal corresponds to a chemical modification within the first five residues of $A\beta_{40}$ ($D_1A_2E_3F_4R_5$). Given a mass measurement error of ±1 Da, and supporting **L2-b** binding experiments performed using an $A\beta_{40}$ F4A sequence variant, as well as acetylated analogs (Figure 2.6), we can eliminate alterations to F4 as a source of the product observed and show that free primary amines are critical for binding and subsequent Aβ degradation. While no direct observations of the Cu(II)–**L2-b**-bound $A\beta_{42}$ form were indicated by MS, the 89.24 Da mass loss product was detected (gray, Figure 2.4a(v)) upon addition of both **L2-b** and Cu(II) to the samples, implying the generation of a transient ternary $A\beta_{42}$–Cu(II)–**L2-b** complex of unknown stoichiometry. These $A\beta_{40}$/$A\beta_{42}$ fragmentation results also suggest that, as expected, Cu(II) likely binds to Aβ proximal to the site of **L2-b** attachment.[4,7] In all cases, neither **L2-b** nor Cu(II) was detected in complex with the identified Aβ degradation product. Detailed structures of these ternary complexes will be the subject of future studies.

To study the molecular level structural dynamics by which **L2-b** redirects metal–Aβ aggregation pathways, IM-MS experiments of the complexes produced were performed.

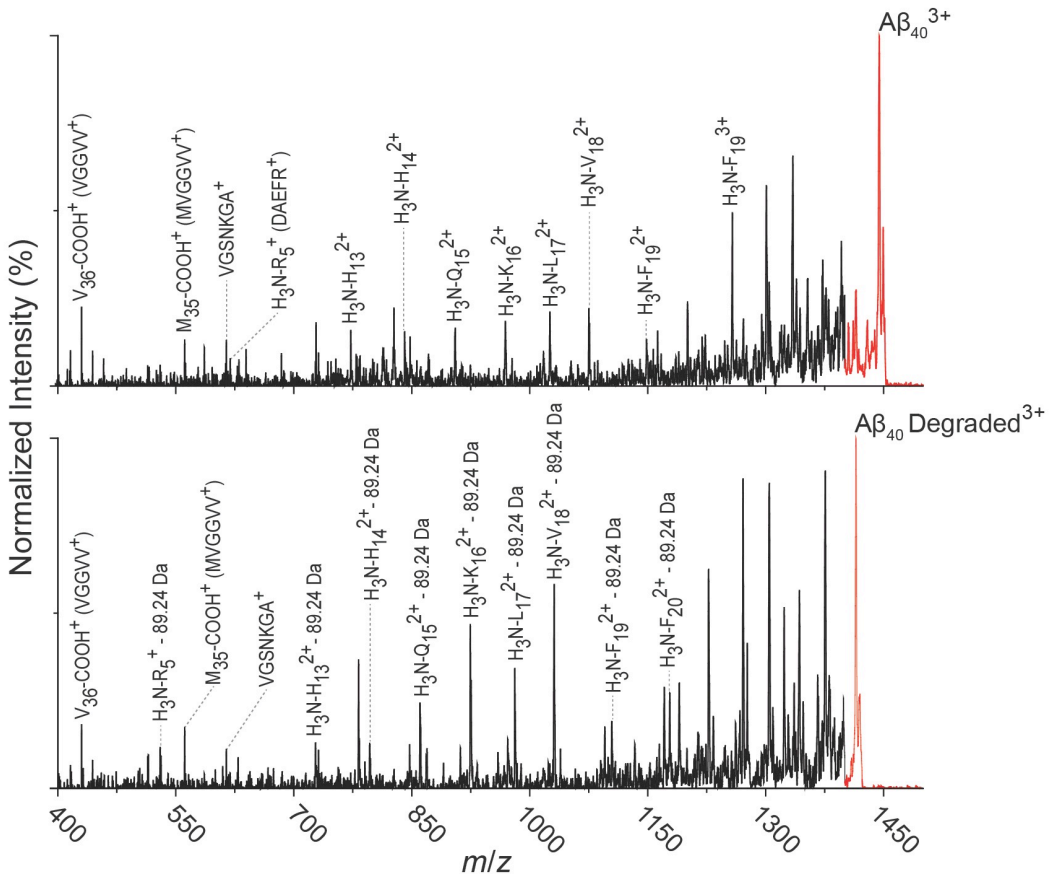

Figure 2.5. Comparison of tandem MS/MS sequencing of Aβ_{40} (top) and the identified Cu(II)–**L2-b**-dependent chemical modification product (bottom), using the quadrupole isolated 3+ charge state (trap collision energy 90 V). These data support that in the presence of both Cu(II) and **L2-b**, the Aβ amino acid sequence is chemically modified at a position between the primary amine on the N-terminus and R5, resulting in a calculated mass shift of 89.24 Da. Aβ_{40} F4A MS data, shown below (Fig. S4), support the conclusion that F4 is not the target of this modification. Spectra depicted in black represent a 5X base signal magnification.

A comparison of the arrival time distributions of the metal-free Aβ_{40} form with the different ligated states supports an increasing level of structural compaction as additional components (*i.e.*, Cu(II) and **L2-b**) associate with Aβ_{40} (Figure 2.4b and Table 2.2). Analyzing the arrival time distributions for all complex states presented, along with the nESI-MS data, our IM-MS investigations demonstrate that **L2-b** is capable of specifically interacting with Cu(II)-bound Aβ over metal-free Aβ, subsequently promoting a high level of structural compaction of the complex. This binding of **L2-b** to metal–Aβ with increased structural compactness could be a key property for the distinguishable reorganization of metal–Aβ aggregation pathways, similar to the previously suggested

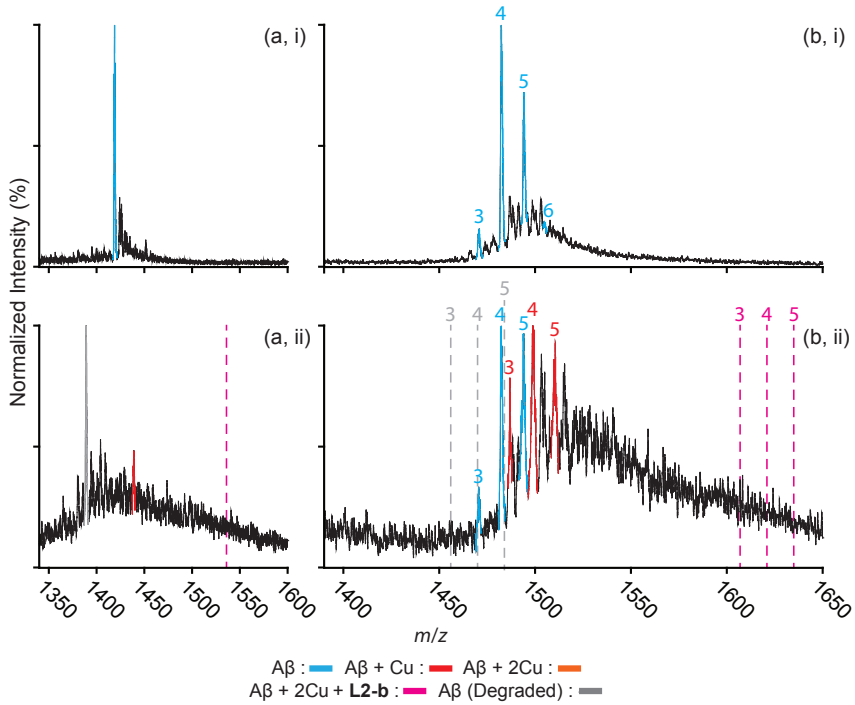

Figure 2.6. MS analyses of $A\beta_{40}$ F4A and acetylated $A\beta_{40}$ in the presence and absence of both **L2-b** and Cu(II). (a) Data for the 4+ charge states of $A\beta_{40}$ F4A (18 μM) incubated with (ii) and without (i), **L2-b** (80 μM) and Cu(II) (40 μM). Data support the conclusion that F4 is not required to promote the **L2-b** and Cu(II) dependent chemical modification observed (gray signal, ii). (b) Data for the 4+ charge states of acetylated $A\beta_{40}$ (18 μM) incubated with (ii) and without (i), **L2-b** (80 μM) and Cu(II) (40 μM). While Cu(II) binding is still observed (red signals, ii), data support the conclusion that at least one $A\beta_{40}$ primary amine is required to stabilize the interaction between $A\beta_{40}$ and **L2-b,** as neither the bound nor chemically modified species is observed (pink dashed lines indicate location of the expected m/z values for bound states). Numerals shown above the MS peaks indicate the number of acetyl modifications detected for a given peak. Mass analysis supports a range of 3 to 6 acetylated primary amines under our experimental conditions (of a possible 6).[35]

molecular level mode of action of EGCG toward metal–Aβ complexes which promotes the generation of nontoxic unstructured aggregates *via* off-pathway aggregation.[24,31]

2.2.4. Targeting and reacting with metal–Aβ complexes in living cells and in the brain of 5XFAD AD mice

The effect of **L2-b** on metal–$A\beta_{40}$/$A\beta_{42}$-induced toxicity was first examined using N2a cells, as an indication of its interaction with metal–Aβ complexes. An increase (*ca.* 10–20%) in cell *via*bility for both $A\beta_{40}$ and $A\beta_{42}$ was displayed upon treatment of cells incubated with Cu(II) or Zn(II), Aβ, and **L2-b** (10 μM each; Figure 2.7). Moving forward, the ability of **L2-b** to penetrate the BBB and interact with metal–Aβ species in the brain

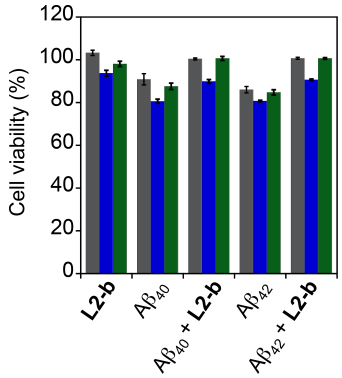

Figure 2.7. Influence of **L2-b** on the cytotoxicity of $A\beta_{40}$ and $A\beta_{42}$ in the absence and presence of metal ions. Viability of cells (%) was determined by the MTT assay in the absence (gray) and presence of $CuCl_2$ (blue) or $ZnCl_2$ (green) and calculated relative to that of cells incubated only with 1% v/v DMSO. Error bars represent the standard de*via*tion from three independent experiments. Conditions: [Aβ] = 10 μM; [Cu(II) or Zn(II)] = 10 μM; [**L2-b**] = 10 μM; 24 h incubation.

was verified in the 5XFAD AD mouse model. Zn(II) found in Aβ plaques was visualized in the brain tissue slices by a fluorophore specific for Zn(II), 6-methoxy-(8-p-toluenesulfonamido)quinolone (**TSQ**; Figure 2.8).[36] Administration of **L2-b** to 5XFAD AD mice intraperitoneally for three weeks on a daily basis starting at the age of three months resulted in drastically diminished fluorescence of **TSQ** in the plaques (arrows shown in Figure 2.8c). Additionally, in the hippocampal mossy fiber terminals, a Zn(II)-rich region in the brain,[37] there was no difference in the fluorescence of **TSQ** between wild type and 5XFAD AD mice treated daily with the vehicle, whereas **L2-b** reduced fluorescence by *ca.* 13% ($P < 0.05$) in 5XFAD AD mice over the same time span (Figure 2.8d). Thus, these *in vivo* studies suggest that **L2-b** is BBB permeable and can enter the brain to interact with intracerebral metals, including those found in Aβ plaques.

2.2.5. Reduction of amyloid pathology in 5XFAD AD mice

To identify the direct involvement of metal–Aβ complexes in amyloid pathology leading to improved cognition, the 5XFAD mouse model of AD[26] was chosen. **L2-b** (1 mg kg^{-1}) was injected into nontransgenic littermates (wild type) and 5XFAD AD mice *via* the intraperitoneal route for three weeks on a daily basis starting at the age of three months. All mice survived the consecutive treatments, which rarely caused changes in body weight (Table 2.3). Necropsy of all major organs in **L2-b**-treated mice revealed no gross changes.

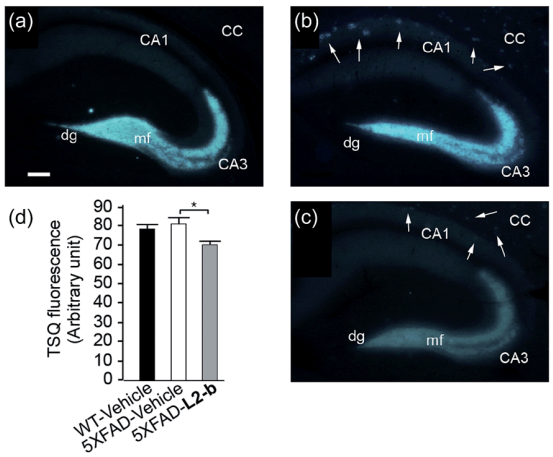

Figure 2.8. Levels of Zn(II) in the brain tissues of nontransgenic wild type (WT) and 5XFAD transgenic mice. Amounts of Zn(II) were determined using a fluorescent dye, 6-methoxy-(8-p-toluenesulfonamido)quinoline (**TSQ**), in the mossy fiber region (mf) of brains from (a) WT and (b and c) 5XFAD transgenic mice after intraperitoneal administration of (a and b) the vehicle or (c) **L2-b** (1 mg per kg per day) for three weeks beginning at three months of age (scale bar = 100 μm). The fluorescence response of **TSQ** was also shown in the zone of amyloid plaques in 5XFAD mice (shown by arrows; b and c). CC, corpus callosum; CA, cornu amonis; dg, dentate gyrus. (d) The fluorescence intensity of **TSQ** was quantified in the mossy fiber region (mf in a–c) of vehicle-treated WT (black bar; n = 6) and 5XFAD male mice (white bar; n = 10), or **L2-b**-treated 5XFAD male mice (gray bar; n = 9), where the measurement was performed using five sagittal sections selected randomly from each animal and denoted as an arbitrary unit of the **TSQ** fluorescence [mean ± standard error of the mean (S.E.M)]. *P < 0.05 by one-way analysis of variance (ANOVA).

The potential association of **L2-b** with amyloid pathology was investigated by first observing the amyloid plaque load in the brain tissue of 5XFAD AD mice. When the brain tissue slices of **L2-b**-administered 5XFAD AD mice were stained with an APP/Aβ specific antibody (4G8) or a compact core amyloid plaque indicator (Congo red), it was found that the amyloid plaque burden was ameliorated (Figure 2.9). Reduction (*ca.* 15%) of both the area of 4G8-immunoreactive deposits and the number of congophilic amyloid plaques was revealed in the cortex of **L2-b**-treated 5XFAD AD mice when compared to vehicle-treated 5XFAD AD mice (Figure 2.9c, f). The changes in the amount of both $A\beta_{40}$ and $A\beta_{42}$ in the brain tissues of 5XFAD AD mice following **L2-b** administration were also assessed. Total amounts of Aβ peptides were analyzed by an enzyme-linked immunosorbent assay (ELISA) in sodium dodecyl sulfate (SDS)- and formic acid (FA)-soluble brain tissue lysates (Figure 2.9a, b and 2.10), as well as oligomeric and fibrillar Aβ aggregates in the phosphate buffered saline (PBS)-soluble fraction (Figure 2.10c, d).[38] Relative to vehicle-treated 5XFAD mice, the **L2-b**-treated 5XFAD mice showed diminished cerebral levels of both $A\beta_{40}$ and $A\beta_{42}$ in all fractions

Table 2.3. Changes in body weight in nontransgenic littermates and 5XFAD mice during the period of vehicle or L2-b treatment.

Treatment	Wild type (WT) Vehicle	5XFAD Vehicle	5XFAD **L2-b**
Number of animals	6	15	16
Day	Body weight (g) on day of treatment*		
1	21.3 ± 0.5	20.5 ± 0.6	20.8 ± 0.4
2	21.8 ± 0.5	20.3 ± 0.6	20.9 ± 0.4
3	21.3 ± 0.6	20.3 ± 0.5	20.6 ± 0.4
7	21.2 ± 0.7	20.4 ± 0.5	20.5 ± 0.5
14	21.3 ± 0.8	20.6 ± 0.5	20.6 ± 0.5
21	22.2 ± 0.7	21.1 ± 0.4	21.1 ± 0.5

mean ± S.E.M.

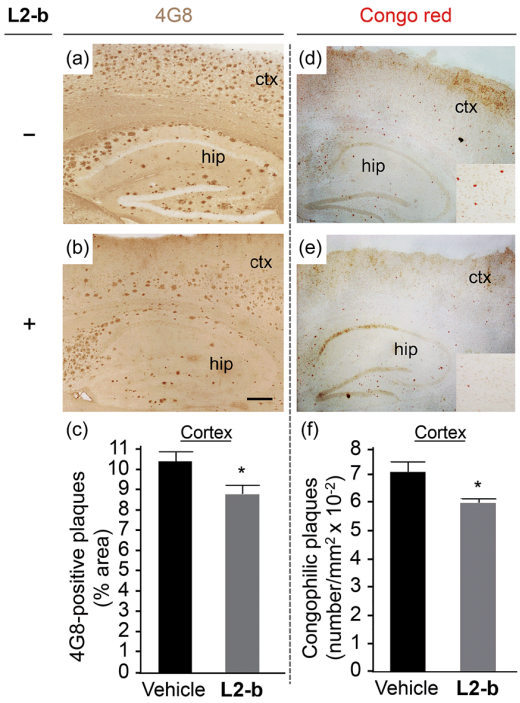

Figure 2.9. Effect of daily treatments with **L2-b** for three weeks on the amyloid deposits in the brains of 5XFAD male mice. Representative microscopic images of (a and b) 4G8-immunostained or (d and e) Congo red stained brain sections of 5XFAD mice, which were given daily (a and d) the vehicle or (b and e) **L2-b** (1 mg per kg per day) *via* intraperitoneal injection for three weeks starting at three months of age (magnification = 40×; scale bar = 100 μm). Inset in (d) and (e): enlarged micrographs of congophilic amyloid plaques in the cortical area (magnification, 400×; hip, hippocampus; ctx, cortex). To evaluate the amyloid pathology of the vehicle (black bars; n = 5)- or **L2-b** (gray bars; n = 7)-treated male 5XFAD mice, (c) the load of 4G8-immunoreactive amyloid deposits and (f) the number of congophilic amyloid plaques in the cortex were measured in five brain sections taken from each animal. *P < 0.05 by one-way ANOVA.

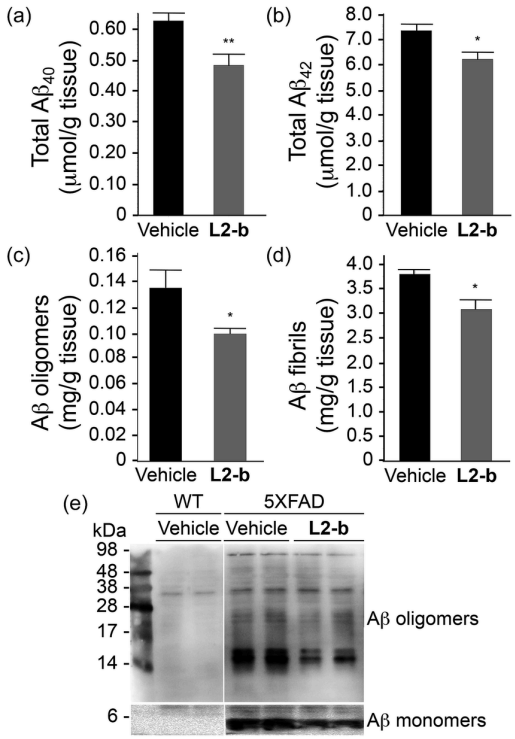

Figure 2.10. Levels of Aβ in whole brain tissues of three-month-old male 5XFAD mice. The amounts of (a) total $A\beta_{40}$, (b) total $A\beta_{42}$, (c) PBS-soluble Aβ oligomers, and (d) Aβ fibrils were assessed using ELISA after three weeks of treatment with vehicle (black bars; n = 5) or **L2-b** (1 mg per kg per day; gray bars; n = 7). Bars denote the levels of Aβ, which were calculated from three independent experiments and expressed as values per gram of tissue. *P < 0.05 or **P < 0.01 by one-way ANOVA. (e) 4–20% (lower panels) and 16.5% (upper panels) tris-glycine gel/Western blot analyses were performed to visualize the Aβ monomers and aggregates, respectively, in the brain tissue lysates of wild type (WT; left panels) and 5XFAD male mice (right panels).

(*ca.* 15–20%, P < 0.05, Figure 10a, b). Oligomeric and fibrillar Aβ species in the PBS fraction were additionally abated by 27% and 15%, respectively (P < 0.05, Figure 2.10c, d). Similarly, the overall reduction of Aβ species was also indicated by gel/Western blot, where Aβ monomers and oligomers were noticeably decreased in brain tissue lysates from **L2-b**-treated 5XFAD AD mice (Figure 2.10e). Together, these studies demonstrate that daily administration of **L2-b** to the AD model mitigates amyloid pathology in AD, including the load of amyloid plaque deposits and the levels of a wide range of conformations from monomers to fibrils.

2.2.6. Cognitive improvement in 5XFAD AD mice

Investigation of behavioral performance was carried out by administering **L2-b** to 5XFAD AD mice which suffer from deficits in learning and memory capabilities as amyloid pathology progresses.[26] The Morris water maze was used to evaluate different

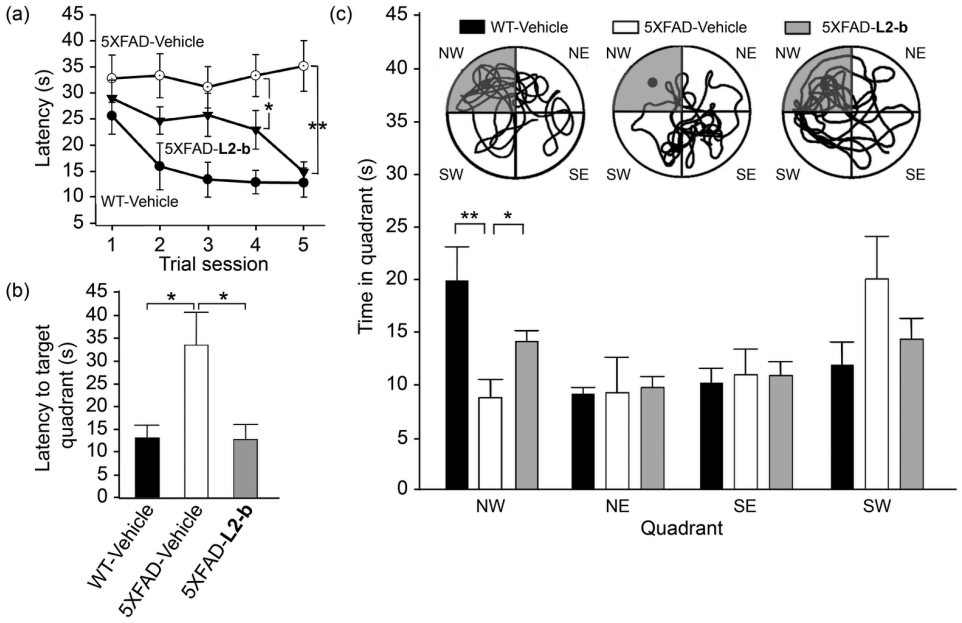

Figure 2.11. Learning and memory abilities of three-month-old male wild type (WT) and 5XFAD male mice treated with vehicle (black and white bars) and **L2-b** (gray), measured using the Morris water maze task. (a) The escape latency time was counted every day during the period of the 21st–25th daily treatments of either vehicle or **L2-b** and the probe trials were performed on the day of the final 25th treatment to measure (b) how quickly the mice reach and (c) how long they spend in the target quadrant (NW, highlighted in gray; circles show images of the representative tracks of the mice in the water maze). **P* < 0.05 or ***P* < 0.01 by one-way ANOVA (n = 6, 13, and 14 for vehicle-treated WT and vehicle-/**L2-b**-treated 5XFAD mice, respectively).

aspects of spatial learning and memory in three-month-old 5XFAD AD mice.[26] The wild type mice, which were consecutively injected with vehicle during the experimental period, normally took shorter times upon repetition of the training trial to find the escape platform, located in the northwest (NW) quadrant (Figure 2.11a and b). In contrast, vehicle-treated 5XFAD AD mice spent longer times searching for and reaching the platform indicating they had difficulties with learning and memory (Figure 2.11).

Administration of **L2-b** to 5XFAD AD mice led to a remarkable improvement in the performance of the task. **L2-b**-treated 5XFAD AD mice were capable of finding the target in a comparable time to the wild type mice displaying significantly better memory and learning abilities than their untreated 5XFAD AD littermates (*P* < 0.05, Figure 2.11a, b). Additionally, **L2-b**-treated 5XFAD AD mice took a more direct and easier path than the vehicle-treated 5XFAD AD mice to search for the platform (*P* < 0.05, Figure 2.11c). Therefore, **L2-b**, a chemical reagent specific for metal–Aβ, ameliorates cognitive defects in the AD mouse model, along with the attenuation of amyloid pathology. These

overall *in vivo* observations and results indicate that metal–Aβ complexes could be directly linked to AD pathogenesis.

2.3. Conclusions

In summary, for the first time, experimental evidence affirms that metal–Aβ complexes can be directly associated with AD pathogenesis, by applying the first *in vivo* chemical tool which specifically targets metal–Aβ complexes and ameliorates metal–Aβ reactivity (*i.e.*, metal–Aβ aggregation, formation of toxic oligomers, and ROS production) in 5XFAD AD mice. Our findings presented herein demonstrate the feasibility of developing small molecules as *in vivo* chemical tools for studying metal–Aβ. In addition, our studies indicate that research efforts toward understanding metal–Aβ-induced pathological pathways and identifying interrelated partners with metal–Aβ in AD onset and progression at the molecular level should continue to be made. The current and future outcomes, obtained from metal–Aβ-involved AD research, can open new directions for our long-term goal, the discovery of effective drugs for this fatal neurological disorder.

2.4. Experimental section

2.4.1. Materials and methods

All reagents were purchased from commercial suppliers and used as received unless otherwise noted. $A\beta_{40}$ and $A\beta_{42}$ (the sequence of $A\beta_{42}$: DAEFRHDSG-YEVHHQKLVFFAEDVGSNKGAIIGLMVGGVVIA) were purchased from Anaspec Inc. (Fremont, CA, USA). Compound **L2-b** was prepared using the previously reported procedures.[27] Trace metals were removed from buffers and solutions used in Aβ experiments (*vide infra*) by treating with Chelex overnight (Sigma-Aldrich, St. Louis, MO, USA). Optical spectra for the measurement of Aβ concentrations were recorded on an Agilent 8453 UV-visible (UV-vis) spectrophotometer. Absorbance values for biological assays, including cell *via*bility and antioxidant assays, were measured on a Molecular Devices SpectraMax 190 microplate reader (Sunnyvale, CA, USA).

2.4.2. Aβ aggregation experiments

Aβ experiments were performed according to previously published methods.[27,29-31,39] Prior to experiments, $A\beta_{40}$ or $A\beta_{42}$ was dissolved in ammonium hydroxide (NH_4OH; 1% v/v, aq). The resulting solution was aliquoted, lyophilized overnight, and stored at −80 °C. A stock solution of Aβ was then prepared by dissolving lyophilized peptide in 1% NH_4OH (10 μL) and diluting with ddH_2O. The concentration of the solution was determined by measuring the absorbance of the solution at 280 nm (ε = 1450 $M^{-1}cm^{-1}$ for $A\beta_{40}$; ε = 1490 $M^{-1}cm^{-1}$ for $A\beta_{42}$). The peptide stock solution was diluted to a final concentration of 25 μM in Chelex-treated buffered solution containing HEPES (20 μM, pH 6.6 for Cu(II) samples; pH 7.4 for metal-free and Zn(II) samples) and NaCl (150 μM). For the inhibition studies, **L2-b** (final concentration 50 μM, 1% v/v DMSO) was added to the sample of Aβ (25 μM) in the absence and presence of a metal chloride salt ($CuCl_2$ or $ZnCl_2$; 25 μM) followed by incubation at 37 °C with constant agitation for 4 or 24 h. For the disaggregation studies, Aβ with and without a metal chloride salt was incubated for 24 h at 37 °C with constant agitation to generate preformed Aβ aggregates. The resulting samples were then treated with **L2-b** (50 μM) and incubated with constant agitation for additional 4 or 24 h.

2.4.3. Gel electrophoresis and Western blotting

The samples from the inhibition and disaggregation experiments were analyzed by gel electrophoresis followed by Western blotting using an anti-Aβ antibody (6E10) following previously established procedures.[27,29-31,39] Samples (10 μL) were separated on a 10-20% Tris-tricine gel (Invitrogen, Grand Island, NY, USA). Following separation, the proteins were transferred onto nitrocellulose membranes and blocked with bovine serum albumin (BSA, 3% w/v, Sigma-Aldrich, St. Louis, MO, USA) in Tris-buffered saline (TBS) containing 0.1% Tween-20 (TBS-T) for 2 h at room temperature or overnight at 4 °C. The membranes were incubated with an anti-Aβ antibody (6E10, 1:2000, Covance, Princeton, NJ, USA) in a solution of 2% BSA (w/v in TBS-T) for 4 h at room temperature or overnight at 4 °C. After washing with TBS-T (3x, 10 min), a

horseradish peroxidase-conjugated goat antimouse secondary antibody (1:5000 in 2% BSA w/v in TBS-T; Cayman Chemical Company, Ann Arbor, MI, USA) was added for 1 h at room temperature. The ThermoScientific SuperSignal West Pico Chemiluminescent Substrate (Thermo Scientific, Rockford, IL, USA) was used to visualize protein bands.

2.4.4. Dot blot analysis

Dot blots were performed following previously established procedures with slight modifications.[33] These experiments were prepared by placing 2.5 μL of the samples from inhibition and disaggregation experiments on nitrocellulose membranes. The samples were allowed to dry and then blocked overnight at 4 °C in 3% BSA w/v in TBS containing 0.01% Tween-20 (dilute TBS-T). The membranes were then incubated with either an anti-Aβ antibody (6E10, 1:2000), an anti-Aβ oligomer antibody (A11, 1:5000 in 2% BSA w/v in dilute TBS-T; Invitrogen), or an anti-Aβ fibril antibody (OC, 1:5000 in 2% BSA w/v in dilute TBS-T; Millipore, Temecula, CA, USA) for 2 h at 4 °C followed by washing with dilute TBS-T (3x, 7 min). The addition of a horseradish peroxidase-conjugated goat antimouse secondary antibody for 6E10-treated membranes or a horseradish peroxidase-conjugated antirabbit secondary antibody (1:10000 in 2% BSA w/v in dilute TBS-T; Promega, Madison, WI, USA) for A11- and OC-treated membranes was subsequently followed. After incubating with the secondary antibody for 1 h at 4 °C, the membranes were washed with dilute TBS-T (3x, 7 min). The Biosesang ECL Plus kit (Biosesang, Gyeonggi-do, Korea) was used to visualize the results on a ChemiDoc MP Imaging System (Bio-Rad, Hercules, CA, USA).

2.4.5. Transmission electron microscopy (TEM)

Samples for TEM were prepared according to a previously reported method using glow-discharged grids (Formar/Carbon 300-mesh, Electron Microscopy Sciences, Hatfield, PA, USA).[27,29-31,39] Images from each sample were taken on a JEM-2100 Transmission Electron Microscope (JEOL Ltd., Tokyo, Japan).

2.4.6. Ion mobility–mass spectrometry (IM–MS)

All IM-MS experiments were carried out on a Synapt G2 (Waters, Milford, MA).[40,41]

Samples were ionized using a nano-electrospray source operated in positive ion mode. MS instrumentation was operated at a backing pressure of 2.7 mbar and sample cone voltage of 40 V. Aliquots of Aβ peptides (final concentration 18 μM) were sonicated for 10 sec prior to preincubation with, or without, a source of Cu(II) (copper(II) acetate) at 37 °C for 10 min. After preincubation, samples were treated with or without **L2-b** at 37 °C for 50 min prior to analysis. Solution conditions were 100 mM ammonium acetate (pH 7.5, unless otherwise stated) with 1% v/v DMSO. Acetylation of $A\beta_{40}$ peptides was carried out using methods described previously,[35] prior to overnight dialysis into 100 mM ammonium acetate (pH 7.5). Collision cross-section (CCS) measurements were externally calibrated using a database of known values in helium, using values for proteins that bracket the likely CCS and ion mobility values of the unknown ions.[42,43] CCS values are the mean average of a minimum of five replicates (maximum of eight), with errors reported as the least square analysis output for all measurements. This least square analysis combines inherent calibrant error from drift tube measurements (3%), the calibration R^2 error and two times the replicate standard de*via*tion error. All other conditions are consistent with previously published methods.[30]

2.4.7. Cell viability measurements

Murine neuroblastoma N2a cell line was purchased from the American Type Cell Collection (ATCC, Manassas, VA, USA). The cell line was maintained in media containing 45% Dulbecco's modified Eagle's medium (DMEM; Gibco, Life Technologies, Grand Island, NY, USA) and 45% OPTI-MEM Reduced Serum Media (Gibco), supplemented with 9% fetal bovine serum (FBS; Atlanta Biologicals, Flowery Branch, GA, USA), 1% non-essential amino acids (NEAA), 2 mM glutamine, 100 U/mL penicillin, and 100 mg/mL streptomycin (Gibco). The cells were grown in a humidified atmosphere with 5% CO_2 at 37 °C. For the MTT assay, N2a cells were seeded in a 96 well plate (15,000 cells per 100 μL). The cells were treated with Aβ alone (10 μM), [Aβ + **L2-b** (10 μM, 1% v/v final DMSO concentration)], [Aβ + $CuCl_2$ or $ZnCl_2$ (10 μM)], or [Aβ + $CuCl_2$ or $ZnCl_2$ + **L2-b**]. The N2a cells were also incubated with a metal chloride salt ($CuCl_2$ or $ZnCl_2$; 10 μM), **L2-b** (10 μM), or metal/**L2-b** (1:1 metal:ligand ratio). After 24 h incubation, 25 μL of MTT (Sigma-Aldrich; 5 mg/mL in PBS, pH 7.4; Gibco) was added to

each well, and the plate was incubated for 4 h at 37 °C. Formazan produced by the cells was solubilized by addition of an acidic solution of *N,N*-dimethylformamide (50% v/v) and sodium dodecyl sulfate (SDS; 20% w/v, aq) overnight at room temperature in the dark. The absorbance was measured at 600 nm by a microplate reader. Cell *via*bility was calculated relative to that of cells containing an equivalent amount of DMSO. Error bars were calculated as standard errors from three independent experiments.

2.4.8. Antioxidant assay

The antioxidant activity of **L2-b** was determined by the Trolox equivalent antioxidant capacity (TEAC) assay employing cell lysates following the protocol of an antioxidant assay kit purchased from Cayman Chemical Company with modifications employing the N2a cell line.[29] Cells were seeded in a 6 well plate and grown to approximately 80-90% confluence. Cell lysates were prepared following the previously reported method with modifications.[44] N2a cells were washed once with cold PBS (pH 7.4; Gibco) and harvested by gently pipetting off adherent cells with cold PBS. The cell pellet was generated by centrifugation (2,000 x g for 10 min at 4 °C). This cell pellet was sonicated on ice (5x for 5 sec pulses with 20 sec intervals between each pulse) in 2 mL of cold assay buffer (5 mM potassium phosphate, pH 7.4, containing 0.9% NaCl and 0.1% glucose). The cell lysates were centrifuged at 5,000 x g for 10 min at 4 °C. The supernatant was removed and stored on ice until use. 10 μL of the supernatant was delivered followed by addition of compound, metmyoglobin, 2,2'-azino-bis(3-ethylbenzothiazoline-6-sulphonic acid (ABTS), and H_2O_2 in the specified order to sample wells on a 96 well plate. After 5 min incubation at room temperature on a shaker, absorbance values at 750 nm were recorded. The percent inhibition was calculated according using the measured absorbance [% inhibition = $(A_0 - A)/A_0$, where A_0 is the absorbance of the supernatant of cell lysates] and was plotted as a function of compound concentration. The TEAC value of ligands was calculated as a ratio of the slope of the standard curve of the compound to that of Trolox (Sigma-Aldrich; Trolox = 6-hydroxy-2,5,7,8-tetramethylchroman-2-carboxylic acid; dissolved in DMSO). Duplicate measurements were conducted in three different experiments.

2.4.9. Brain uptake studies

Brain uptake experiments were carried out using male CD1 mice (purchased from Vital River Laboratory Animal Technology Co. Ltd., Beijing, China) by Contract Research Organization, Shanghai ChemPartner Co., Ltd. (Shanghai, China). The studies reported here adhere to the principles of the Association for Assessment and Accreditation of Laboratory Animal Care (AAALAC) International. **L2-b** (10 mg kg^{-1}, single dose in sterile water) was administrated to mice by oral gavage. At 30 min postdose (n = 3 at each time point), 150 μL of blood was withdrawn *via* retro orbital puncture or cardiac puncture and transferred into tubes with spray-coated K_2EDTA as an anticoagulant. Blood samples were put on ice and centrifuged to obtain plasma samples (2000 g, 5 min, 4 °C). Immediately following blood collection, mice were euthanized by pure CO_2 inhalation. The whole brain was collected, rinsed with cold saline, dried on filter paper, and weighed. The brain samples were immediately homogenized with three volumes (v/w) of homogenizing solution (PBS). Both plasma and brain samples were added with an internal standard (propranolol) in acetonitrile (CH_3CN; protein precipitation). The mixture was vortexed for 2 min and centrifuged at 14,000 rpm for 5 min and an aliquot of the supernatant was analyzed for concentration of **L2-b** by LC-MS/MS (UPLC/MS-MS API-5500, Framingham, MA, USA), with the analytical lower limit of quantitation (LLOQ) values for **L2-b** at 2 ng/mL (plasma), 8 ng/mL (brain), and 30 ng/mL (CSF). The supernatant was stored at −80 °C prior to analysis.

2.4.10. Metabolic stability

The susceptibility of **L2-b** to metabolism was determined by a Contract Research Organization (Shaghai ChemPartner Co., Ltd) using **L2-b** (1 mM) and ketanserin (1 mM; as a reference) in human liver microsomes (0.75 mg/ml) for 0 min, 5 min, 15 min, 30 min, 45 min, 60 min, 75 min, 90 min, and 120 min. The reaction mixtures also contained potassium phosphate buffer (100 mM, pH 7.4) and reduced nicotinamide adenine dinucleotide phosphate (NADPH; 6 mM). Metabolic reactions were initiated by the addition of NADPH and stopped at designated time points by the addition of CH_3CN (135 μL). Precipitate was removed by centrifugation. Supernatant (50 μL) was

transferred to a 96 well plate containing 50 μL of millipore water for LC/MS analysis.

2.4.11. Animals and drug administration

Animal studies using male 5XFAD AD model mice were performed in accordance with the Guidelines for Laboratory Animal Care and Use of the Asan Institute for Life Sciences, Asan Medical Center (Seoul, Korea), where they were given free access to chow and drinking water under a 12 h light/dark cycle. 5XFAD transgenic mice overexpress mutant human APP_{695} [K670N/M671L (Swedish), I716V (Florida), and V717I (London)] and PSEN1 (M146L and L286V); thus, the mice rapidly develop pathological features of AD, such as intraneuronal and extracellular Aβ deposition, neurodegeneration, and behavioral disabilities.[26] In this study, each mouse was given an injection with freshly prepared vehicle (1% v/v DMSO in 20 mM HEPES, pH 7.4, 150 mM NaCl) or **L2-b** (1 mg kg^{-1} of body weight) into the lower right or left quadrant of their abdomen every day for three weeks using Ultra-Fine™ II insulin syringes (Becton Dickinson, Franklin Lakes, NJ, USA). The body weight of the animal was measured immediately before the injection. Three hours after the final injection, the mice were sacrificed under deep anesthesia. A necropsy was performed to evaluate if there was drug-induced damage and the brain tissues were quickly collected and frozen with liquid nitrogen and stored at –80°C.

2.4.12. Tissue preparation

The right brain hemisphere of the mice was quickly frozen with liquid nitrogen for biochemical analyses. The left hemispheres were sagittally dissected at the thickness of 12 μm on a cryostat (HM550; Microm, Walldorf, Germany), mounted onto 1% poly-L-lysine-coated glass slides, and thereafter used for histological evaluations.

2.4.13. Measurement of synaptic Zn(II)

Freshly prepared brain sections (12 μm thickness) were stained with *N*-(6-methoxy-8-quinolyl)-*p*-toluenesulfonamide (TSQ; 4.5 μM, Invitrogen) in 100 μL of 140 mM sodium barbital/sodium acetate buffer (pH 10.0) for 90 sec.[37] After rinsing briefly in physiological saline (0.9% NaCl, pH 7.2), fluorescence of TSQ on the sections was

photographed under a fluorescence microscope (Eclipse 80i, Nikon) with a 100X Plan Fluor lens and a UV-2A filter (dichroic, 400 nm; excitation, 330-380 nm; barrier, 420 nm; Nikon) using a digital camera (DS-Fi1/DS-U2; Nikon) and computer-assisted imaging software (NIS-Elements F; Nikon). The mean fluorescence intensity of TSQ in the mossy fiber area was measured using a computer-assisted image analysis program (Image-Pro Plus; Media Cybernetics, Silver Spring, MD, USA) and the level of synaptic Zn(II) was determined by subtracting background fluorescence as obtained at an area outside of the tissue section.

2.4.14. $A\beta_{40}/A\beta_{42}$ quantification

The amounts of $A\beta_{40}/A\beta_{42}$ were measured in the brain according to the methods as described previously.[38] Briefly, the protein homogenate fractions were collected in PBS (pH 7.4) containing Complete™ Protease Inhibitor cocktail (Roche Diagnostics, Mannheim, Germany), in 2% SDS (aq), and then in 70% formic acid (FA) by serial centrifugations. The EC buffer-diluted protein fractions were subjected to ELISA using the human $A\beta_{40}/A\beta_{42}$ ELISA kit (Invitrogen), where FA-fractions were neutralized with 1 M Tris (pH 11.0) prior to the dilution. In addition, the amounts of the aggregated or oligomeric Aβ in PBS fractions were also measured using Aβ Oligomers ELISA kit (82E1-specific; IBL International, Hamburg, Germany). The colorimetric quantifications were determined at 450 nm with the Synergy H1 Hybrid microplate reader (BioTek, Winooski, VT, USA), and the cerebral $A\beta_{40}/A\beta_{42}$ amount was calculated as moles per gram of wet brain tissue.

2.4.15. Quantification of Aβ deposition

In order to evaluate the development of extracellular Aβ deposits, immunohistochemistry studies were performed on the sagittal brain sections using an anti-human Aβ(17-24) antibody (4G8, 1:1000; Covance, Princeton, NJ, USA). After being immunologically reacted with 4G8 and biotynylated anti-mouse secondary antibody (Vector Laboratories, Burlingame, CA, USA), the tissue sections were developed in PBS containing 0.015% diaminobenzidine and 0.001% H_2O_2 (Vector Laboratories) and then examined or photographed under a light microscope (Eclipse

80i; Nikon, Tokyo, Japan). Next, the congophillic amyloid plaques were detected by staining the tissues with Accustain® Congo Red amyloid staining solution (Sigma-Aldrich, St. Louis, MO, USA). The loads of amyloid deposits in the cortex were given as the percent area of 4G8-immunoreactive deposits or the number of congophilic plaques per mm^2 of cortex area.

2.4.16. Immunoblot analysis of Aβ

Immediately after the brains were collected from the mice, the tissue lysates were prepared in PBS (pH 7.4) containing Complete™ Protease Inhibitor Cocktail (Roche Diagnostics) and stored in liquid nitrogen. The protein amount was measured using a bicinchoninic acid assay (Bio-Rad). Boiled proteins were separated with the sample buffer (62.5 mM Tris, pH 6.8, 2% SDS, 10% glycerol, 0.01% bromophenol blue, 5% mercaptoethanol, and 50 mM dithiothreitol) on 4-20% or 16.5% Precise Tris-Glycine Gel (Thermo Fisher Scientific, Rockford, IL, USA) and then transferred onto polyvinylidene difluoride membranes (Merck Millipore, Billerica, MA, USA) using semidry blotters (TE70 PWR; Amersham Biosciences, Uppsala, Sweden). After blocking in TBS-T buffer with 5% skimmed milk and 1% BSA (Bovostar; Bovogen, Melbourne, Australia), the blots were reacted with an anti-Aβ antibody (6E10, 1:1000; Covance) and then with horseradish peroxidase-conjugated secondary antibody (1:5000). Immunoreactive proteins were detected using Immobilon Western Chemiluminescent HRP Substrate (Merck Millipore) on the Davinch-Chemi® Chemiluminescence Imaging System (CAS-400SM; CoreBio, Seoul, Korea).

2.4.17. Behavioral evaluation

Spatial learning and memory abilities were assessed using the Morris water maze task, which was composed of a cylindrical platform (15 cm in diameter) submerged 0.5 cm below the surface of opaque water at the center of a target quadrant in the circular pool. The mice were subjected to three training trials per day to swim and locate the hidden platform for a maximum of 60 sec. The task was conducted at 3 h after each drug injection over a period of five consecutive days starting on the day of the 21st injection, during which vehicle or **L2-b** was still administered. The time and swimming

track taken to reach the escape platform were recorded and analyzed on SMART Video Tracking System (Harvard Apparatus, Holliston, MA, USA). Three hours later, the mice entered water again to swim in the absence of the platform for 60 sec and the time spent in each quadrant area was collected.

2.4.18. Statistics

All values are presented as the means ± standard errors of the mean (SEMs) unless otherwise noted. Statistical analysis was performed using one-way analysis of variance (ANOVA) with Student-Newman-Keuls *post hoc* test, or the unpaired *t*-test. Differences with P values < 0.05 were considered significant.

2.5. Acknowledgements

This work was supported by the Ruth K. Broad Biomedical Foundation, the 2013 Research Fund (Project Number 1.130068.01) of Ulsan National Institute of Science and Technology (UNIST), and the National Research Foundation of Korea (NRF) grant funded by the Korean government (MSIP) (NRF-2014R1A2A2A01004877) (to M.H.L.); the Korea Healthcare Technology R&D Project, Ministry for Health and Welfare, Republic of Korea (A092042) and the Basic Science Research Program, National Research Foundation of Korea, Ministry of Education, Republic of Korea (NRF-2012R1A1A2006801) (to J.-Y.L.); the University of Michigan Protein Folding Disease Initiative (to B.T.R. and M.H.L.).

2.6. References and notes

(1) Fargo, K.; Beiler, L. *Alzheimers Dement.* **2014**, *10*, e47.
(2) Corbett, A.; Pickett, J.; Burns, A.; Corcoran, J.; Dunnett, S. B.; Edison, P.; Hagan, J. J.; Holmes, C.; Jones, E.; Katona, C.; Kearns, I.; Kehoe, P.; Mudher, A.; Passmore, A.; Shepherd, N.; Walsh; F.; Ballard, C. *Nat. Rev. Drug Discovery* **2012**, *11*, 833.
(3) Jakob-Roetne, R.; Jacobsen, H. *Angew. Chem., Int. Ed.* **2009**, *48*, 3030.
(4) Beck, M. W.; Pithadia, A. S.; DeToma, A. S.; Korshavn, K. J.; Lim, M. H. In *Ligand Design in Medicinal Inorganic Chemistry*; Storr, T., Ed. Wiley: Chichester, England, 2014; pp. 256.
(5) Hardy; J. A.; Higgins, G. A. *Science* **1992**, *256*, 184.
(6) Barnham, K. J.; Masters, C. L.; Bush, A. I. *Nat. Rev. Drug Discovery* **2004**, *3*, 205.
(7) Kepp, K. P. *Chem. Rev.* **2012**, *112*, 5193.
(8) Savelieff, M. G.; Lee, S.; Liu, Y.; Lim, M. H. *ACS Chem. Biol.*, **2013**, *8*, 856.
(9) Lee, H. J.; Korshavn, K. J.; Kochi, A.; Derrick, J. S.; Lim, M. H. *Chem. Soc. Rev.* **2014**, *43*, 6672.
(10) Greenough, M. A.; Camakaris, J.; Bush, A. I. *Neurochem. Int.* **2013**, *62*, 540.
(11) DeToma, A. S.; Salamekh, S.; Ramamoorthy A.; Lim, M. H. *Chem. Soc. Rev.* **2012**, *41*, 608.
(12) Lovell, M. A.; Robertson, J. D.; Teesdale, W. J.; Campbell, J. L.; Markesbery, W. R.; *J. Neurol. Sci.* **1998**, *158*, 47.
(13) Que, E. L.; Domaille; D. W.; Chang, C. J. *Chem. Rev.* **2008**, *108*, 1517.
(14) Viles, J. H. *Coord. Chem. Rev.* **2012**, *256*, 2271.
(15) Young, T. R.; Kirchner, A.; Wedd, A. G.; Xiao, Z. *Metallomics* **2014**, *6*, 505.
(16) Ayton, S.; Lei, P.; Bush, A. I. *Free Radical Biol. Med.* **2013**, *62*, 76.
(17) Pithadia, A. S.; Lim, M. H. *Curr. Opin. Chem. Biol.* **2012**, *16*, 67.
(18) Faller, P.; Hureau, C.; La Penna, G. *Acc. Chem. Res.* **2014**, *47*, 2252.
(19) Crouch, P. J.; White, A. R.; Bush, A. I. *FEBS J.* **2007**, *274*, 3775.
(20) Rodríguez-Rodríguez, C.; Telpoukhovskaia, M.; Orvig, C. *Coord. Chem. Rev.* **2012**, *256*, 2308.
(21) Perez, L. R.; Franz, K. J. *Dalton Trans.* **2010**, *39*, 2177.
(22) Ritchie, C. W.; Bush, A. I.; Mackinnon, A.; Macfarlane, S.; Mastwyk, M.; MacGregor, L.; Kiers, L.; Cherny, R.; Li, Q.-X.; Tammer, A.; Carrington, D.; Mavros, C.; Volitakis, I.; Xilinas, M.; Ames, D.; Davis, S.; Beyreuther, K.; Tanzi, R. E.; Masters, C. L. *Arch. Neurol.* **2003**, *60*, 1685.
(23) Adlard, P. A.; Cherny, R. A.; Finkelstein, D. I.; Gautier, E.; Robb, E.; Cortes, M.; Volitakis, I.; Liu, X.; Smith, J. P.; Perez, K.; Laughton, K.; Li, Q.-X.; Charman, S. A.; Nicolazzo, J. A.; Wilkins, S.; Deleva, K.; Lynch, T.; Kok, G.; Ritchie, C. W.; Tanzi, R. E.; Cappai, R.; Masters, C. L.; Barnham, K. J.; Bush, A. I. *Neuron* **2008**, *59*, 43.
(24) Savelieff, M. G.; DeToma, A. S.; Derrick, J. S.; Lim, M. H. *Acc. Chem. Res.* **2014**, *47*, 2475.
(25) Mancino, A. M.; Hindo, S. S.; Kochi, A.; Lim, M. H. *Inorg. Chem.* **2009**, *48*, 9596.

(26) Oakley, H.; Cole, S. L.; Logan, S.; Maus, E.; Shao, P.; Craft, J.; Guillozet-Bongaarts, A.; Ohno, M.; Disterhoft, J.; Eldik, L. V.; Berry, R.; Vassar, R. *J. Neurosci.* **2006**, *26*, 10129.
(27) Choi, J.-S.; Braymer, J. J.; Nanga, R. P. R.; Ramamoorthy, A.; Lim, M. H. *Proc. Natl. Acad. Sci. USA* **2010**, *107*, 21990.
(28) Kung, H. F.; Lee, C.-W.; Zhuang, Z.-P.; Kung, M.-P.; Hou, C.; Plössl, K. *J. Am. Chem. Soc.* **2001**, *123*, 12740.
(29) Savelieff, M. G.; Liu, Y.; Senthamarai, R. R. P.; Korshavn, K. J.; Lee, H. J.; Ramamoorthy, A.; Lim, M. H. *Chem. Commun.* **2014**, *50*, 5301.
(30) Lee, S.; Zheng, X.; Krishnamoorthy, J.; Savelieff, M. G.; Park, H. M.; Brender, J. R.; Kim, J. H.; Derrick, J. S.; Kochi, A.; Lee, H. J.; Kim, C.; Ramamoorthy, A.; Bowers; M. T.; Lim, M. H. *J. Am. Chem. Soc.* **2014**, *136*, 299.
(31) Hyung, S.-J.; DeToma, A. S.; Brender, J. R.; Lee, S.; Vivekanandan, S.; Kochi, A.; Choi, J.-S.; Ramamoorthy, A.; Ruotolo, B. T; Lim, M. H. *Proc. Natl. Acad. Sci. USA* **2013**, *110*, 3743.
(32) As presented in ref. 27, the initial aggregation studies using **L2-b** were conducted only for metal-induced $A\beta_{40}$ aggregation at one incubation time (*i.e.*, 24 h).
(33) Kayed, R.; Head, E.; Thompson, J. L.; McIntire, T. M.; Milton, S. C.; Cotman, C. W.; Glabe, C. G. *Science* **2003**, *300*, 486.
(34) Kayed, R.; Head, E.; Sarsoza, F.; Saing, T.; Cotman, C. W.; Necula, M.; Margol, L.; Wu, J.; Breydo, L.; Thompson, J. L.; Rasool, S.; Gurlo, T.; Butler, P.; Glabe, C. G. *Mol. Neurodegener.* **2007**, *2*, 18.
(35) Hermanson, G. T. In *Bioconjugate Techniques* 2nd ed; Hermanson, G. T. Ed. Academic Press: New York, USA ,2008; pp. 1003.
(36) Frederickson, C. J.; Kasarskis, E. J.; Ringo, D.; Frederickson, R. E. *J. Neurosci. Methods* **1987**, *20*, 91.
(37) Lee, J.-Y.; Kim, J. S.; Byun, H.-R.; Palmiter, R. D.; Koh, J.-Y. *Brain Res.* **2011**, *1418*, 12.
(38) Oh, S. B.; Byun, C. J.; Yun, J.-H.; Jo, D.-G.; Carmeliet, P.; Koh, J.-Y.; Lee, J.-Y. *Neurobiol. Aging* **2014**, *35*, 511.
(39) Liu, Y.; Kochi, A.; Pithadia, A. S.; Lee, S.; Nam, Y.; Beck, M. W.; He, X.; Lee, D.; Lim, M. H. *Inorg. Chem.* **2013**, *52*, 8121.
(40) Giles, K.; Williams, J. P.; Campuzano, I. *Rapid Commun. Mass. Spectrom.* **2011**, *25*, 1559.
(41) Zhong, Y.; Hyung, S.-J.; Ruotolo, B. T. *Analyst* **2011**, *136*, 3534.
(42) Ruotolo, B. T.; Benesch, J. L. P.; Sandercock, A. M.; Hyung, S.-J.; Robinson, C. V. *Nat. Protoc.* **2008**, *3*, 1139.
(43) Bush, M. F.; Hall, Z.; Giles, K.; Hoyes, J.; Robinson, C. V.; Ruotolo, B. T. *Anal. Chem.* **2010**, *82*, 9557.
(44) Spencer, V. A.; Sun, J.-M.; Li, L.; Davie, J. R. *Methods* **2003**, *31*, 67.

Chapter 3
Structural similarity of small molecules, but distinct targets and reactivities in amyloidogenic diseases through multiple modes of action

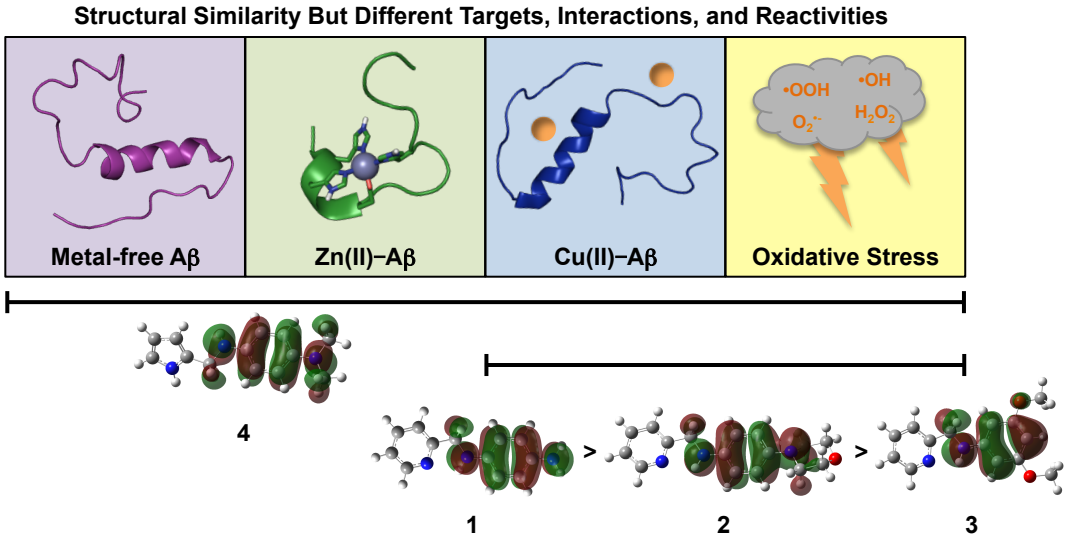

I thank Professor Kwang Soo Kim, Dr. Han Lee, Dr. Woo Cho, and Dr. Zahra Tehrani for performing the computational calculations. I am grateful for Professor Bing Ye and Dr. Masha Savelieff conducting the primary neuron culture experiments. I also appreciate Professor Scott Larsen for the assistance in the design of the molecules. Milim Jang carried out living cell experiments and the antioxidant capacity assay. Juhye Kang obtained TEM images. I would like to also acknowledge Dr. Akiko Kochi, Jeffrey Derrick, Jillian Charon, and Arkah Ghosh for their assistance with the PAMPA assay, the deoxyribose assay, initial solution speciation studies, and initial metal binding studies, respectfully. I performed the purification and synthesis of the compounds, the analysis by gel electrophoresis with Western blot, inhibition of Fenton-like reactions, the BBB permeability test, and mechanistic studies in solution.

3.1. Introduction

Metal ion dyshomeostasis, misfolded protein aggregation, and increased oxidative stress have been implicated in having a central role in the pathogenesis and progression of neurodegenerative diseases, including Alzheimer's disease (AD), Parkinson's disease (PD), and amyloid lateral sclerosis (ALS).[1-8] It has been suggested that these factors are inter-related through the development of metal–protein complexes that could lead to the misfolding and stabilization of abnormal protein conformations that facilitate and accelerate toxic aggregate formation and lead to the production of reactive oxygen species (ROS) through Fenton-like chemistry by redox-active metals.[1-5,9-12] Progress in generating molecules suitable to target these metal–protein complexes as potential treatments or as chemical tools to study their properties has been made; however, most of these tools share the same structural components, lack specificity for particular forms of metal–protein complexes, and have not had their molecular level mode of action elucidated.[2,13]

To gain a better understanding of this aspect and provide new insight into tool development, four small molecules were designed and prepared based onto a *p*-iodostilbene framework with slight differences in their structures (Figure 3.1). We report that despite the structural changes being relatively minor, they have different activities toward our model targets [*i.e.*, amyloid-β (Aβ); the amyloidogenic peptide associated primarily with AD, metal ions [Cu(II) or Zn(II)], ROS, and other free radicals]. By employing biochemical and computational approaches, it is demonstrated that these compounds can target and interact with metal-free Aβ and/or complexes of metal and Aβ (metal–Aβ) through structure-dependent modes of action leading to the redirection of the aggregation route to generate off-pathway forms mediating their reactivity (*i.e.*, toxic aggregate formation, and ROS generation) to varying degrees. These studies demonstrate that slight structural variations to one framework can govern small molecules' targeted capabilities of regulating multiple pathological factors found in neurodegenerative diseases.

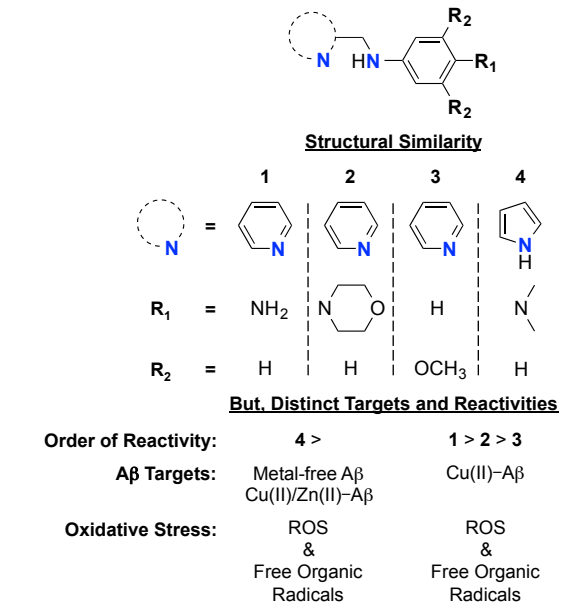

Figure 3.1. Structures of 1-4 and summary of reactivity. **1**, N^1-(pyridin-2-ylmethyl)benzene-1,4-diamine; **2**, 4-morpholino-*N*-(pyridin-2-ylmethyl)aniline; **3**, 3,5-dimethoxy-*N*-(pyridin-2-ylmethyl)aniline; **4**, N^1-((1H-pyrrol-2-yl)methyl)-N^4,N^4-dimethylbenzene-1,4-diamine.

3.2. Results and discussion

3.2.1. Rational selection of small molecules and the model peptide system

Four derivatives (**1**-**4**) of the known amyloid-interacting framework, *p*-iodostilbene, (Figure 3.1) were selected for our studies.[2,14-18] These molecules have two nitrogen (*N*,*N*) donor atoms for metal chelation that are provided by 2-picolylamine (**1**-**3**) or [1*H*-pyrrol-2-yl]methylamine (**4**) groups. The structures were varied further by installing amine (**1**), morpholino (**2**), 3,5-dimethoxy (**3**), or dimethylamino (**4**) functionalities (Figure 3.1). These changes should effect the interaction with metal–Aβ with the differences in the metal binding site mainly varying the metal binding properties while the other structural changes that vary hydrogen bonding and hydrophobicity of the compounds should effect the interaction with Aβ. **1**-**4** were obtained from commercial sources and **1**, **3**, and **4** were recrystallized before use. In addition to the commercially obtained **1**, this compound was also synthesized in two steps though the reduction of the nitro containing compound produced from the previously reported S_NAr reaction between 1-fluoro-4-nitrobenzene and 2-(aminomethyl)pyridine.[19,20] The product was then isolated as the HCl salt (85% yield; Figure 3.2).

In addition to having well known Aβ and metal–Aβ interacting properties, many *p*-iodostilbene derivatives are known to penetrate the blood-brain barrier (BBB).[14-18] In

Table 3.1. Calculated and measured BBB permeability parameters for **1**-**4**.

Parameters	1	2	3	4	Lipinski's rules and others
MW[a]	199	269	244	215	≤ 450
*c*LogP[b]	1.96	1.05	1.73	1.86	≤ 5.00
HBA[c]	3	4	4	3	≤ 10
HBD[d]	3	1	1	2	≤ 5
PSA (Å^2)[e]	50.9	37.9	43.4	31.1	≤ 90
logBB[f]	−0.563	−0.272	−0.249	−0.047	< −1.0 poorly distributed in the brain
$-\log P_e$[g]	5.0(1)	4.6(5)	4.2(8)	4.9(0)	$-\log P_e$ < 5.4 (CNS+); $-\log P_e$ > 5.7 (CNS-)
CNS +/− Prediction	CNS+	CNS+	CNS+	CNS+	

[a]MW, molecular weight; [b]*c*logP, calculated log of water–octanol partition coefficient.; [c]HBA, hydrogen bond acceptor; [d] HBD, hydrogen bond donor; [e] PSA, polar surface area; [f]logBB = −0.0148 × PSA + 0.152 × *c*logP × 0.130. [g]Determined using the parallel artificial membrane permeability assay adapted for BBB (PAMPA-BBB).

order to assess if the structures (**1**-**4**) generated *via* slight variations could also be available in the brain, the ability to cross BBB was examined through several methods. First, adherence to Lipinski's rules and calculated logBB values were confirmed (Table 3.1). All calculated values suggest that **1**-**4** could be able to cross the BBB. The results from solution speciation studies were also considered as uncharged species can passively diffuse across the BBB more easily than charged species.[21] Since all of the tested compounds were shown to be predominately neutral at physiological pH (Figure 3.3; **1**, pK_{a1} = 4.7(6), pK_{a2} = 6.0(2), *ca*. 80% neural ligand (L) at pH 7.4; **2**, pK_{a1} = 4.0(8),

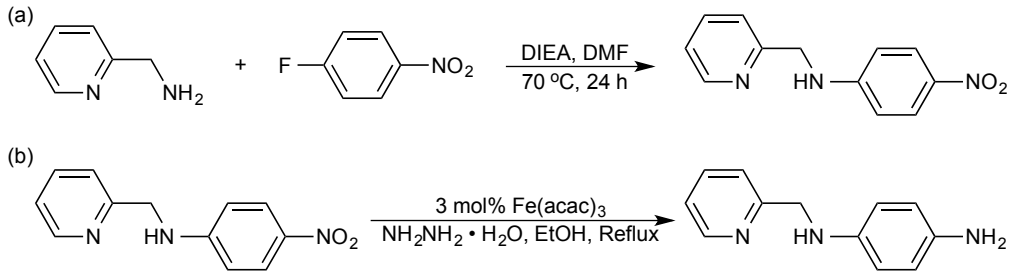

Figure 3.2. Synthesis of (a) 4-nitro-*N*-(pyridin-2-ylmethyl)aniline and (b) **1**.

pK_{a2} = 5.5(1), *ca*. 95% L at pH 7.4; **3** pK_{a1} = *n/a*, pK_{a2} = 5.0(8), *ca*. 100% L at pH 7.4; **4** not tested *vide infra*), an *in vitro* parallel artificial membrane permeability assay

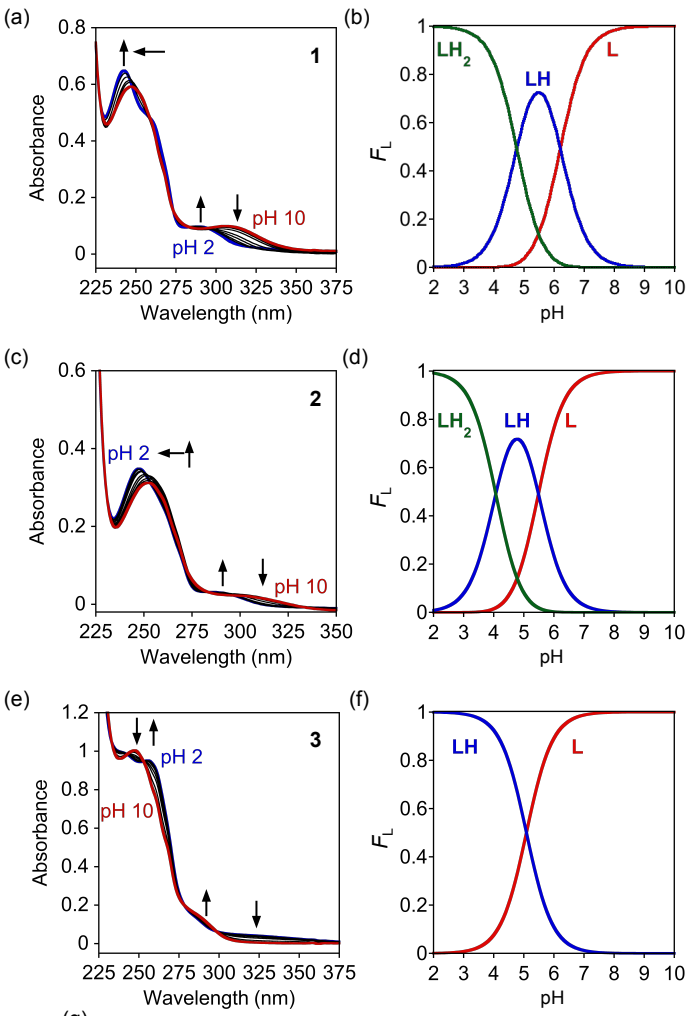

L=	pK_a 1	2	3
pK_{a1}: LH$_2$ ⇌ LH + H	4.7(6)	4.0(8)	–
pK_{a2}: LH ⇌ L + H	6.0(2)	5.5(1)	5.0(8)

Figure 3.3. Solution speciation studies of **1**-**3.** Variable pH titrations of (a) **1** (50 μM), (c) **2** (20 μM), or (e) **3** (100 μM) were monitored by UV-Vis. The resulting spectra were fit to obtain (g) pK_a values and plot (b,d,f) speciation diagrams. F_L = Fraction of ligand with at the specified protonation state. Charges omitted for clarity. Note that **4** was not determined for solution speciation due to limited stability in solution (100 mM NaCl, 10 mM NaOH).

adapted for the BBB (PAMPA-BBB) was used to confirm BBB permeability. Permeability values (–logP_e; Table 3.1) were obtained and when analyzed together with the calculated values and solution speciation studies, the PAMPA-BBB assay suggests that **1**-**4** can passively diffuse across the BBB and be viable structural frameworks, even with structural variations, for studying the inter-relationship of multiple factors involved in the

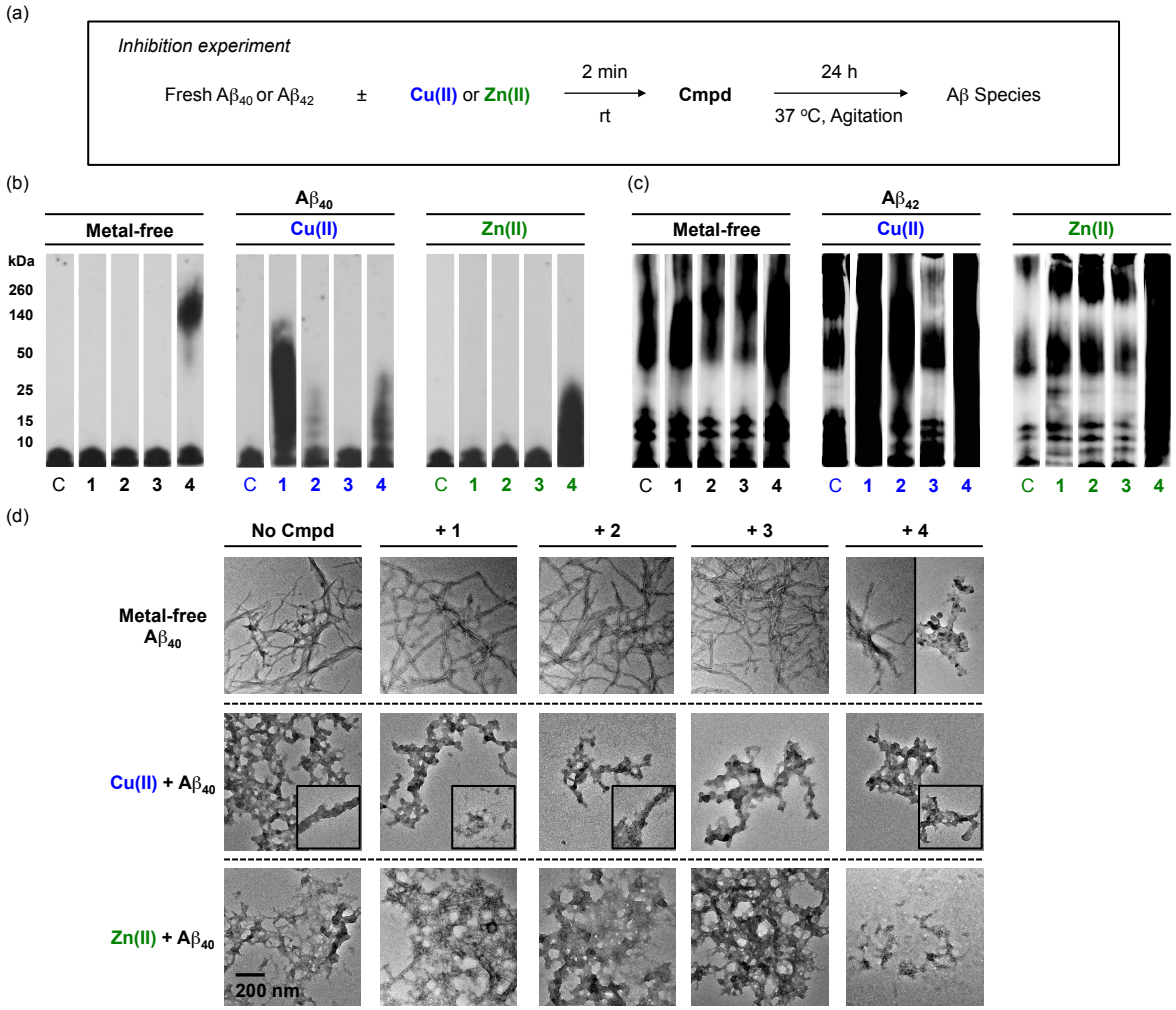

Figure 3.4. Effect of the compounds on metal-free and metal-induced Aβ aggregation. (a) Scheme of inhibition experiments: freshly prepared Aβ (25 μM) in the presence or absence of Cu(II) (blue, 25 μM) or Zn(II) (green, 25 μM) was mixed without (lane C) or with compounds **1**-**4** (50 μM, lanes 1-4) and incubated at 37 °C with constant agitation for 24 h. Gel/Western blot analysis of the molecular weight distribution of the resulting (b) $A\beta_{40}$ and (c) $A\beta_{42}$ species using anti-Aβ antibody (6E10). (d) Morphologies of the $A\beta_{40}$ aggregates as observed using TEM (scale bar = 200 nm).

pathogenesis of neurodegenerative diseases in the brain.

As the model peptide, Aβ was chosen for these studies due to its interactions with metal ions being relativity well studied *in vitro.*[2,9-11,22-28] Cu(I/II), Zn(II), and Fe(II) have been shown to coordinate to the Aβ peptide *in vitro* and the formation of these metal–Aβ complexes can direct the aggregation pathway of Aβ to generate and/or stabilize toxic forms. Additionally, when Aβ binds to redox-active metal ions [*i.e.*, Fe(II/III), Cu(I/II)], the production of ROS occurs though Fenton-like chemistry.[2,9-11,22-28] These *in vitro* observations demonstrate a clear interrelationship between Aβ, metal ions, and

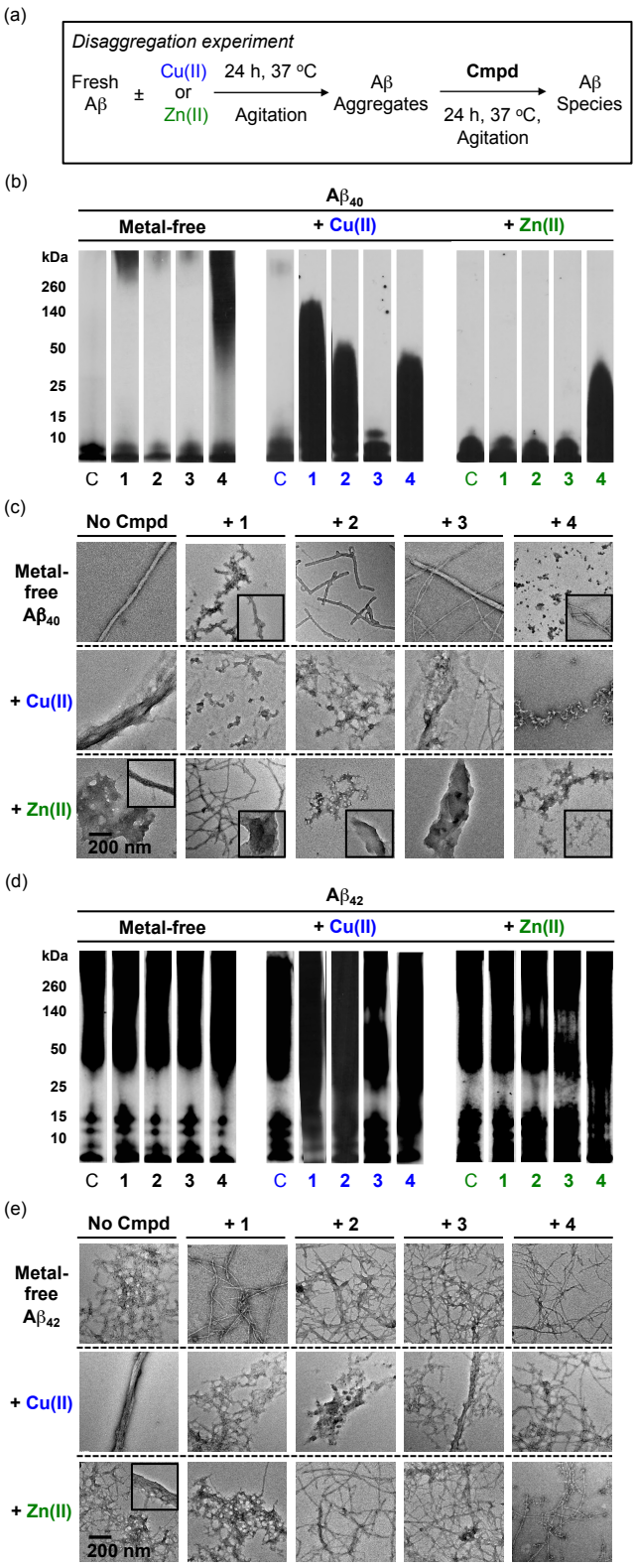

Figure 3.5. Ability of **1**-**4** to disrupt pre-formed metal-free and metal–Aβ aggregates. (a) Disaggregation experiment scheme: Metal-free and metal induced aggregates of Aβ were generated by incubating mixtures of freshly prepared $A\beta_{40}$ or $A\beta_{42}$ (25 μM) in the presence or absence of Cu(II) (blue, 25 μM) or Zn(II) (green, 25 μM) at 37 °C with agitation. After 24 h, samples were treated with **1-4** (50 μM) and

incubated for an additional 24 h. Gel electrophoresis and Western blot analysis of the molecular weight distribution of the resulting (b) $A\beta_{40}$ and (d) $A\beta_{42}$ species using anti-Aβ antibody (6E10). Morphologies of the (c) $A\beta_{40}$ and (e) $A\beta_{42}$ species as observed using TEM (scale bar = 200 nm).

oxidative stress linked through metal–Aβ complexes.[2,4,9,10,12,29,30] This makes Aβ good model system for studying the ability of small molecules to target and mediate the reactivity of apparent metal–amyloid interactions.

3.2.2. Reactivity I: Modulation of metal-free and metal-induced peptide aggregation by 1-4

The effect of the small structural differences on the ability of **1**-**4** to redirect the aggregation of both metal-free Aβ and metal–Aβ in inhibition (Figure 3.4a) and disaggregation experiments (Figure 3.5a) was evaluated using gel electrophoresis followed by Western blotting (gel/Western blot) with an anti-Aβ antibody (6E10) to determine the molecular weight (MW) distribution of the resulting peptide species in addition to observing the morphologies of the aggregates by transmission electron microscopy (TEM). Experiments were carried out with the two major Aβ isoforms, $A\beta_{40}$ and $A\beta_{42}$, found in the brain of AD.[9,31]

First, the alteration of metal-free Aβ aggregation was studied. The compounds (**1**-**3**) with different substituents on the phenyl ring (Figure 3.1) did not lead to noticeable diversion of the metal-free aggregation pathway (Figures 3.4b-d, 3.5b-e, and 3.6). Changing the pyridine (**1**-**3**) to a pyrrole (**4**), however, had a pronounced influence on metal-free Aβ aggregation. Treatment of $A\beta_{40}$ with **4** produced forms that were greater than 50 kDa in both inhibition and disaggregation samples, while in the case of $A\beta_{42}$ increased species ≤ 50 kDa were detected by gel/Western blots, which was more evident in settings of the inhibition than the disaggregation (Figures 3.4b,c and 3.5b,c). Additionally, in the $A\beta_{40}$ inhibition and disaggregation, TEM images smaller and more amorphous species were observed (Figures 3.4d, 3.5c,e, and 3.6); however, these changes were less noticeable in the $A\beta_{42}$ samples (Figures 3.5e and 3.6).

Next, the ability to control Cu(II)- and Zn(II)-induced aggregation was evaluated. Compound **1** demonstrated the capacity to redirect only Cu(II)-promoted $A\beta_{40}$ and $A\beta_{42}$ aggregation (Figures 3.4b,c and 3.5b,d), even when higher Zn(II) concentrations